HYDROGEOLOGY OF A FRUITLAND FORMATION AQUIFER, SAN JUAN BASIN - NEW MEXICO AND COLORADO, WITH EMPHASIS ON USING TEMPERATURE DISTRIBUTION DATA TO ESTIMATE LATERAL GROUNDWATER VELOCITY

by

John Philip McCord

Submitted in Partial Fulfillment of
the Requirements for the Degree
of Masters of Science in
Hydrology

NEW MEXICO INSTITUTE OF MINING AND TECHNOLOGY

SOCORRO, NEW MEXICO

October, 1988

ACKNOWLEDGMENTS

Numerous people and organizations have contributed to the successful completion of this study. Foremost among these were the Gas Research Institute which provided funding to obtain basic hydrogeologic data; Dr. Marshall Reiter of the New Mexico Bureau of Mines and Geology who provided both the high quality temperature data used in this study and helpful guidance in its interpretation; and Dr. Fred Phillips who helped me formulate this research.

Other individuals who provided data and encouragement included Dr. K.C. Bowman, Dr. George Saulnier, Craig Rightmire, Raoul Choate, Bruce Kelso, Paul Oldaker, and Frank Campbell.

In addition, I wish to express my thanks to all the Waterdogs whose friendship I value, and whose inability to make the play was a constant source of amusement.

Finally, I thank my wife Stephanie, without whose support I would not have been able to undertake this adventure.

TABLE OF CONTENTS

Table of Contents (con't)

LIST OF FIGURES

List of Figures (con't)

List of Figures (con't)

List of Figures (con't)

LIST OF TABLES

LIST OF PLATES

ABSTRACT

Currently the Fruitland Formation is considered to be part of a thick confining interval within the San Juan Basin hydrogeologic system. However, this study establishes that a Fruitland Formation aquifer characterized by laterally extensive, thick coalbeds, has the potential to be a major aquifer within this system.

As part of this study, data appropriate to defining the hydraulic head distribution for the Fruitland Formation has been compiled and analyzed. This data includes direct water-level elevations around the periphery of the basin and pressure head data obtained from drill-stem tests in the basin interior. The potentiometric surface defined by this data indicates that in the north and central portions of the basin, a Fruitland Formation aquifer may have the highest hydraulic potential of any aquifer within the hydrogeologic system.

Lithologically, this aquifer is characterized by thick coalbeds. Recent coalbed correlation efforts based on bed position relative to the Huerfanito Bentonite Bed suggest that individual thick coalbeds may extend up to 40 km in the northeast-southwest direction. In the study area, four of these major coalbeds overlap in an en echelon fashion with vertical separation between the individual beds of less than 30 meters. If some hydraulic connection between these individual thick coalbeds can be assumed, a lateral hydraulic continuity in coalbeds of more than 100 km is a possibility.

Coalbed aquifer properties will be primarily determined by the genetic fracture system in coal called cleat. However, this fracture permeability has been shown to be highly stress-sensitive. This indicates that aquifer/reservoir tests in coal intervals probably underestimate hydraulic conductivity.

An alternative method to estimate hydraulic conductivity involving the analyses of regional temperature distribution data is explored in this study. Analyses of high quality and correlatable temperature data gathered as part of a geothermal investigation in the San Juan Basin area, indicates that within the study area there is a lateral temperature gradient approximately perpendicular to the flow direction as defined by Fruitland Formation hydraulic head distribution. This temperature gradient is not due to depth variation, but rather, is due to a lateral change in conductive heat flow. Given this lateral temperature gradient, vertical temperature gradients through the Fruitland Formation can be analyzed to calculate lateral groundwater velocity within this interval.

The general analytical approach to accomplish this was developed by Stallman. This study uses both an implicit analytical solution based on Stallman's work, and an analysis of apparent excess heat flow within the assumed aquifer interval, for five well combinations within the study area to calculate lateral groundwater velocity. The calculated groundwater velocities are then combined with the estimated hydraulic gradient between the wells to estimate hydraulic conductivity. The calculated groundwater velocities using these methods seem unreasonably high and result in hydraulic conductivity estimates that are several

calculated groundwater velocities using these methods seem high and result in hydraulic conductivity estimates that are higher than hydraulic conductivities obtained from aquifer/reservoir tests. However, the techniques used to estimate lateral groundwater velocity are conceptually correct and given more detailed temperature and thermal conductivity profiles, could result in accurate estimations of lateral groundwater velocity.

INTRODUCTION

OBJECTIVE

The objective of this study is to develop an understanding of a proposed Fruitland Formation aquifer in the San Juan Basin, northwest New Mexico and southwest Colorado. Within the framework of the regional hydrodynamics, this formation is currently lumped together with the overlying Kirtland Shale to form the Kirtland/Fruitland confining unit. Aquifer units overlying and underlying this aquitard are the Ojo Alamo Sandstone and the Pictured Cliffs Sandstone, respectively. This study will show that a Fruitland Formation aquifer, characterized by laterally extensive, thick coalbeds is potentially a major aquifer within the regional hydrogeologic system.

STUDY MOTIVATION

The San Juan Basin of southwest Colorado and northwest New Mexico is one of the most active areas of coalbed methane exploration and development in the United States. A recent estimate of the potential magnitude of this resource in the San Juan Basin is 50 TCF (Kelso and Wicks, 1988). The bulk of this resource is found in the coalbeds of the Fruitland Formation. Prior to the recent efforts to develop these coalbeds as gas reservoirs, the Fruitland Formation had been considered as part of a confining unit within the regional aquifer system. However, industry experience has shown that the production of natural gas from this interval is often accompanied by the production of significant quantities of water. This water is important both in terms of production economics and reservoir performance. Therefore, developing an understanding of the Fruitland Formation aquifer characteristics, and of its role within the regional hydrologic system will contribute to the successful development of this resource.

APPROACH

The approach to this study has been to compile and analyze all data appropriate to defining the hydraulic head distribution in the Fruitland Formation and utilize existing information to establish its general aquifer characteristics. Data collected to define the potentiometric surface of the Fruitland Formation includes water-level data around the basin periphery and drill-stem test (formation pressure) data in the basin interior. Information utilized to establish Fruitland Formation aquifer characteristics includes:

- regional structure and Fruitland interval stratigraphy
- porosity/permeability characteristics of coal
- existing aquifer/reservoir test results in the Fruitland interval
- regional and interval temperature distribution data

Emphasis in establishing Fruitland Formation aquifer characteristics will be on the discussion of coal stratigraphy and porosity/permeability, and on the analyses of temperature data to estimate lateral groundwater velocity.

PREVIOUS WORK

This study was aided by a large body of previous work in the San Juan Basin accomplished for a variety of different purposes. The references cited in this section represent only a small part of this existing work. However, they do include those studies that have been most useful in addressing subjects important in the defining and understanding of a Fruitland Formation aquifer, and of its role within the regional hydrodynamic system. Important regional geology studies include those by Silver (1951), Kelley (1950, 1951), and Sears et al. (1941). Important regional hydrogeologic information is found in Stone

et al. (1983), Berry (1959), Frenzel and Lyford (1982), Myers and Villanueva (1986), and Brimhall (1973). Fruitland Formation coal geology is best defined by the classical work of Fassett and Hinds (1971) with other important contributions by Fassett (1988). Important studies related to San Juan Basin coalbed methane and coalbed reservoir characteristics include Choate (1984), Kelso and Wicks (1988) and Meissner (1984). Finally, critical geothermal thermal investigations include Reiter and Mansure (1983), Reiter and Clarkson (1983), Clarkson and Reiter (1987).

REGIONAL SETTING

LOCATION OF THE STUDY AREA

The primary area considered in this study is in the north-central portion of the San Juan Basin, northwest New Mexico and southwest Colorado. Figure 1 (after Fassett, 1988) shows the geographic location of that part of the San Juan Basin encompassing the Fruitland Formation. In this figure the basin outline is based on the outcrop contact of the Fruitland Formation and the Pictured Cliffs Sandstone. The study area, highlighted on Figure 1, includes an area of approximately 1000 square miles in those townships between 29N and 32N (Colorado), and ranges between 5W and 10W.

GENERAL GEOLOGY

Structure

The San Juan Basin of this study is limited to the Central Basin as defined by Kelley (1951). This central Basin is a roughly circular area bounded by the steeply inward dipping Hogback monocline to the west, north and east, and by the gently inward dipping Chaco Slope to the south. The San Juan Mountain batholith is located just to the

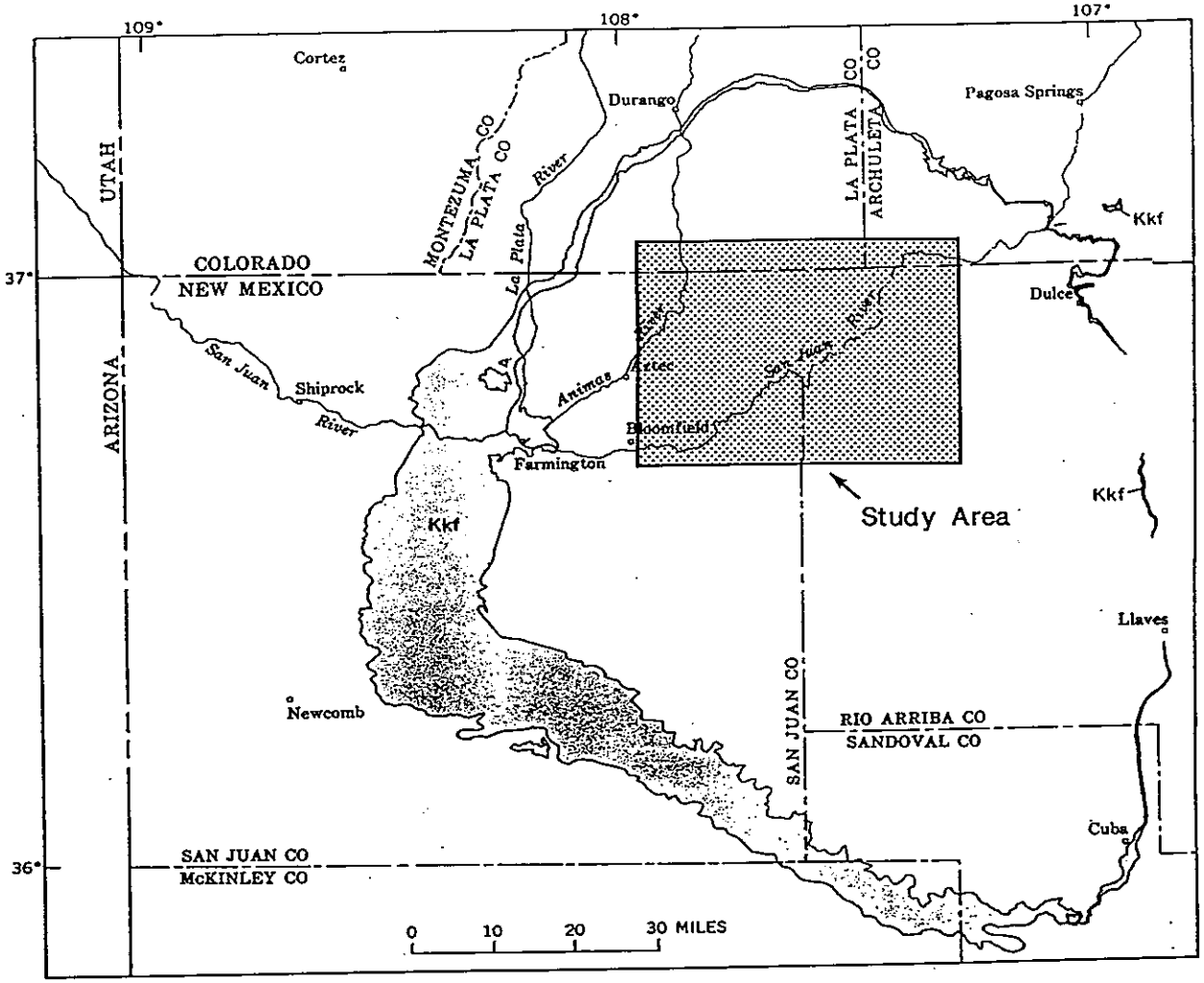

Figure 1 - Index map showing location of the study area within the San Juan Basin. Basin outline is the outcrop of the Fruitland Formation (after Fassett, 1988).

north of the basin. Figure 2 (Stone et al., 1983) shows the structural elements of the San Juan Basin.

Central basin structure is best defined by a structure contour map of the Huerfanito Bentonite Bed (Figure 3). This marker bed datum was defined by Fassett and Hinds (1971). Figure 3 shows that the basin synclinal axis approximately bisects the study area on a northwest-southeast trend. Figure 4 (modified from Kelso and Wicks, 1988) is a structure contour map of the top of the Pictured Cliffs Sandstone (base of the Fruitland Formation) in the north half of the basin. This map indicates Fruitland Formation structural dips in the study area south of the synclinal axis are less than 1 degree to the northeast, while dips north of the synclinal axis get only as high as 2 degrees to the southwest. These small structural dips indicate that within the study area strata are essentially horizontal. On a more local scale, small fold and faults may be present. But on the scale mapped these potential features are not evident.

Stratigraphy

Jurassic and Cretaceous sedimentary strata crop out in thin steeply dipping bands coincident with the Hogback monocline and in broader areas over the more gently dipping Chaco Slope region. Tertiary sedimentary rocks define the surficial geology of the Central Basin area. Figure 5 (Stone et al., 1983) is a schematic north-south stratigraphic cross-section summarizing geologic formation nomenclature (Triassic-Tertiary) in the San Juan Basin. The primary stratigraphic unit of interest in this study is the Upper Cretaceous Fruitland Formation. Other units that will be discussed relative to the Fruitland Formation will include the underlying Lewis Shale and

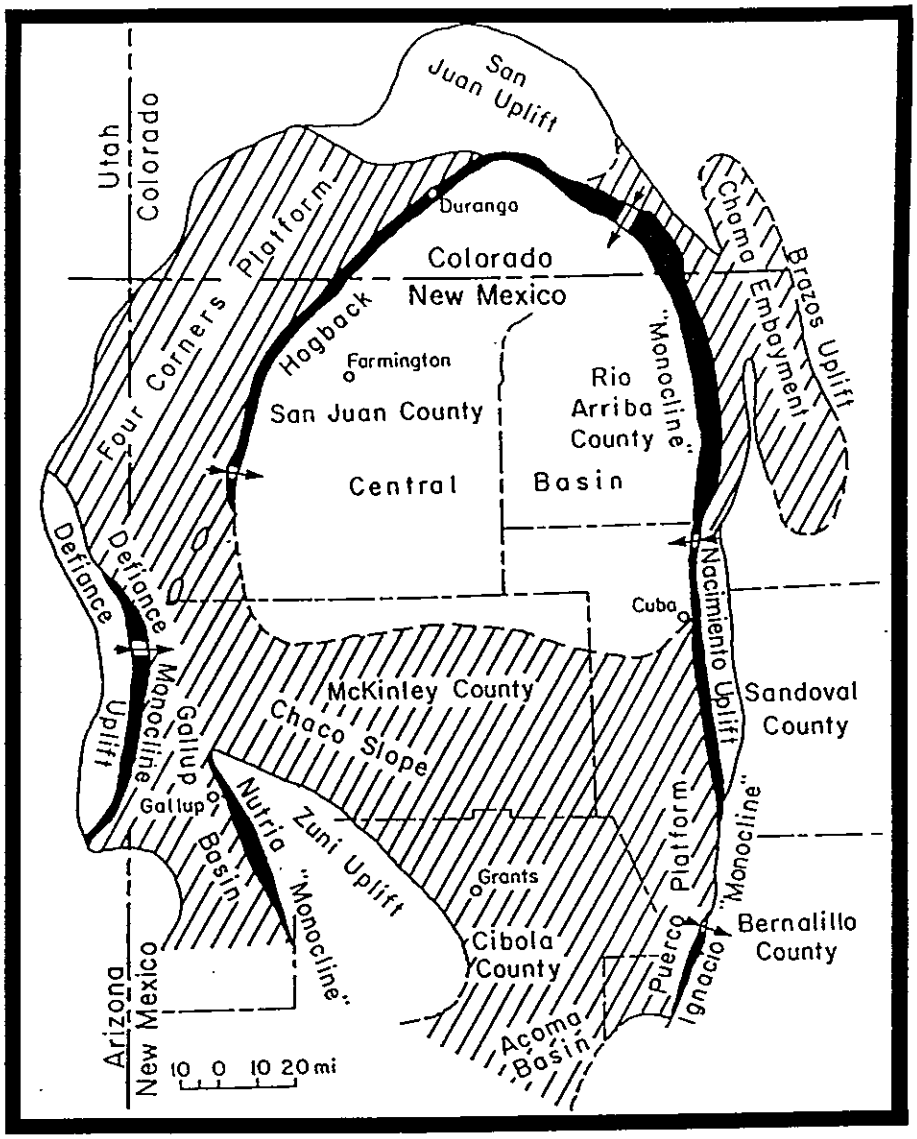

Figure 2 - Structural elements in the San Juan Basin (from Stone et al., 1983 [modified from Kelley, 1951]).

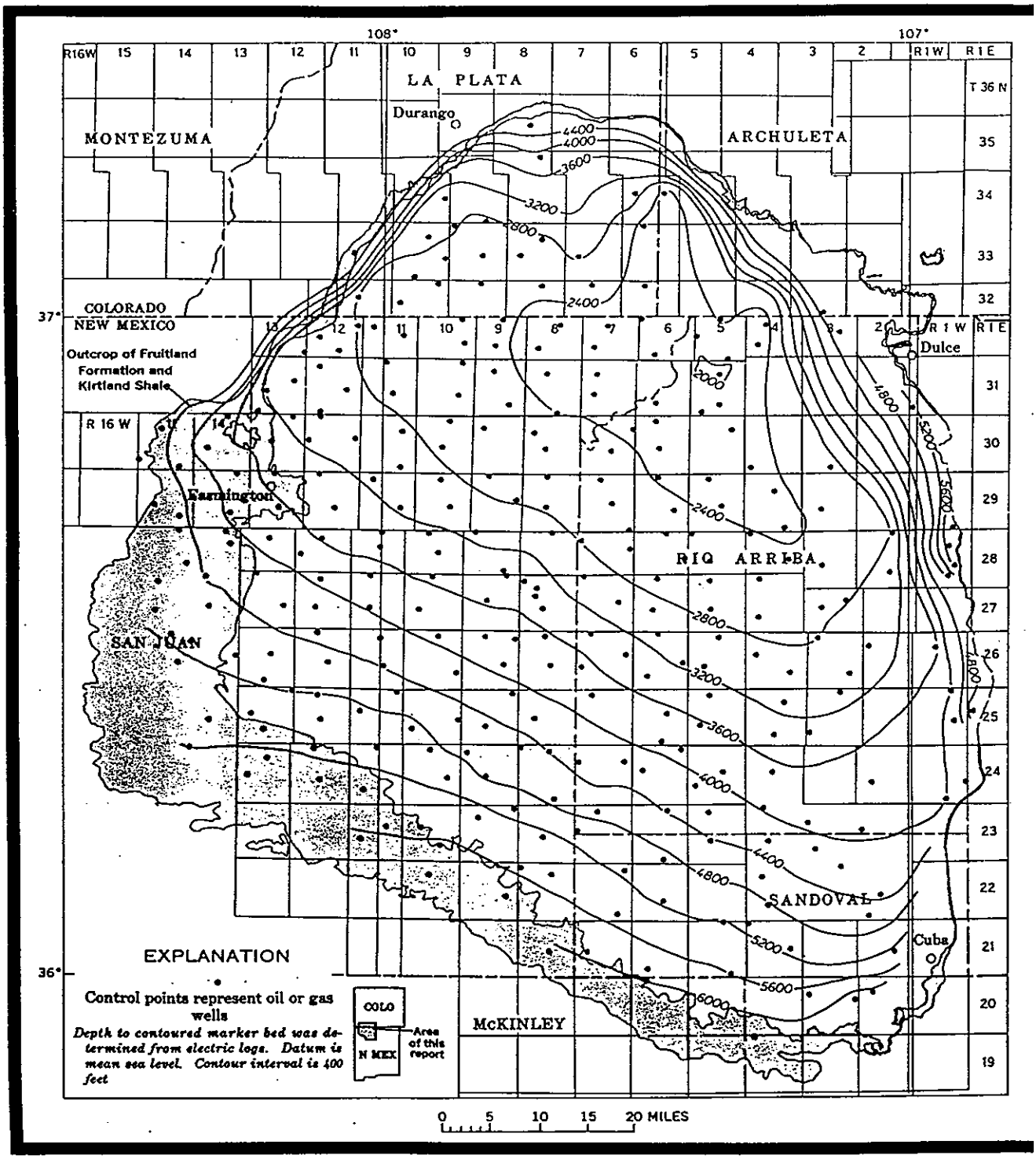

Figure 3 - Structure contour map of the Huerfanito Bentonite Bed of the Lewis Shale (from Fassett and Hinds, 1971).

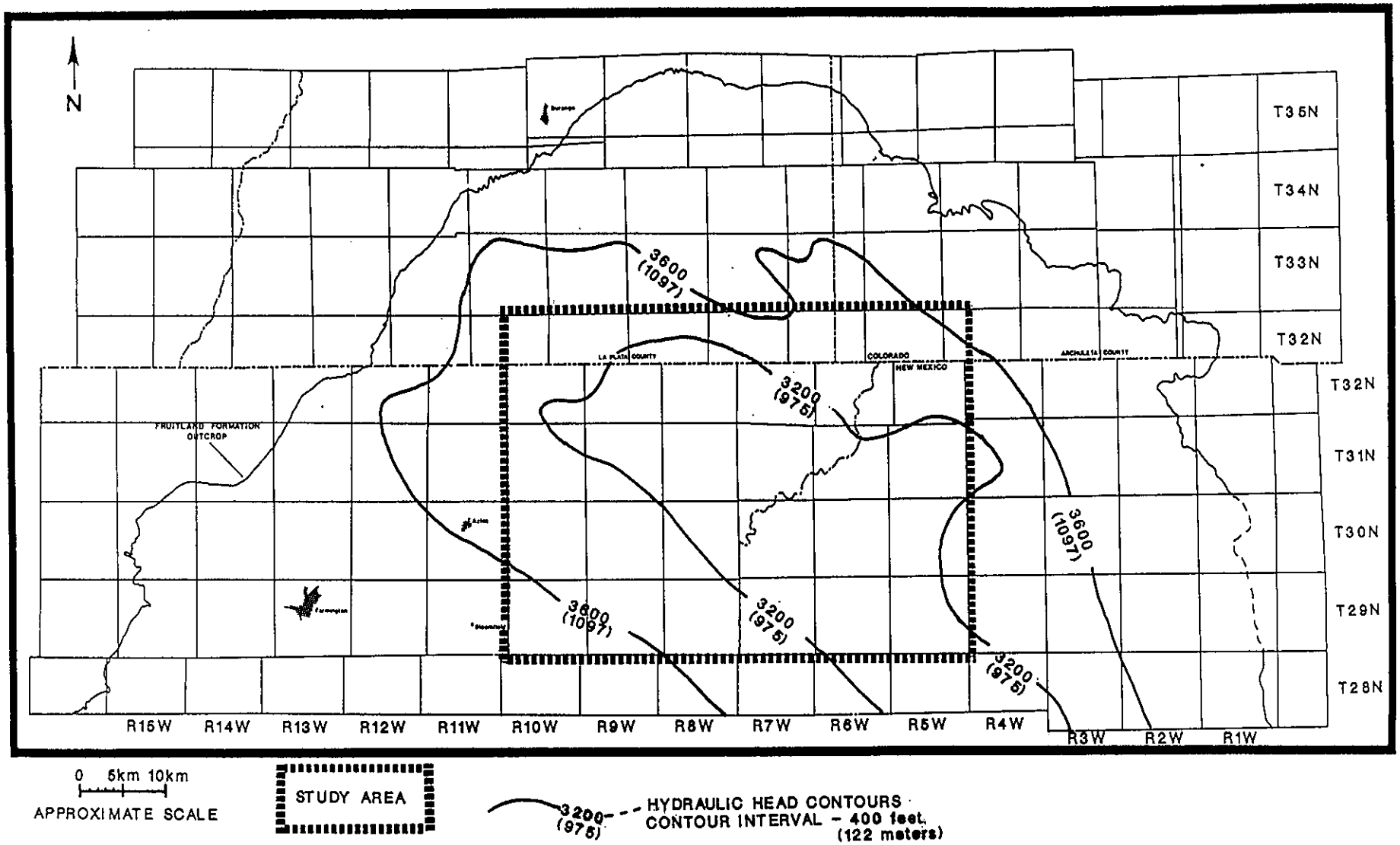

Figure 4 – Structure contour map of the Pictured Cliffs Sandstone (after Kelso and Wicks, 1988)

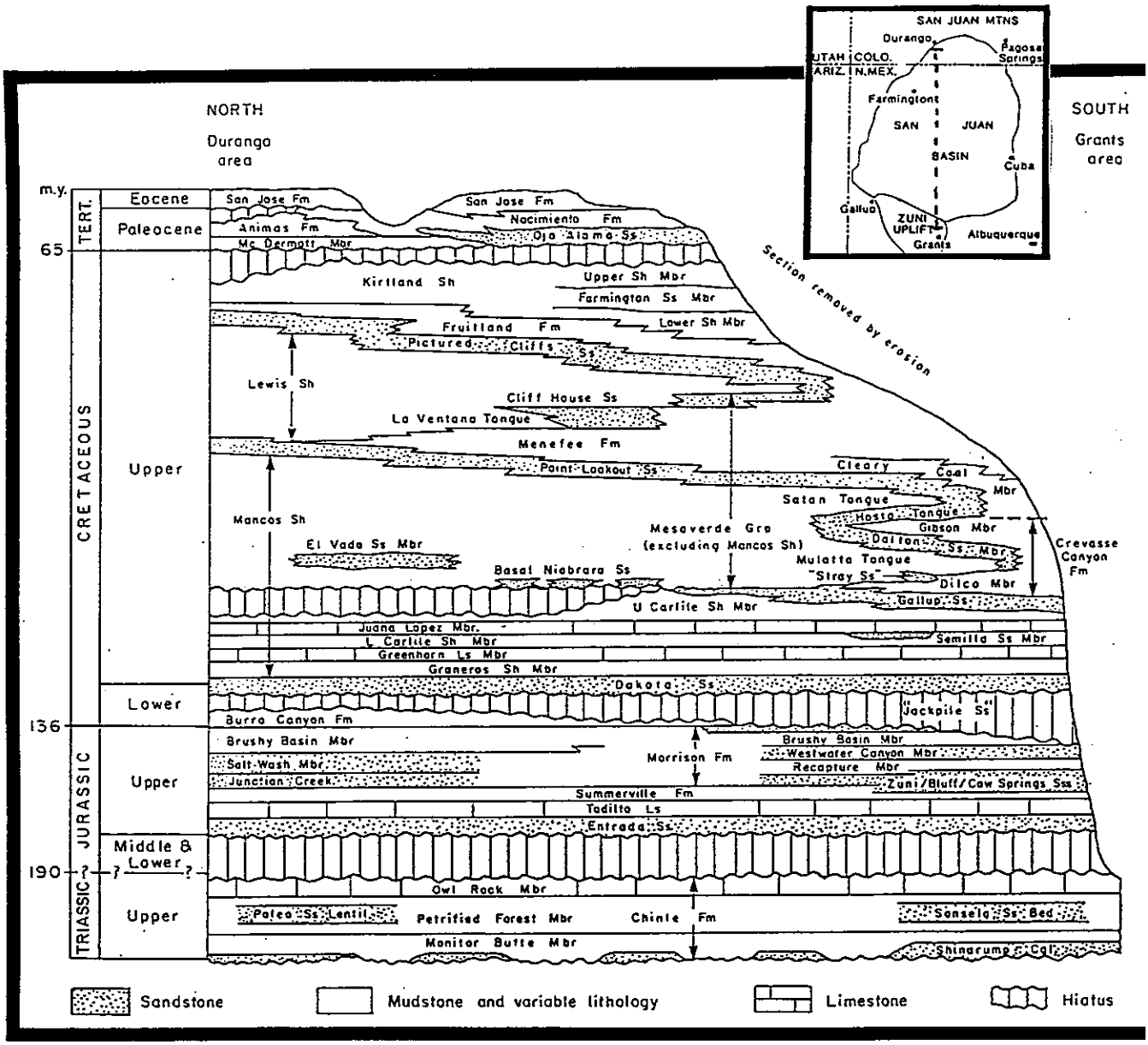

Figure 5 - North-south trending stratigraphic section showing the Triassic-Tertiary nomenclature of the San Juan Basin (from Stone et al., 1983).

Pictured Cliffs Sandstone, and the overlying Kirtland Shale and Ojo Alamo Sandstone.

The Fruitland Formation was deposited in continental fluvial and paludal environments (Fassett and Hinds, 1971) behind a northeastward regressing, northwest trending shoreline. The partially time-equivalent shoreline sandstones and marine shales, the Picture Cliffs Sandstone and Lewis Shale, were being deposited contemporareously to the northeast. Southwest from the Fruitland deltaic depositional setting, the fine-grain sediments of the Kirtland Shale were deposited in a low energy fluvial (upper alluvial plain) environment.

The Lewis Shale is a thick, relatively homogeneous, gray to black marine shale, containing scattered interbeds of sandstone, silty limestone, calcareous concretions, and bentonite (Fassett and Hinds, 1971). The approximate thickness of the Lewis Shale underlying the study area ranges from 450 to 600 meters. The important marker datum, the Huerfanito Bentonite Bed is found near the middle of this unit. Contact with the overlying Pictured Cliffs is conformable and gradational. This contact is arbitrarily placed to include predominantly sandstone in the Pictured Cliffs and predominantly shale in the Lewis (Fassett and Hinds, 1971).

The Pictured Cliffs Sandstone ranges in thickness from approximately 30 to 90 meters and is characterized by a general coarsening upward sequence (Meissner, 1984). The lowermost unit in this sequence consists of a shaley siltstone which is conformable and gradational with the underlying Lewis Shale. This unit grades upward into a thin-bedded fine-grained sandstone unit. The uppermost unit is a fine- to medium-grained, cross-laminated sandstone (Meissner, 1984). Regionally, the Pictured Cliffs Sandstone becomes younger and rises

stratigraphically northeastward across the basin. Figure 6 (from Fassett, 1988) are three northeast trending basin cross-sections showing the northeastward stratigraphic rise of the Pictured Cliffs. Porosity ranges from 15 to 20 percent and is generally best developed in the uppermost sandstone unit. Permeabilities for the Pictured Cliffs Sandstone tend to be low and highly variable. Published permeabilities range from .5 to 100 millidarcies with an average value of 5.45 millidarcies (Four Corners Geological Society, 1978). These low permeabilities are caused primarily by the precipitation of authigenic illite-smectite clay (Meissner, 1984). It has been hypothesized (Law et al., 1983; Meissner, 1984) that this clay infill is related to the highly reactive fluids expelled from the overlying Fruitland Formation coals during coal maturation. The Pictured Cliffs Sandstone underlies and locally intertongues with the Fruitland Formation throughout most of the basin. The contact between the Pictured Cliffs and the Fruitland Formation is taken as the top of the first well developed sandstone below the base of the lowermost Fruitland coal (Berry, 1959). In areas where local transgressions have resulted in an intertonguing relationship, a thin (10-20 m) Fruitland siltstone/coal interval is found 30-50 meters below this contact.

The Fruitland Formation ranges in thickness from approximately 37 to 127 meters and consists of interbedded shales, siltstones, fine-grained channel sandstones, and coal. Locally, thin limestone beds are found in the lower part of the formation (Fassett and Hinds, 1971; Meissner, 1984). In general, the different rock units are laterally discontinuous with individual beds pinching out usually within 100 meters (Fassett and Hinds, 1971). However, thick well developed

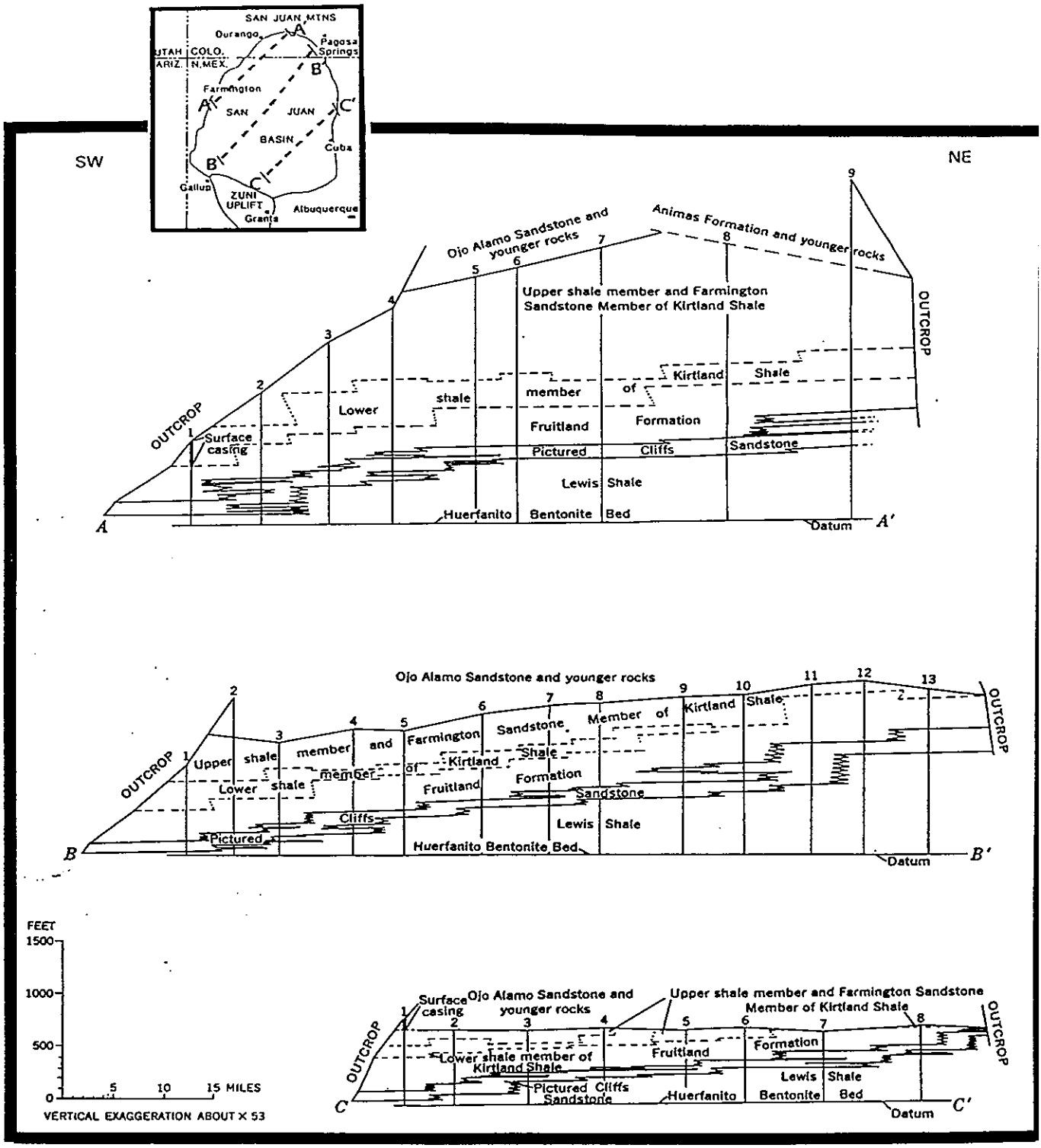

Figure 6 - Northeast trending stratigraphic cross-sections showing the northeastward stratigraphic rise of the Pictured Cliffs Sandstone (from Fassett, 1988).

coalbeds can be fairly continuous with individual beds extending for up to 40 km (Fassett, 1988).

Because of its complex and discontinuous lithologic nature, characterizations of Fruitland Formation porosity and permeability is problematic. Locally, sandstone units within the Fruitland have porosities ranging from 10 to 16 percent and permeabilities from .1 to 1 millidarcies (Four Corners Geological Society, 1978). Porosity and permeability for coals, the most laterally continuous formation units will be discussed later. The contact between the Fruitland and the overlying Kirtland is gradational and is generally placed at the top of the highest coal or carbonaceous shale bed in the section (Fassett and Hinds, 1971). However, this criterion is not universal in that thin carbonaceous shales and coals are locally present within the lower part of the Kirtland (Fassett, 1988). In the eastern third of the basin, the Fruitland is overlain unconformably by the Tertiary Ojo Alamo sandstone (Fassett, 1988). In this area, the Fruitland thins to the east and is truncated near the east side of the basin (Fassett, 1988).

The Kirtland Shale outcrops around the north, west, and south sides of the basin, and is missing in the eastern portion of the basin. As described by Fassett and Hinds (1971), the Kirtland Shale includes two units. The lower unit is predominantly grey shale containing a few thin interbeds of siltstone and sandstone. The upper unit includes the Farmington Sandstone member and an overlying shale. This unit is generally comprised of a series of interbedded sandstone lenses and shale. The shale interbeds in the Farmington Sandstone interval are lithologically similar to the lower unit shale. However, the shale interbeds near the top of the Kirtland tend to be varicolored. Thickness of the lower shale unit ranges from zero on the east side of

the basin to 140 meters in the western portion of the basin. Average thickness is 60-70 meters. Thickness of the upper unit ranges from zero the east side of the basin to approximately 460 meters in the northwestern portion of the basin (Fassett and Hinds, 1971). Like the Fruitland Formation, characterization of the porosity and permeability of the Kirtland Shale is problematic. Locally, sandstone lenses in the Farmington Sandstone portion of the upper unit have produced oil and gas. However, there is no extensive and systematic porosity/ permeability development in the Kirtland Shale. Therefore, on both a regional and local basis, this unit should be considered as a very low permeability interval.

The Paleocene Ojo Alamo Sandstone overlies the Kirtland Shale within the study area. The nature of this contact is generally thought to be unconformable, but varying interpretations (Dane, 1936; Baltz, 1967; Fassett and Hinds, 1971), call into question the proper relationship. The Ojo Alamo is composed of interbedded sandstone, conglomeratic sandstone, and shale. Thickness of this unit generally ranges between 15 and 30 meters (Fassett and Hinds, 1971). Individual sandstone beds can be laterally continuous.

GENERAL HYDROGEOLOGY

An overview of the regional hydrogeology of the San Juan Basin was presented by Stone et al. (1983). The following brief summary of the general hydrogeology is taken primarily from this work.

Aquifer Units

In general, San Juan Basin aquifer units are artesian (that is, they rise above the upper confining surface). Confining intervals include the low permeability marine shales. However, confinement is

not complete and vertical leakage does occur at very low rates (10^{-8} - 10^{-11} cm/sec). Major sandstone aquifers have transmissivities between 1.07 - 2.15 cm^2/sec (100 and 200 ft^2/day) over large areas. These major aquifers include the Ojo Alamo Sandstone, Gallup Sandstone, Morrison Formation and Entrada Sandstone. Other minor aquifers produce locally, generally in the range of 10 gallons per minute, and include valley-fill alluvium, the Tertiary San Jose and Nacimiento Formations and Cretaceous sandstones of the Mesa Verde Group and the Dakota Sandstone. Figure 7 (Stone et al., 1983) shows a schematic hydrogeologic cross-section of the San Juan Basin. On this cross-section the Fruitland/Pictured Cliffs interval is depicted as being part of the Lewis to Kirtland confining interval. Head potential across this interval is shown as downward from the overlying units and upward from the underlying units. Figures 8 and 9 show the estimated potentiometric surfaces for the Ojo Alamo sandstone (after Stone et al., 1983; Tansey, 1984) and the Mesa Verde Group (Cliff House Sandstone) (after Berry, 1959) in the vicinity of the study area.

Regional Flow

Regional groundwater flow is generally from the topographically high outcrop areas around the periphery of the basin toward the topographically low alluvial valleys. The San Juan River Valley west of the study area is thought to be a major discharge area. Basin-wide steady-state inflow/outflow rates are estimated to be 5.66 x 10^5 cm^3/sec (20 ft^3/sec) for Tertiary aquifers and 11.33 x 10^5 cm^3/sec (40 ft^3/sec) for the Cretaceous and Jurassic aquifers (Stone et al., 1983).

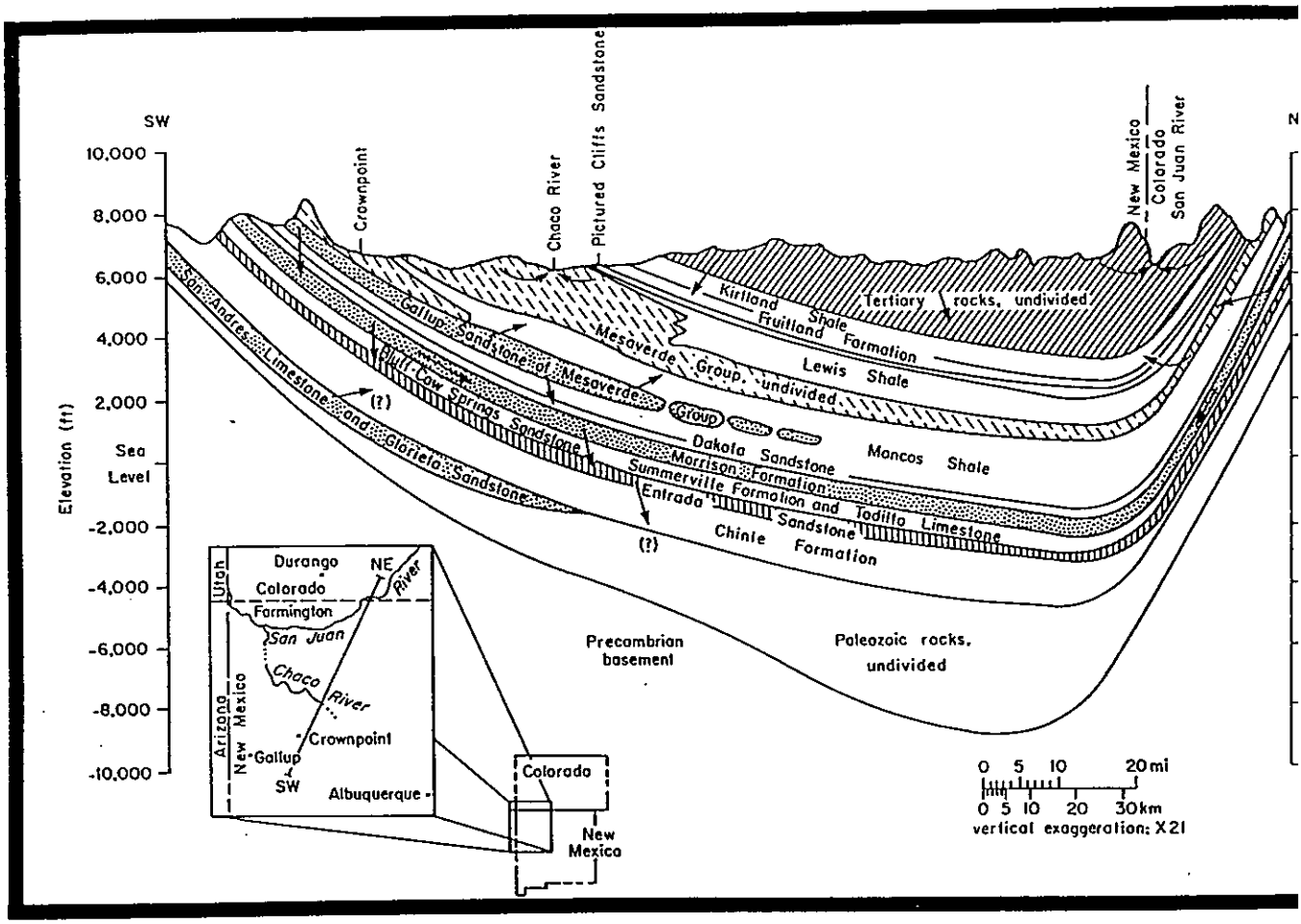

Figure 7 - Generalized hydrogeologic cross-section. Major aquifers are highlighted. Confining units are blank. Directions of flow are indicated (from Stone et al., 1983).

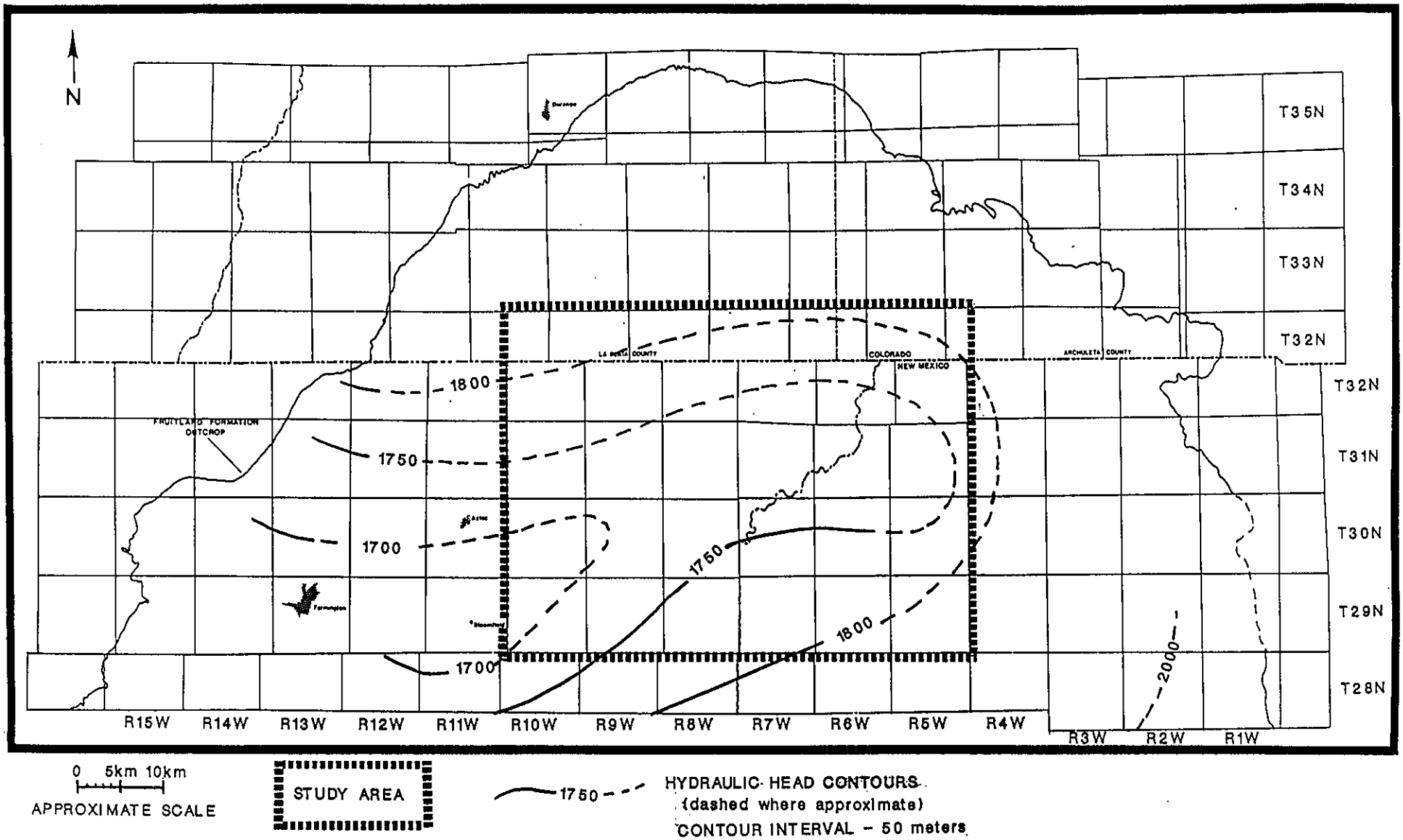

Figure 8 - Estimated potentiometric surface of the Ojo Alamo Sandstone (after Stone, et al 1983 and Tansey, 1984)

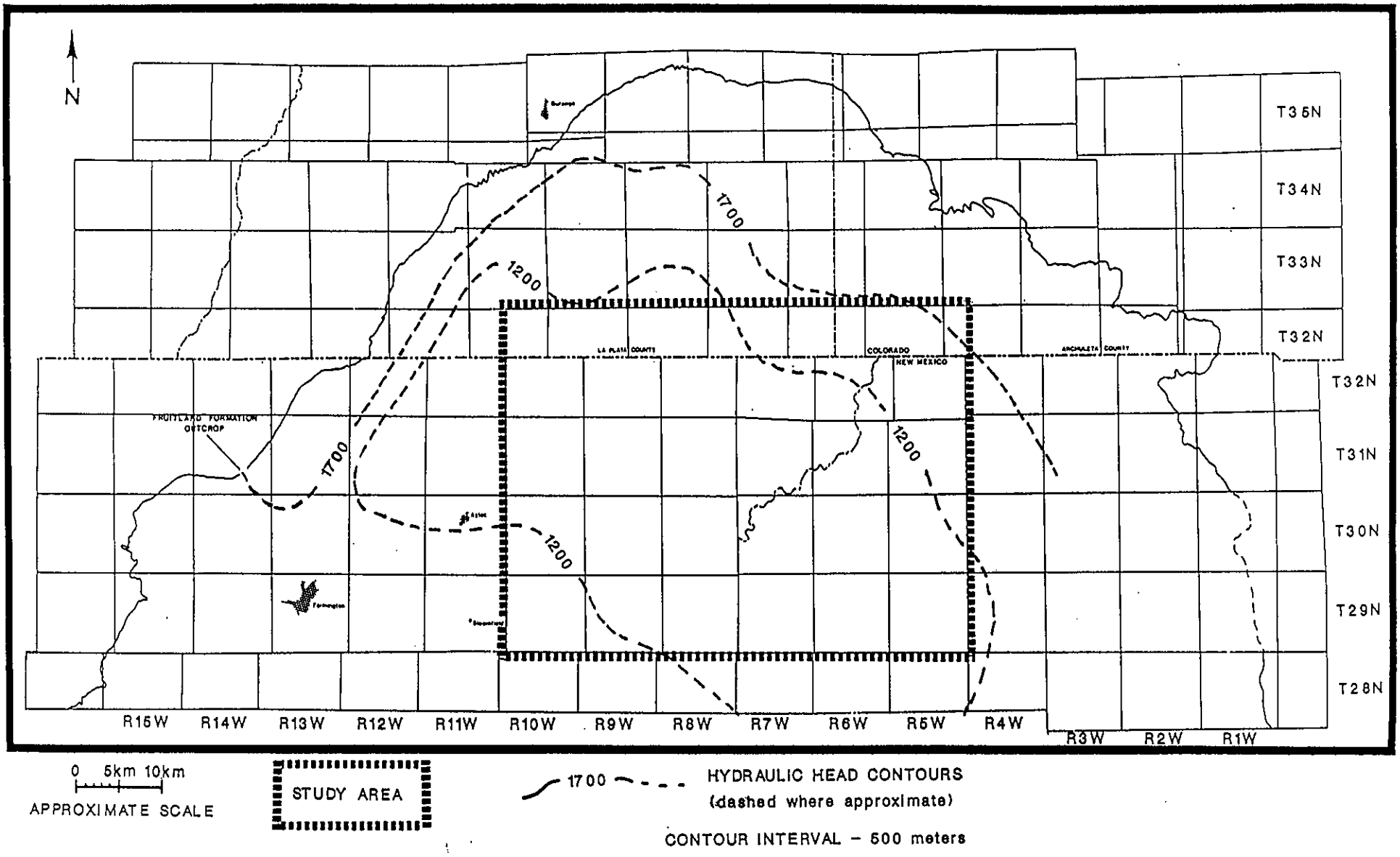

Figure 9 – Estimated potentiometric surface of the Mesa Verde Group Cliff House Sandstone (after Berry,1951)

HEAT FLOW

Geothermal and heat-flow investigations were carried out in the late 1970's. Significant studies related to these investigations include Reiter and Mansure (1983), Reiter and Clarkson (1983), and Clarkson and Reiter (1987).

Figure 10 (modified from Clarkson and Reiter, 1987) shows heat-flow data in the northern San Juan Basin area. Heat flow data in the San Juan volcanic field indicates a mean regional conductive heat flow in this area of 127 mWm^{-2}. Heat flow data south of the central basin area on the Chaco Slope location indicates a mean regional conductive heat flow of 67 mWm^{-2}. Generally, the temperature gradients obtained in the Lewis or Mancos Shales were used in heat flow calculations. These units were selected because they were generally more homogeneous (less variability in thermal conductivity) and less permeable (less perturbation due to groundwater advection). These characteristics were felt to contribute to giving the best representative conductive heat flow at each location. Review of Figure 10 shows a trend of increasing heat-flow north from the Chaco Slope toward the San Juan Mountain volcanic field. To explain this trend, Reiter and Clarkson (1983a) developed steady-state heat-flow models which suggest a deep replenishing heat source underlying the northern San Juan Basin and San Juan volcanic field. Figures 11a and 11b (Reiter and Mansure, 1983) are subsurface temperature profiles running east-west (a) and north-south (b) across the basin. Figure 11a indicates that within the central part of the basin there is very little lateral temperature variation in the east-west direction below an elevation of 1200 meters. However, Figure 11b indicates that there is a north-south lateral

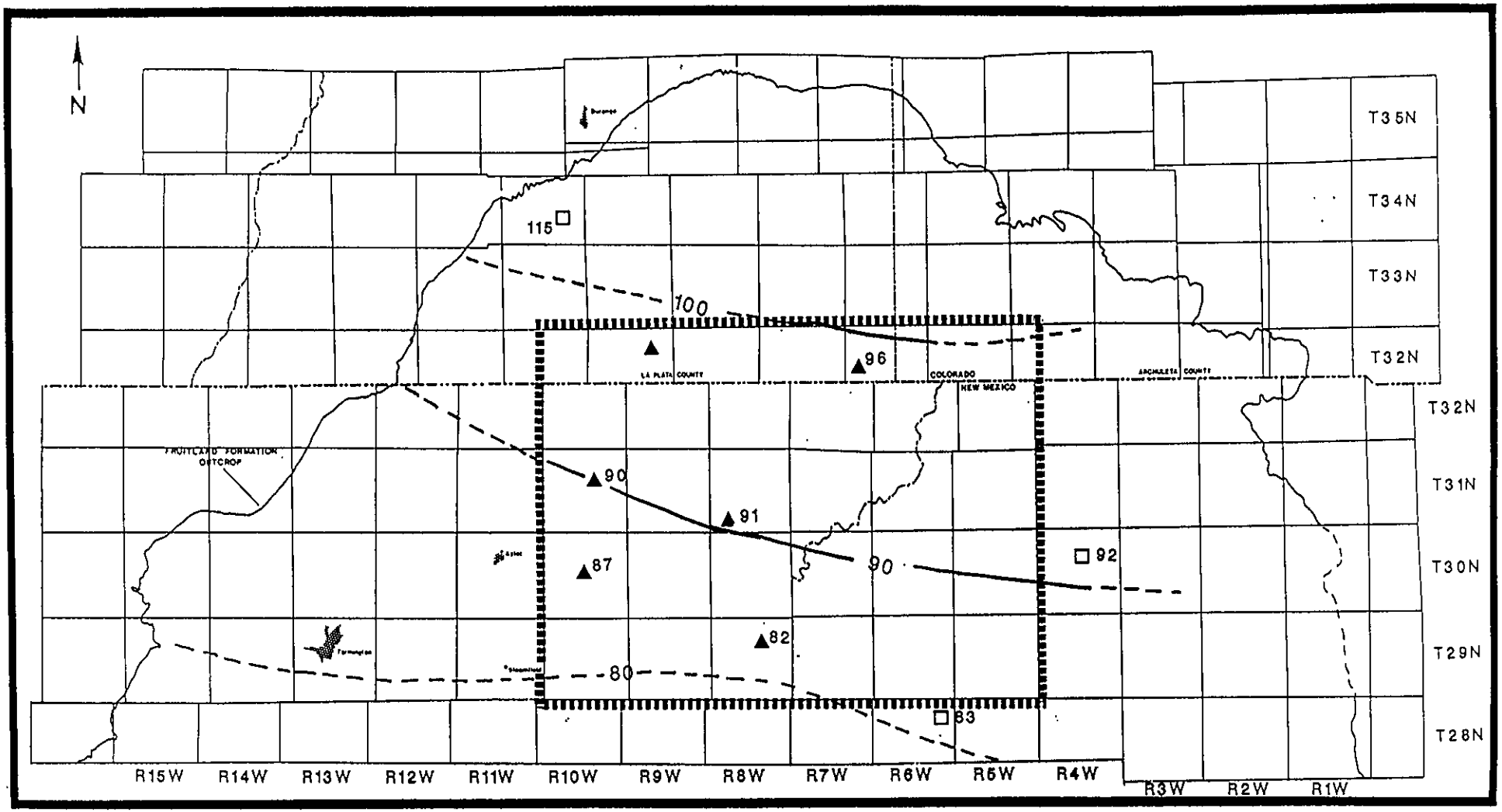

Figure 10. Conductive heat flow contours (after Reiter and Mansure, 1983).

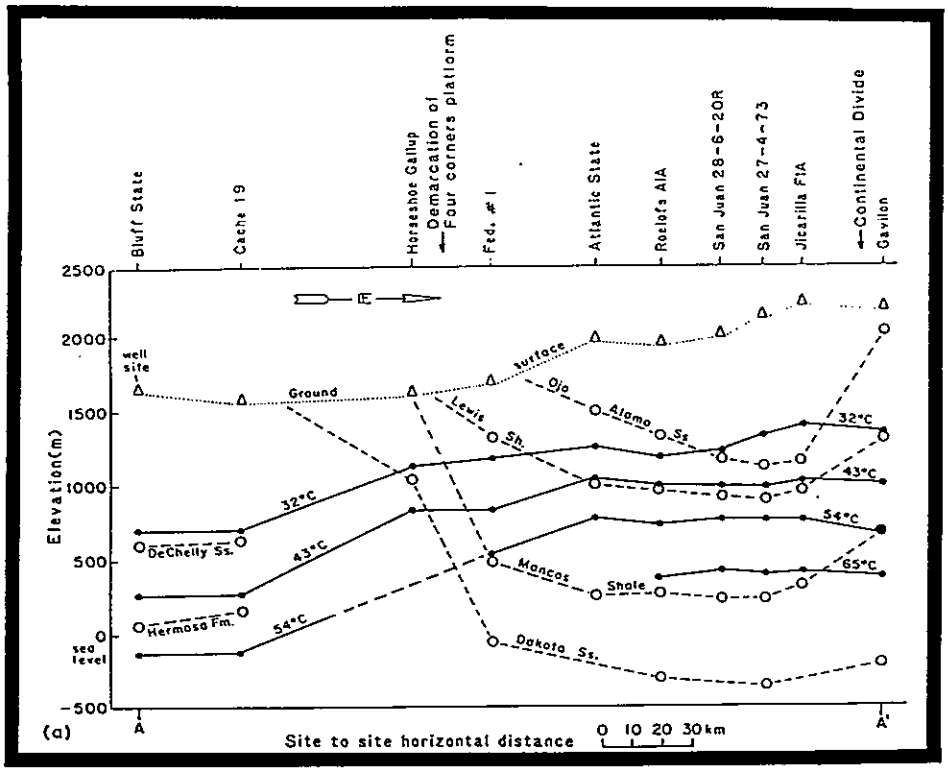

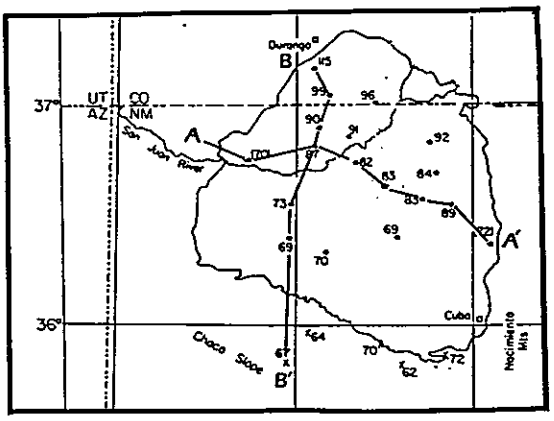

Index Map

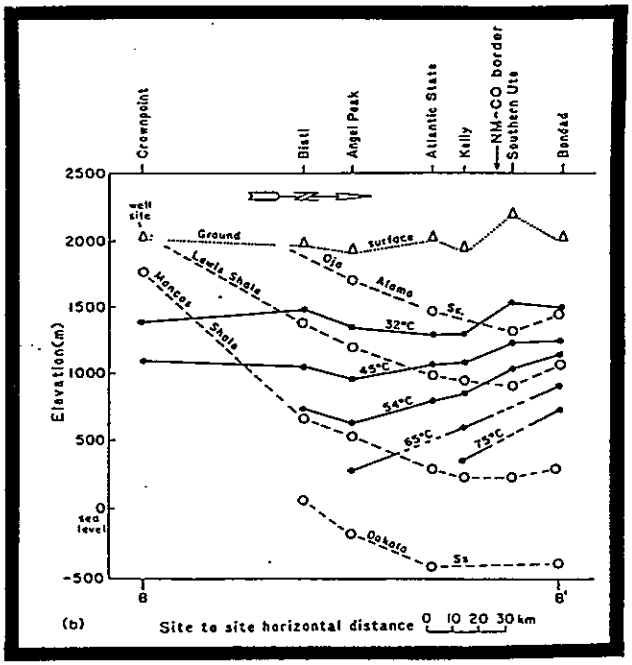

Figure 11 - Subsurface temperature profiles
a. East-west
b. North-south
(from Reiter and Mansure, 1983
and Clarkson and Reiter, 1987).

temperature gradient of between 1.9×10^{-4} to 2.7×10^{-4} °C/m at an elevation of 1000 to 1200 meters.

HEAT TRANSPORT AND FLUID FLOW IN POROUS MEDIA

Temperature distributions within the earth are primarily the result of a local/regional geothermal regime. This local/regional geothermal regime contributes a characteristic, uniform, conductive heat flow for a given area. However, perturbations to the uniform heat flow are apparent in the shallow subsurface (0 to 2000 m). One of the mechanisms that contributes to these geothermal anomalies is groundwater flow. In this section basic principals and parameters related to terrestrial heat flow are summarized. In addition, the utility of temperature data to hydrologic analyses is discussed in detail.

GENERAL GEOTHERMICS

The following discussion is based on information from two sources. These are:

> Geothermics with Special Reference to Applications (1974) by O. Kappelmeyer and R. Haenel
>
> Geothermics (1976) by J. Goguel (translated by A. Rite and edited by S.J. Weinberg).

Geothermics is the study of temperature distributions and terrestrial heat flows within the earth. Fundamentally this area of study is concerned with heat transfer from the earth's interior to its surface primarily through the mechanism of heat conduction.

Terrestrial Heat Flow

Terrestrial heat conduction can be expressed with the following equation:

$$\vec{q}_H = K_T \text{ grad } T \tag{1}$$

$\vec{q}_H$ = heat flow vector

K_T = isotropic, homogeneous thermal conductivity for rock unit

T = temperature

In geothermics, the following assumptions are generally made.

1. Heat conduction is essentially vertical and at steady state.
2. Thermal conductivity is isotropic and homogeneous.

Therefore terrestrial heat flow, $\vec{q}_H$, can be defined as:

$$\vec{q}_H = K_T \frac{\partial T}{\partial z} \tag{2}$$

which is the product of thermal conductivity of rock and the vertical temperature gradient.

Thermal Conductivity

Thermal conductivity is a fundamental thermal property of rocks. This property is defined by Fourier's Law which states that for a given heat flow, the thermal conductivity of a material is inversely proportional to the temperature gradient through that material. Figure 12 (Kappelmeyer and Haenel, 1974) shows the thermal conductivity for a variety of geologic materials. In a system of horizontal layers of different rock types, the effective vertical thermal conductivity for the system can be calculated by the harmonic mean of the individual thermal conductivities. That is

$$K_{T\ (\text{effective})} = \frac{\Sigma\, b_i}{\Sigma \frac{K_i}{b_i}} \tag{3}$$

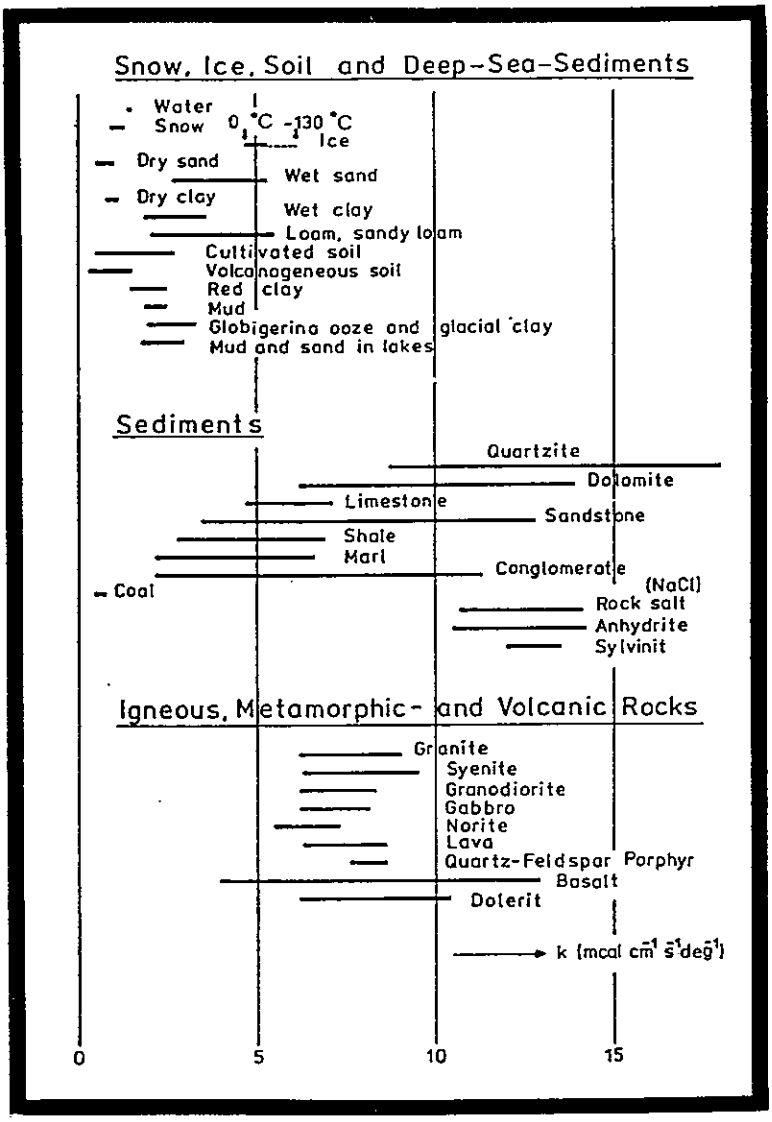

Figure 12 - Thermal conductivity for different type rocks (from Kappelmeyer and Haenel, 1974).

b_i = thickness of layer i

K_i = thermal conductivity of material in layer

Measuring Thermal Conductivity

The principal method of measuring thermal conductivity involves putting a known quantity of heat into a sample and measuring the resulting steady state temperature gradient across the sample. Rearranging equation 2 yields:

$$K_T = q_H/(\Delta T/\Delta z) \tag{4}$$

To calculate K_T for a given sample, q_H and $\Delta T/\Delta z$ must be determined.

The typical laboratory technique to establish the necessary data uses some modification of a divided bar apparatus. Normally, this apparatus consists of an insulated heating element designed to direct heat output vertically through a radially insulated sample disk into a constant temperature sink. Using an apparatus of this type, q_H is calculated by determining the power output of the heating element and dividing by the surface area of the sample. Thermocouples are used to determine the temperature difference (ΔT) across the sample. Finally the thickness of the sample disk is measured. This data is then used to calculate K_T. Sample disks are either cut from whole rock cores or are fashioned from rock chips embedded in a matrix of known thermal conductivity. For sample disks of both types, a correction to account for fluid filled porosity is required. In addition, for the composite sample disk containing rock chips, a correction for chip orientation or aspect anisotropy is required.

Temperature Gradient

The temperature gradient in the subsurface is primarily determined by the local terrestrial heat flow and the thermal conductivity of the strata.

The temperature gradient in a region can be determined through the analyses of mine and well-bore bottom hole temperatures, or measured in a well-bore by using either discontinuous or continuous temperature logs. In a single well-bore, a temperature log through strata with markedly different thermal conductivities will show different temperature gradients. Figure 13 (after Kappelmeyer and Haenel, 1973) is a schematic representation of the changes in temperature gradient corresponding to changes in strata thermal conductivity. Review of this figure indicates that strata with high thermal conductivity will show a relatively low temperature gradient and that temperature gradients will increase with a decrease in rock thermal conductivity.

APPLICATIONS OF TEMPERATURE DATA TO HYDROLOGIC ANALYSES

In addition to heat conduction, fluid convection can also contribute to subsurface heat transfer. Fluid convection can be of two types: natural convection and advection. Natural convection is caused by large temperature differences within a fluid body which result in density differences. These temperature/density contrasts result in a local convective cell where heat is transported from the bottom to the top of the cell. Natural convection is not important in this study, and will not be described in any further detail.

Advective fluid movement results from pressure or head differences within and/or between water-bearing strata. Advective fluid movement will redistribute heat in the direction of flow and may result in

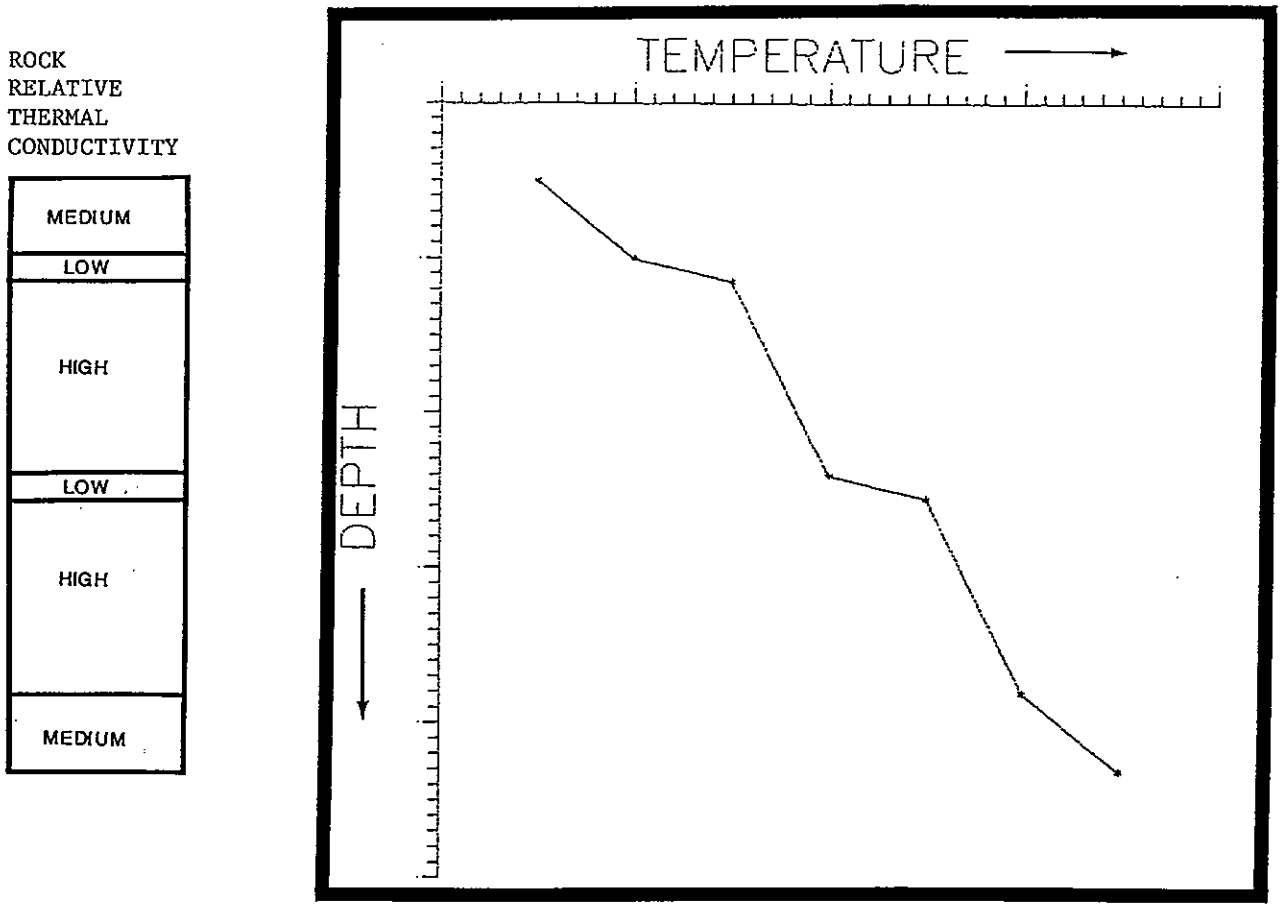

Figure 13 - Schematic representation of temperature gradients through rock units of differing thermal conductivities.

anomalous temperature gradients. Therefore, analysis of temperature data can aid in understanding groundwater flow characteristics.

General Analytical Approach

The general analytical approach that couples conductive and advective heat transfer was fully developed by R.W. Stallman (1963). His purpose in this landmark paper was to "call attention to the possibility of utilizing measurements of the distribution of underground temperatures as an indirect manifestation of groundwater velocity." The following discussion is a detailed review of this paper.

Heat transfer in a saturated, permeable material results from the combination of heat conduction and groundwater advection. These simultaneous processes result in temperature and head distributions which can be described by differential equations. Figure 14 (after Stallman, 1963) represents a control volume of saturated, permeable material and is used to develop these differential equations. This control volume is assumed to be homogeneous, isotropic and saturated. In addition, temperature gradients are assumed to be linear through the control volume.

To define the temperature gradient in one direction (i.e., the x-direction) let the temperature at the center of the control volume be T. Then the temperatures at Faces 1 and 2 (y-z plane) is:

$$T_1 = T - \frac{1}{2} \frac{\partial T}{\partial x} dx \qquad (5)$$

$$T_2 = T + \frac{1}{2} \frac{\partial T}{\partial x} dx \qquad (6)$$

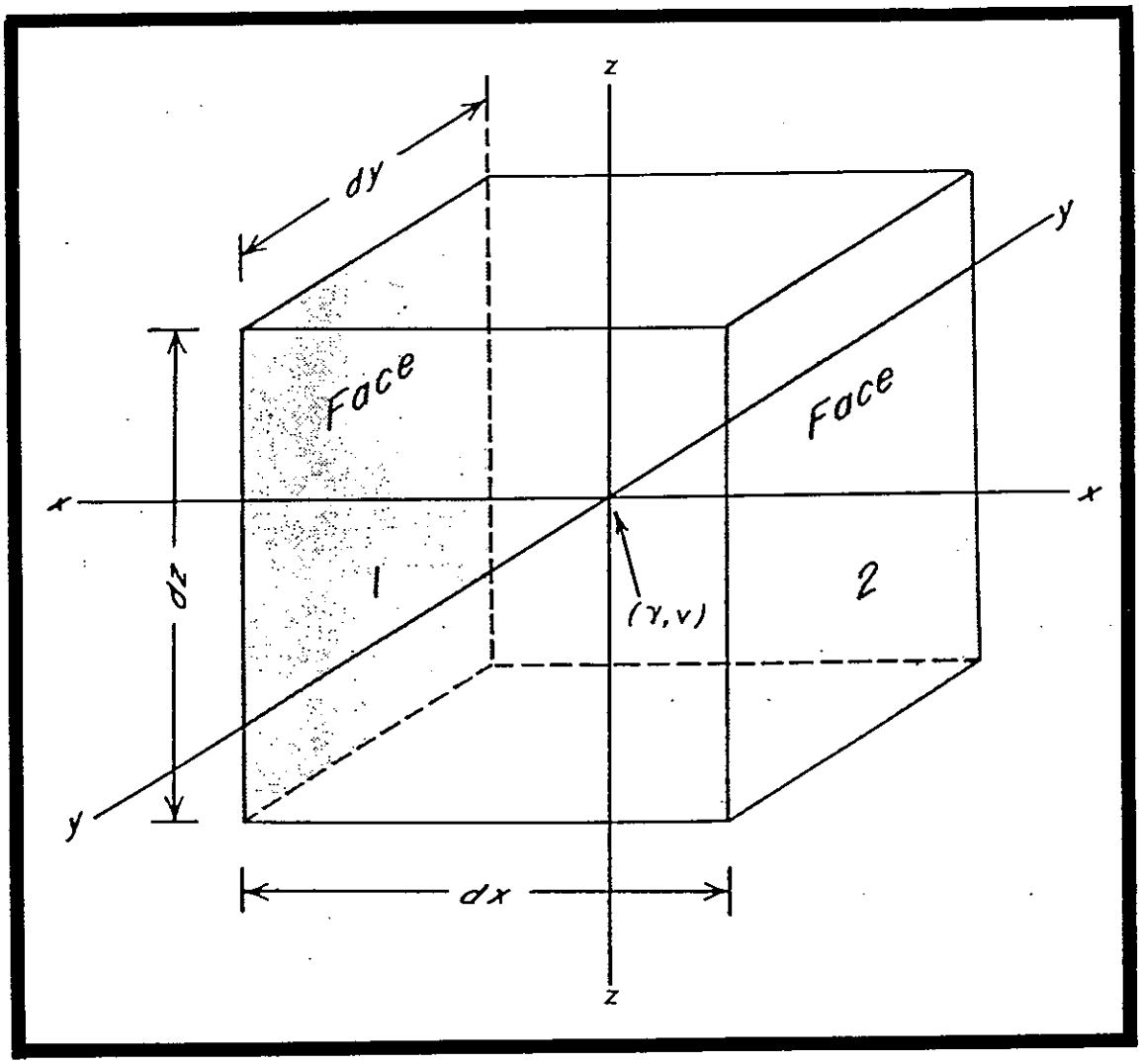

Figure 14 - Schematic diagram of control volume used in the development of the combined fluid and heat transport equation (from Stallman, 1960).

T_1 = temperature at face 1

T_2 = temperature at face 2

From the law of heat conduction, heat flow through these two control volume faces is:

$$q_{C1} = - K_T \frac{\partial T_1}{\partial x} \, dydz \tag{7}$$

$$q_{C2} = - K_T \frac{\partial T_2}{\partial x} \, dydz \tag{8}$$

q_{C1} = conductive heat flow through Face 1

q_{C2} = conductive heat flow through Face 2

K_T = thermal conductivity of the saturated control volume material

Combining these equations with equations 5 and 6 yields:

$$q_{C1} = - K_T \left(\frac{\partial T}{\partial x} - \frac{1}{2} \frac{\partial^2 T}{\partial x^2} \, dx \right) dydz \tag{9}$$

$$q_{C2} = - K_T \left(\frac{\partial T}{\partial x} + \frac{1}{2} \frac{\partial^2 T}{\partial x^2} \, dx \right) dydz \tag{10}$$

The difference between q_{C1} and q_{C2} is the net rate at which heat is added to the control volume by conduction and is equal to:

$$q_{C1} - q_{C2} = K_T \frac{\partial^2 T}{\partial x^2} \, dxdydz \tag{11}$$

Similar equations can be developed to determine the net rate at which heat is added to the control volume by conduction in the y- and z-directions. Combining these equations defines the total rate, q_C, of heat addition to the control volume by conduction where:

$$q_C = K_T \left[\frac{\partial^2 T}{\partial x^2} + \frac{\partial^2 T}{\partial y^2} + \frac{\partial^2 T}{\partial z^2}\right] dxdydz \qquad (12)$$

Specific discharge of water through the same control volume is described by Darcy's Law. In the x-direction:

$$V_x = - K \frac{\partial h}{\partial \ell} \qquad (13)$$

V_x = specific discharge in the x-direction

K = hydraulic conductivity of the material in the control volume

h = head (potential) above reference plane

ℓ = length of the flow path through the control volume.

In the control volume the specific discharges at Faces 1 and 2 in the x-direction are:

$$V_1 = V_x - \frac{1}{2} \frac{\partial V_x}{\partial x} dx \qquad (14)$$

$$V_2 = V_x + \frac{1}{2} \frac{\partial V_x}{\partial x} dx \qquad (15)$$

The rate at which heat is advected into the control volume through Face 1, q_{a1}, is the product of the specific discharge (V_1), the temperature at the boundary and the heat capacity of the fluid.

$$q_{a1} = ([c\rho]\ V_1 T_1)\ dydz \qquad (16)$$

$c\rho$ = heat capacity of the fluid where,

c = specific heat of the fluid

ρ = density of the fluid

Substituting equations 14 and 15 into equation 16 gives:

$$q_{a1} = [c\rho]\left[\left(V_x - \frac{1}{2}\frac{\partial V_x}{\partial x}\,dx\right)\left(T - \frac{1}{2}\frac{\partial T}{\partial x}\,dx\right)\,dydz\right]$$

$$= [c\rho]\left[V_xT - \frac{1}{2}V_x\frac{\partial T}{\partial x}\,dx - \frac{1}{2}T\frac{\partial V_x}{\partial x}\,dx + \frac{1}{4}\frac{\partial V_x}{\partial x}\frac{\partial T}{\partial x}\,(dx)^2\right]\,dydz \quad (17)$$

Assuming no change in fluid density within the control volume, the rate at which fluid is advected out through Face 2 is:

$$q_{a2} = [c\rho]\left[V_xT + \frac{1}{2}V_x\frac{\partial T}{\partial x}\,dx + \frac{1}{2}T\frac{\partial V_x}{\partial x}\,dx + \frac{1}{4}\frac{\partial V_x}{\partial x}\frac{\partial T}{\partial x}\,(dx)^2\right]\,dydz \quad (18)$$

The difference between q_{a1} and q_{a2} is the net rate at which heat is added to the control volume due to advection and is equal to:

$$q_{a1} - q_{a2} = -[c\rho]\frac{\partial(V_xT)}{\partial x}\,dxdydz \quad (19)$$

Similar equations can be developed to determine the net rate at which heat is added to the control volume by advection in the y- and z-directions. Combining these equations defines the total rate, q_a, of heat addition to the control volume by advection where:

$$q_a = -[c\rho]\left[\frac{\partial(V_xT)}{\partial x} + \frac{\partial(V_yT)}{\partial y} + \frac{\partial(V_zT)}{\partial z}\right]\,dxdydz \quad (20)$$

The total addition of heat to the control volume by both conduction and advection is $q_c + q_a$. Assuming that heat is neither generated nor consumed within the control volume, and that, in the absence of net heat change within the control volume, that the temperature will decay with time the resulting equation completely describing the temperature within the control volume is:

$$q_c + q_a = c_{ws}\rho_{ws} \frac{\partial T}{\partial t} \, dxdydz \tag{21}$$

c_{ws} = specific heat of the saturated material

ρ_{ws} = the density of the saturated material

t = time

Substituting equations 12 and 20 and rearranging terms gives the most general differential equation describing heat transfer within the control volume.

$$\frac{\partial^2 T}{\partial x^2} + \frac{\partial^2 T}{\partial y^2} + \frac{\partial^2 T}{\partial z^2} = \frac{c\rho}{K_T} \left[\frac{\partial (V_x T)}{\partial x} + \frac{\partial (V_y T)}{\partial y} + \frac{\partial (V_z T)}{\partial z} \right] + \frac{c_{ws}\rho_{ws}}{K_T} \frac{\partial T}{\partial t} \tag{22}$$

Expanding the bracketed part of the first term on the right hand side of equation 22 results in:

$$V_x \frac{\partial T}{\partial x} + V_y \frac{\partial T}{\partial y} + V_z \frac{\partial T}{\partial z} + T \left(\frac{\partial V_x}{\partial x} + \frac{\partial V_y}{\partial y} + \frac{\partial V_z}{\partial z} \right) \tag{23}$$

From the continuity equation:

$$\frac{\partial V_x}{\partial x} + \frac{\partial V_y}{\partial y} + \frac{\partial V_z}{\partial z} = - S \frac{\partial h}{\partial t} \tag{24}$$

S = storage coefficient of the saturated, permeable material

Assuming steady-state fluid flow:

$$- S \frac{\partial h}{\partial t} = 0 \tag{25}$$

This reduces equation 23 to:

$$V_x \frac{\partial T}{\partial x} + V_y \frac{\partial T}{\partial y} + V_z \frac{\partial T}{\partial z} \qquad (26)$$

Substituting equation 26 back into equation 22 gives:

$$\frac{\partial^2 T}{\partial x^2} + \frac{\partial^2 T}{\partial y^2} + \frac{\partial^2 T}{\partial z^2} = \frac{[c\rho]}{K_T}\left(V_x \frac{\partial T}{\partial x} + V_y \frac{\partial T}{\partial y} + V_z \frac{\partial T}{\partial z}\right) + \frac{c_{ws}\rho_{ws}}{K_T} \frac{\partial T}{\partial t} \qquad (27)$$

Or in vector notation:

$$\nabla^2 T = \frac{[c\rho]}{K_T} [\vec{V} \cdot \nabla T] + \frac{c_{ws}\rho_{ws}}{K_T} \frac{\partial T}{\partial t}$$

Using this equation together with various simplifying assumptions, Stallman showed that, given the proper temperature and head distribution data set, groundwater velocity (specific discharge) can be calculated.

Subsequent to Stallman's development of the general analytical approach to coupled heat and fluid flow, both hydrologists and geophysicists have applied this approach to analyze the impact of fluid flow on near-surface (0-2000 meter depth) temperature distribution. Examples of these applications and the application used in this study are discussed next.

Previous Applications of Temperature Data to Hydrologic Analyses

Analysis of Vertical Leakage

One of the initial applications making use of Stallman's general analytical approach was the development by J.D. Bredehoeft and I.S. Papadopulos (1965) of an analytical solution describing steady-state, vertical (1-D) flow of groundwater and heat through an isotropic, homogeneous, and fully saturated semi-confining layer. Using the

assumptions of steady-state, one-dimensional (vertical) fluid and heat flux, Stallman's most general differential equation describing heat transfer (equation 27) is reduced to:

$$\frac{\partial^2 T}{\partial z^2} - \frac{[c\rho V_z]}{K_T} \frac{\partial T}{\partial z} = 0 \qquad (28)$$

Given a temperature gradient through a semi-confining layer, boundary conditions can be established. These boundary conditions are:

$$\text{at } z = 0 \qquad T_z = T_o$$

$$\text{at } z = L \qquad T_z = T_L$$

where,

T_z = temperature measurement at any depth z

T_o = uppermost temperature measurement

T_L = lowermost temperature measurement

L = vertical distance between T_o and T_L

Figure 15 shows a schematic diagram of a leaky aquifer system and the parameters of interest. In this figure both z (with origin at T_o) and V_z are positive in a downward direction. Using the given boundary conditions the particular solution for equation 28 is:

$$T_z = \frac{(T_L - T_o)\left[\exp\left(\frac{c\rho V_z L}{K_T}/L\right) - 1\right]}{\exp\left(\frac{c\rho V_z L}{K_T}\right) - 1} + T_o \qquad (29)$$

Bredehoeft and Papadopulos rearranged and simplified this equation to give:

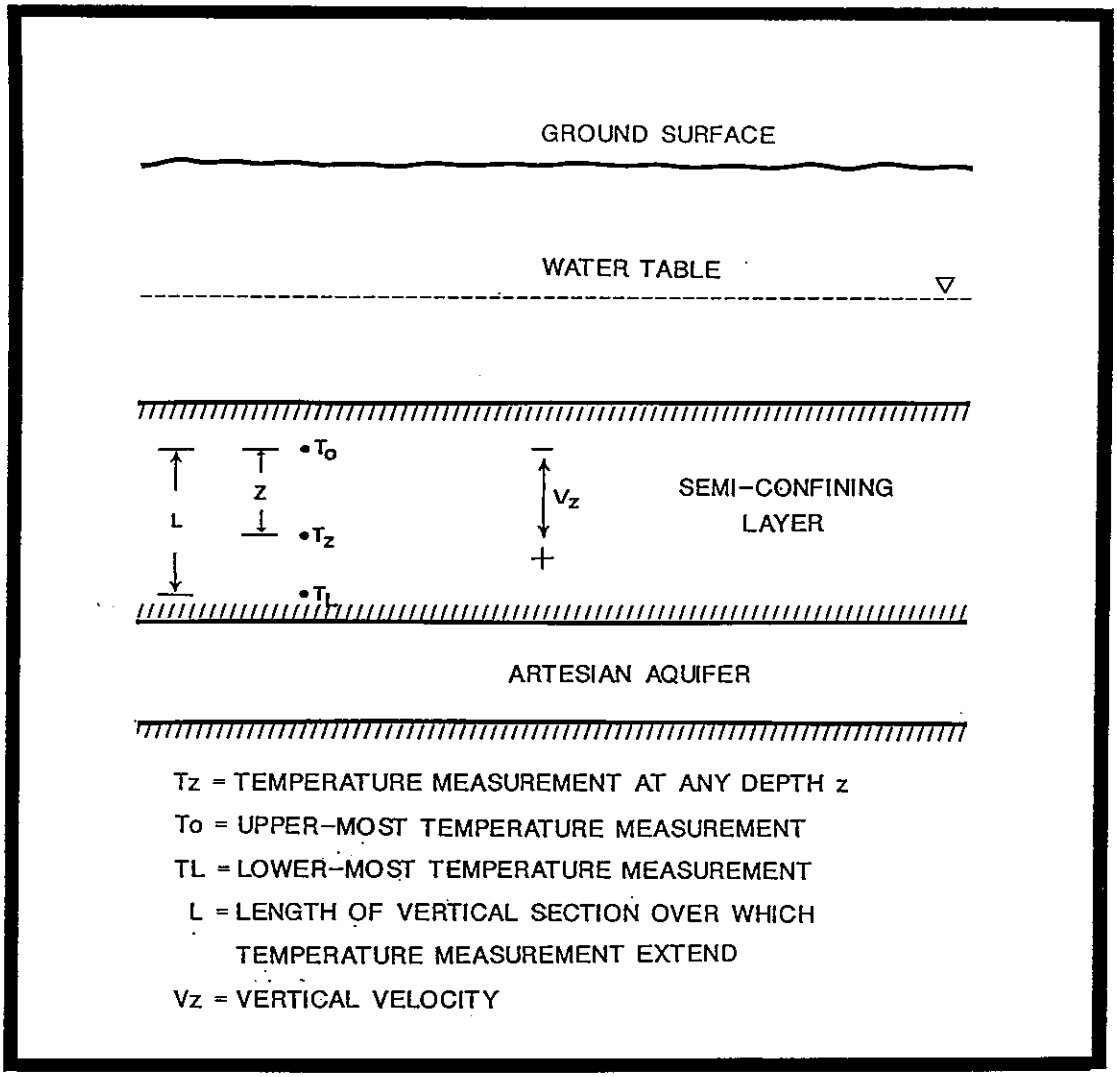

Figure 15 - Schematic diagram of a leaky aquifer showing vertical temperature distribution in the semiconfining layer (after Bredehoeft and Papadopulos, 1965).

$$\frac{(T_z - T_o)}{(T_L - T_o)} = f(\beta, z/L) \tag{30}$$

where:

$$f(\beta, z/L) = [\exp(\beta z/L) - 1]/[\exp(\beta) - 1] \tag{31}$$

and:

$$\beta = \frac{c\rho V_z L}{K_T} \tag{32}$$

From this simplified equation, Bredehoeft and Papadopulos calculated the values of $f(\beta,z/L)$ for selected values of the parameters and created a plot of $f(\beta,z/L)$ vs. z/L to develop type curves for β. To determine vertical groundwater velocity (V_z) from temperature data the appropriate β is found by matching these type curves with a plot of z/L vs. $(T_z - T_o)/(T_L - T_o)$. V_z can then be calculated using:

$$V_z = \beta K_T/Lc\rho \tag{33}$$

An example of a field application of this technique is documented by M. L. Sorey (1971).

This same problem is approached from a different perspective by Mansure and Reiter (1979). In this paper, the primary concern is the recognition of the impact of groundwater movement on heat flow calculations.

Terrestrial heat flow is determined by multiplying logged temperature gradients by rock thermal conductivities. When fluid advection is present within the logged interval, the terrestrial heat flow or total energy flux includes a component carried by the advecting

fluid ('internal heat energy'). This total energy flux is defined as (Mansure and Reiter, 1979):

$$E = - K_T \frac{dT}{dz} + c\rho V \ (T_z - T') \qquad (34)$$

where,

T' = temperature at which the 'internal heat energy' is taken to be zero.

Review of temperature versus depth profiles can offer a qualitative indicator of the direction of vertical fluid movement. Figure 16 (after Mansure and Reiter, 1979) shows schematic temperature vs. depth plots through a homogeneous, isotropic material.

The three cases shown in this figure are:

Case 1: Straight line between T_1 and T_2. This represents no fluid advection (heat transfer by conduction only).

Case 2: Concave line between T_1 and T_2. This represents downward fluid movement and results in fluid at some fixed depth having a lower temperature than would be encountered at that depth if there was no fluid movement.

Case 3: Convex line between T_1 and T_2. This represents upward fluid movement and results in fluid at some fixed depth having a higher temperature than would be encountered at that depth if there was no fluid movement.

The approach used by Mansure and Reiter (1979) to analyze temperature data where potential vertical advection is indicated involved plotting $\Delta T/\Delta z$ (temperature gradient) versus T. Rearranging equation 34 yields:

$$\frac{dT}{dz} = \frac{c\rho V}{K_T} (T_z - T') - E/K_T \qquad (35)$$

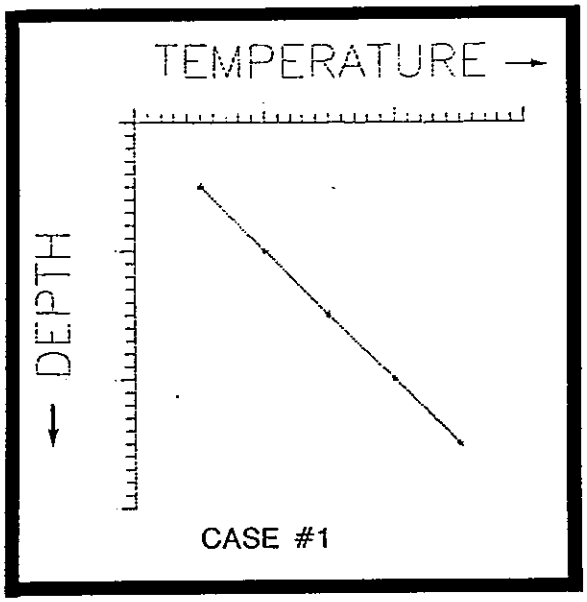

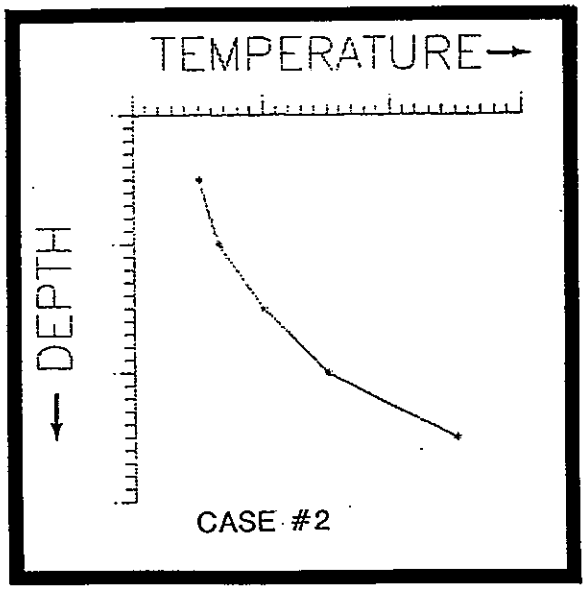

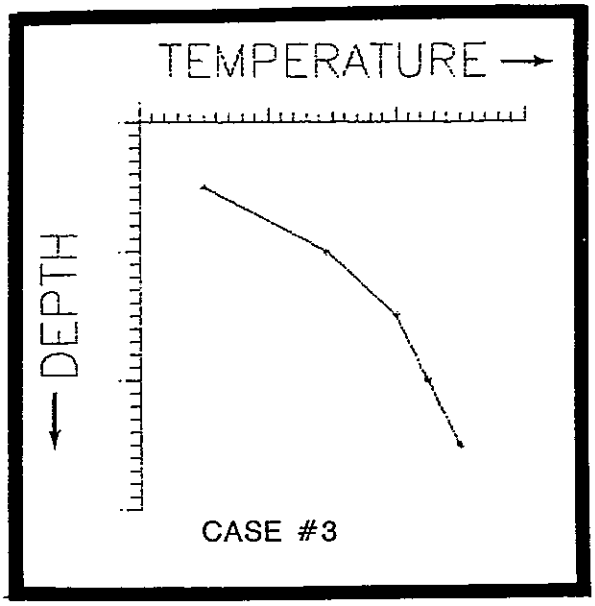

Figure 16 - Schematic representation of temperature versus depth profiles for different cases of vertical advection.

This is a linear equation of the variable T with the slope equal to $\frac{c\rho V}{K_T}$ and the intercept equal to $-E/K_T$. In depth intervals where there is no vertical fluid movement (V = 0.0) this plot results in a horizontal line. In depth intervals with vertical advection (V > 0.0 and $\frac{c\rho V}{K_T}$ = non-zero constant), this plot results in a non-horizontal straight line. Figure 17 from Mansure and Reiter (1979) illustrates this technique. In this figure three regions can be defined. Regions I and III are characterized by nearly horizontal lines indicating little or no vertical advection. In region II the plot is linear with a non-zero slope indicating uniform vertical advection. In this region, the velocity of the vertical advecting fluid can be estimated from the slope of the plot (equation 35).

In their discussion of the applicability of this analysis technique, Mansure and Reiter (1979) caution that if the plot of $\Delta T/\Delta z$ versus T is non-linear, conclusions about vertical advection cannot be made. In a non-linear plot other factors such as horizontal flow, variable thermal conductivity or transient effects could be contributing to the gradient anomaly. An extension of this method involves the plot of heat flow $\left(K_T \frac{\Delta T}{\Delta z}\right)$ versus T. Using this plot, perturbations caused by variations in thermal conductivity can be smoothed out.

Identification of Recharge/Discharge Areas

The other major application of temperature data in hydrology has been in the identification of aquifer recharge/discharge areas. Domenico and Palciauskas (1973) addressed this application using a theoretical analysis of advective heat transfer in a regional flow system. In this analysis, approximate and exact solutions to the

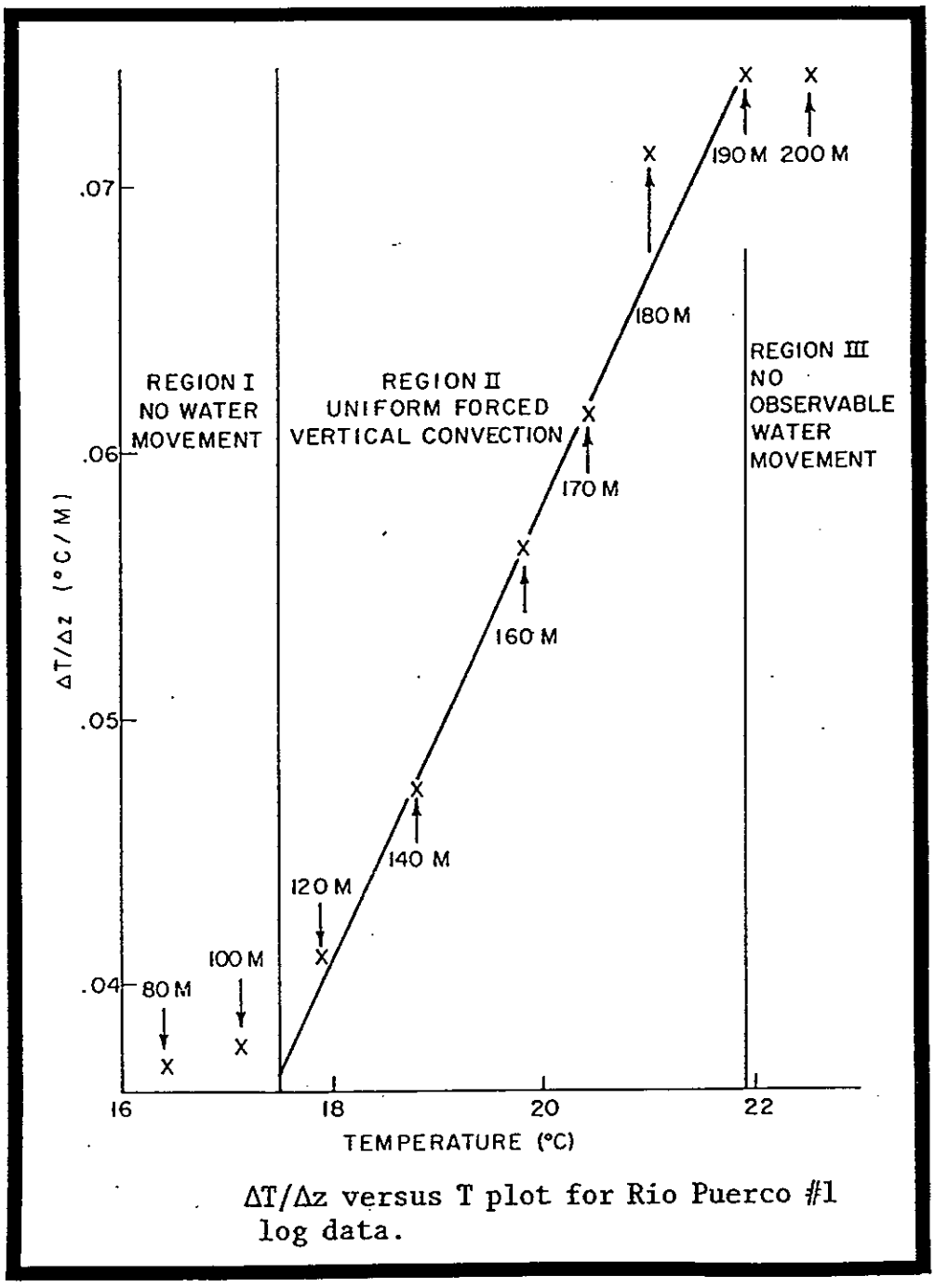

ΔT/Δz versus T plot for Rio Puerco #1 log data.

Figure 17 - Example of a ΔT/Δz versus T plot used to estimate vertical advection (from Mansure and Reiter, 1979).

coupled heat transfer and regional fluid flow equation were developed in order to help better understand regional temperature distributions. These solutions indicate that advective heat losses in recharge areas are balanced by advective heat gains in discharge areas. This in turn indicates that temperature gradients increase with increasing depth in recharge areas and decrease with increasing depth in discharge areas.

Application in this Study

Previous applications utilizing terrestrial heat in hydrologic analyses have primarily been concerned with vertical fluid flow and vertical temperature redistribution. In this study, temperature and head distribution data will be used to estimate lateral fluid flow characteristics. While Stallman (1963) clearly had this application in mind when he developed the general analytical approach previously detailed, he did recognize that where the temperature gradient was zero in the direction of flow this type of analysis would not be feasible. Since local variations in terrestrial conductive heat flow are generally very small within a given geological region (Kappelmeyer and Haenel, 1974), lateral temperature gradients will also be very small. Therefore, it is not surprising that terrestrial heat flow data has been little used in the analysis of lateral fluid flow.

However, geothermal studies in the San Juan Basin (Reiter and Mansure, 1985) have shown a significant and systematic lateral variation in terrestrial heat flow (Figure 10). This characteristic, when combined with other temperature and head distribution data, make this an area where analysis of lateral groundwater flow using temperature data may be feasible. Approaches to this type of analysis and applications/results using temperature and head distribution data from the study area will be discussed later.

CHARACTERISTICS OF A FRUITLAND FORMATION AQUIFER

As mentioned in the introduction, significant water production from gas wells completed in thick Fruitland Formation coals suggested that this interval might be an aquifer. In this section, characteristics important in defining a Fruitland Formation coal interval aquifer are discussed. These include:

- the lateral continuity of the major coalbeds
- porosity and permeability of coal
- regional Fruitland Formation head distribution
- results of aquifer/reservoir testing in coalbeds
- thermal characteristics of the Fruitland Formation

In the following section temperature distribution data will be used to estimate lateral groundwater velocity in a Fruitland Formation aquifer.

COAL STRATIGRAPHY

Spatial Distribution and Lateral Continuity

The Fruitland Formations contains multiple coalbeds with individual beds ranging from less than .5 to more than 12 meters in thickness. Figure 18 (after Fassett and Hinds, 1971) is an isopach map in the vicinity of the study area of the total thickness of Fruitland Formation coals found in beds greater than or equal to .6 meter in thickness. Review of this figure indicates that within the study area cumulative coal thickness is generally greater than 10 m. In addition, the study area includes some of the thickest coal development in the entire basin.

Given that Figure 18 shows cumulative coal development in the study area, it is necessary to relate this to the lateral continuity of individual beds. Individual bed correlation in the San Juan Basin has historically proven to be very difficult. This difficulty is related

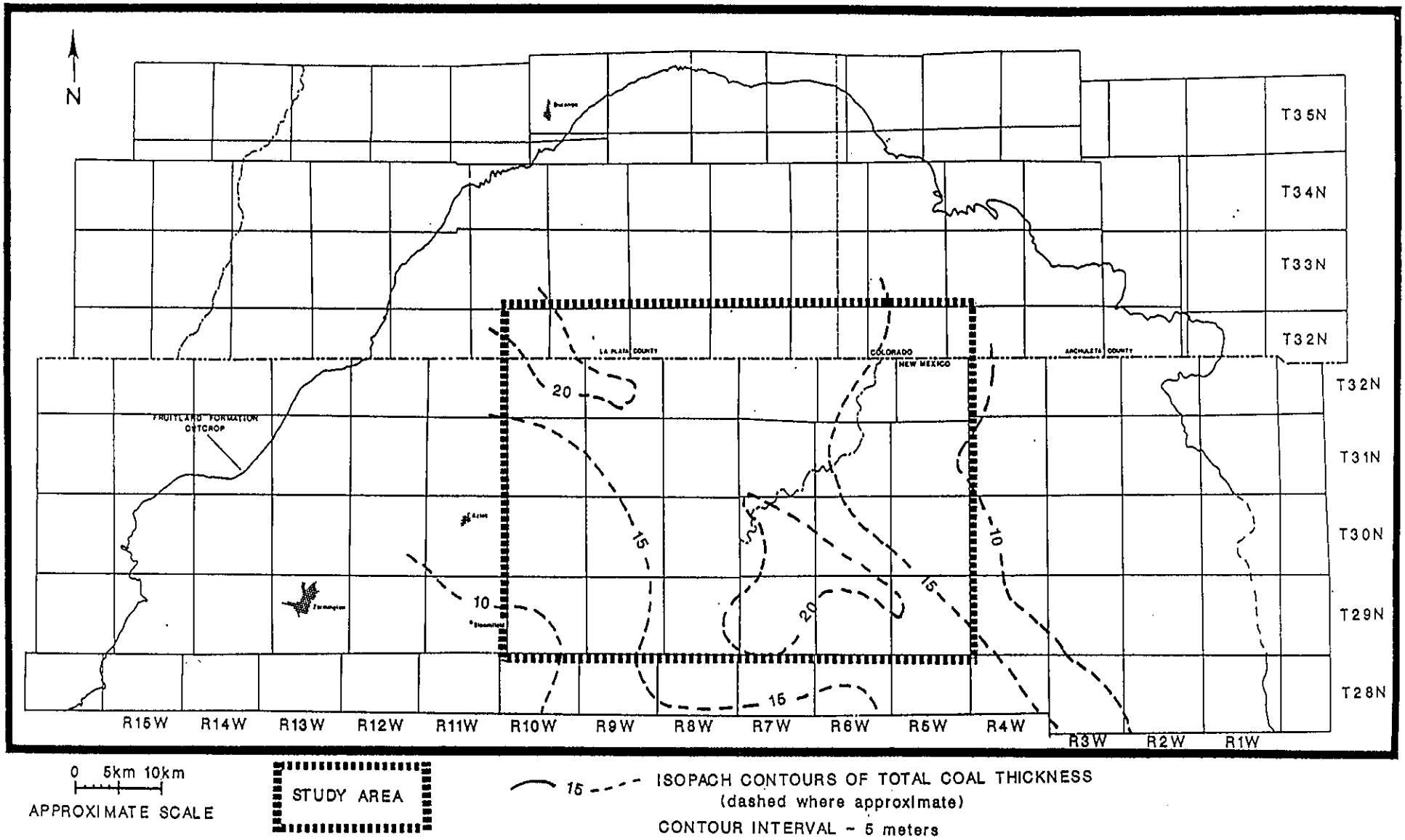

Figure 18 - Isopach map of total coal thickness in the Fruitland Formation (after Fassett and Hinds, 1971).

to both the depositional complexities associated with deltaic environments, and the time-transgressive nature of Pictured Cliffs deposition. Depositional complexities include the evolution and migration of swamp environments and localized interswamp areas (lateral facies changes); erosion features (fluvial channels); and differential sediment compaction. Correlation problems related to the Pictured Cliffs Sandstone is primarily the result of workers utilizing the top of the Pictured Cliffs as the datum for correlation. Historically, workers selected this unit as a regional datum because of its extent and its relatively easy recognizability on geophysical logs. However, with the discovery by Fassett and Hinds (1971) of the Huerfanito Bentonite marker bed within the Lewis Shale, it was shown that the Pictured Cliffs is stratigraphically rising toward the northeast. Therefore, correlations of individual coalbeds relative to the Pictured Cliffs would only be meaningful if that coalbed exhibited the same stratigraphic rise.

Figure 19 (Fassett, 1988) is a northeast trending stratigraphic cross-section utilizing the Huerfanito Bentonite bed as a datum and showing Fruitland Formation coalbeds and the underlying Pictured Cliffs Sandstone. This figure shows that stratigraphically higher coalbeds progressively overlap stratigraphically lower beds from southwest to northeast across the basin. Individual coalbeds are shown to generally parallel the Huerfanito datum.

In Fassett and Hinds (1971) Fruitland coal correlations were generally considered to be more reliable in a northwest-southeast direction parallel to paleoshoreline trends. However, subsequent work by Fassett (1988) has shown that correlation and continuity of individual coalbeds is better along a southwest-northeast trend

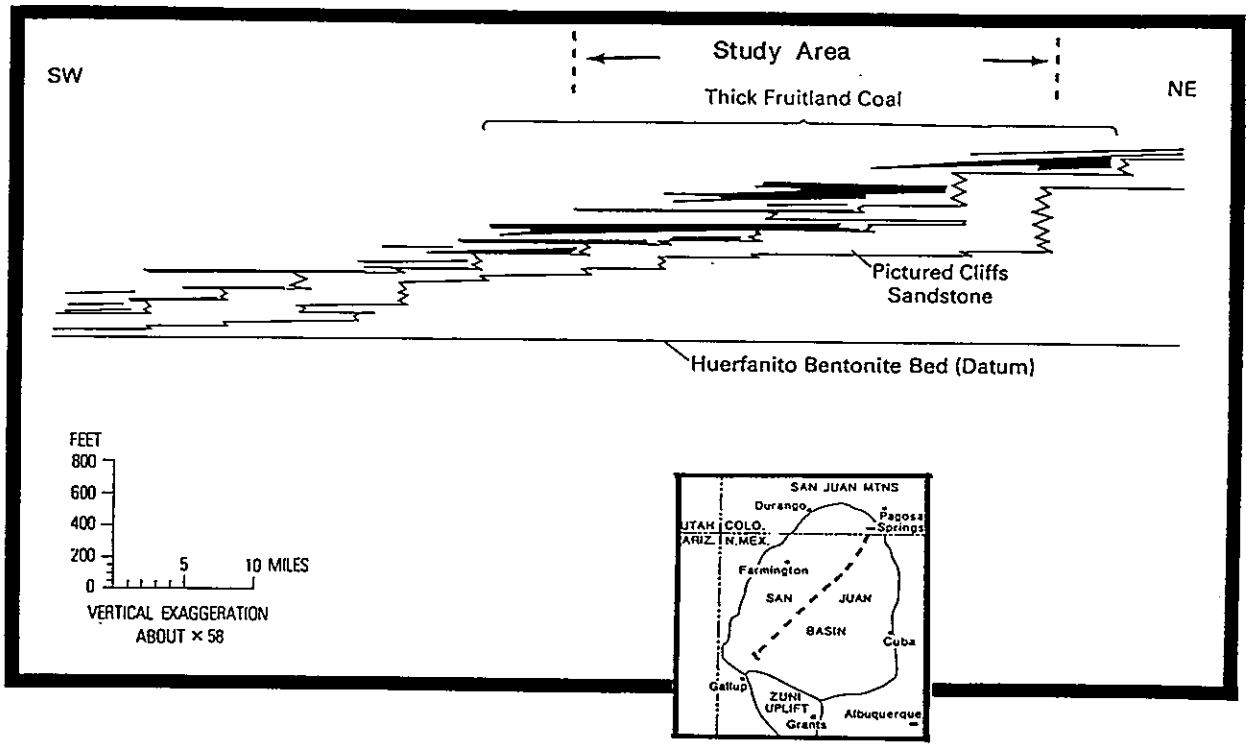

Figure 19 - Northeast-trending stratigraphic cross-section showing Fruitland Formation coalbeds and the underlying Pictured Cliffs Sandstone (from Fassett, 1988).

(perpendicular to Pictured Cliffs paleoshorelines). Figure 19 shows that within the study area there are four major coalbeds with southwest trending lateral continuity exceeding 24 km. In addition, these coalbeds form an en echelon pattern and tend to overlap each other with vertical separations of less than 30 meters. If some hydraulic connection between these individual thick coalbeds can be assumed, a lateral hydraulic continuity in coalbeds on the order of 80-100+ km is a possibility.

Porosity and Permeability

In general, porosity and permeability contribute to hydraulic conductivity, a fundamental aquifer parameter that provides a measure of the ease with which fluid flows through a porous media. In some rock types, particularly medium to coarse grained clastics, fluid flows through interconnected porosity. For these rock types porosity is an important controlling influence on hydraulic conductivity, and permeability is a measure of how well the porosity is interconnected. In other finer grained rocks, porosity may be high, but the degree to which the porosity is interconnected is low. For these rock types, the permeability is low and porosity does not provide a good measure of hydraulic conductivity. Still other rock types have a very low primary porosity. In these types of rocks, permeability results from fractures, and is related to both fracture density and aperture size. Coal might best be placed in this last category. However, coal exhibits some unique porosity/permeability characteristics which make it difficult to quantify its ability to transmit fluid. These characteristics include a complex porosity system and a stress-sensitive genetic fracture system.

Coal has been described as having a dual or two-fold porosity system. This system includes micro-porosity and macro-porosity (Van Krevelen, 1981). Micro-porosity is made up of those pores with radii smaller than 20 Å. Macro-porosity includes both larger radii pores and a genetic fracture system called cleat. Cleat is an orthogonal jointing system where fairly continuous face cleats are joined together by an orthogonal set of short, connecting butt cleats. Figure 20 (Jones et al., 1984) shows a schematic diagram of cleat configuration in a core sample obtained from the Fruitland Formation.

Porosity measurements on Fruitland Formation coal samples range from 4.4 to 8.6 percent with the micro-pores accounting for approximately 90% of this total porosity (Sato, 1981). However, measurement techniques use either small chip samples or powder samples which do not provide a good representation of the fracture porosity. Therefore, measured values of both total porosity and the relative percentage of the macro-pores are low. In addition, mercury injection capillary pressure data for a Fruitland Formation coal sample indicate a high irreducible water saturation of between 75 and 82 percent (Jones et al., 1988). This data suggest that water is strongly sorbed to the internal surfaces of coal within the micro-porosity. This characteristic would effectively eliminate more than 90 percent of the measured porosity from being effective porosity (that porosity effective in transmitting fluid). Therefore, since coal exhibits a very low indicated effective porosity, this parameter will not exert a strong influence on hydraulic conductivity.

As previously discussed relative to coal porosity, coal exhibits a genetic fracture system. While this fracture or cleat system is thought to be a relatively minor contributor to total coal porosity, it

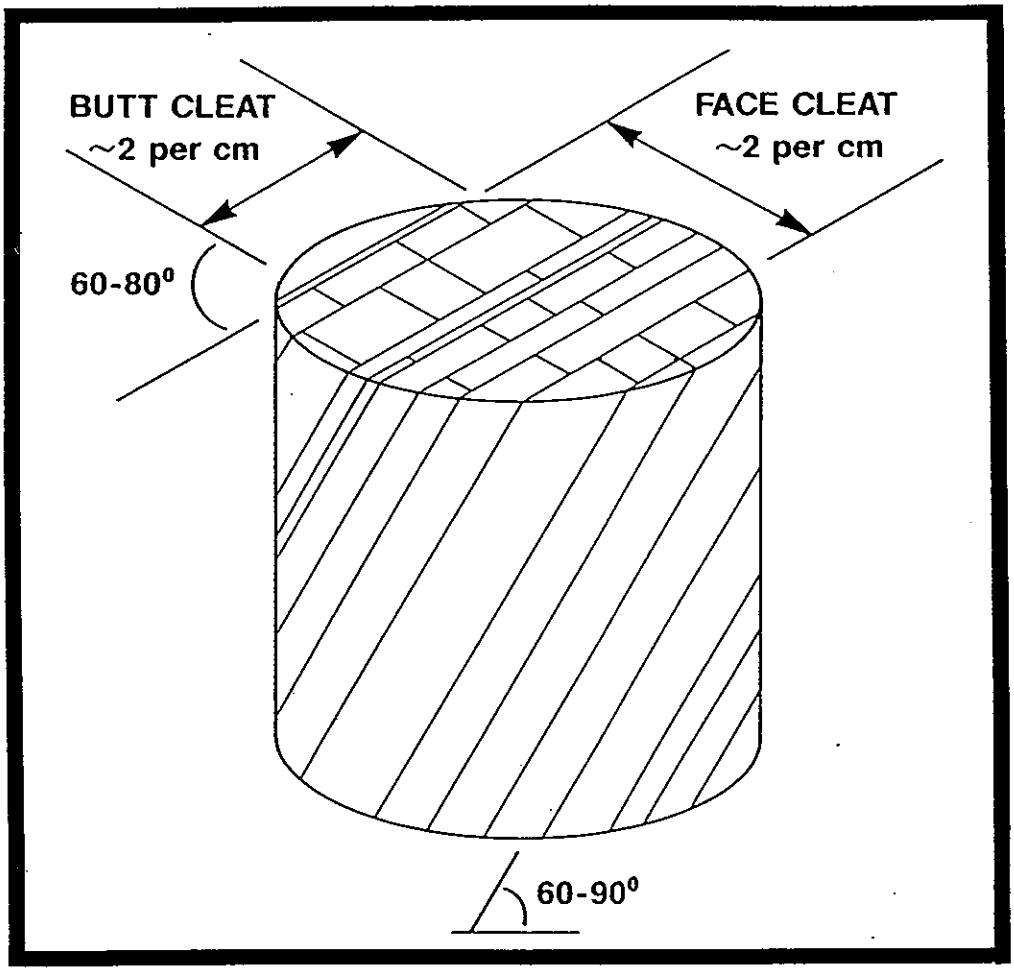

Figure 20 - Example of coal cleat system. Sample is from a San Juan Basin coal core (from Jones et al., 1984).

is the main contributor to basic coal permeability. Permeability measurements can be obtained from laboratory techniques and, in the field, from aquifer/reservoir tests. However, there are significant problems associated with each of the methods. Laboratory permeability measurements are generally obtained on small (core-plug or whole core) samples. Though these samples are assumed to be generally representative, they are invariably damaged during sample collection, preparation and testing (Jones et al., 1988). In the best controlled tests, test procedures will address cleat orientation, and in situ stress and temperature. However, regardless of the details of the test procedures, two factors affect the estimated permeability results. The first factor is that the in situ fluid state (gas and water) cannot be adequately simulated, resulting in a nonrepresentative sample. The second factor is that the size of the sample does not constitute a representative elementary volume relative to the cleat system. Both of these factors will tend to result in minimum values and may significantly underestimate in situ permeability.

Field permeability testing seemingly eliminates most of the problems associated with laboratory testing. In general, field tests provide a good representative measure of aquifer/reservoir response to induced stresses. Aquifer/reservoir damage is always a possibility from drilling, but test analysis techniques can usually assess the extent of any damage. However, coal aquifer/reservoirs provide a unique challenge to field testing and permeability analysis. Early well tests in coal intervals noted a rapid fall-off in pressure/fluid production. This general trend was attributed to a limited reservoir and/or short-lived fracture production. As experience with testing and producing coal aquifer/reservoirs has increased, it has been shown, at

least empirically, that rapid drawdown/pressure reduction results in rapid decline in productivity while a slow, step-wise drawdown/pressure reduction results steady and sustained aquifer/reservoir fluid production. This suggested a possible permeability response to stress. Recent laboratory results (Rose and Foh, 1984; Harpalani and McPherson, 1985) have shown significant decreases in coal permeability with applied stress. These laboratory results have led to on-going analyses of various field results. As part of these analyses, the Gas Research Institute (GRI) initiated and funded compilation of all available coal-interval permeability data. This project resulted in the collection of more than 40 permeability data points. Four of these data points were from the San Juan Basin. Preliminary review of these data suggested a decrease in permeability with increasing depth. This data substantiated laboratory results. Recently McKee et al. (1986 and 1988) have developed mathematical relationships for permeability, porosity and density as a function of effective stress and have compared mathematical results to available permeability/depth data. Figure 21 (McKee et al.) is a semilog plot of coal interval permeabilities in the San Juan and Piceance Basins. The match curve on this figure is from derived formulae. Closed symbols indicate data points where well test data were available for the calculation of equivalent lithostatic depth. Open symbols indicate data points where lithostatic conditions had to be assumed. This figure shows permeability decreasing with increasing depth and indicates a good match between the field data and the derived analytical approach.

While coal permeability has been shown to be stress-dependent, this characteristic has not yet been widely considered relative to aquifer/reservoir tests over coal intervals. Existing data suggest

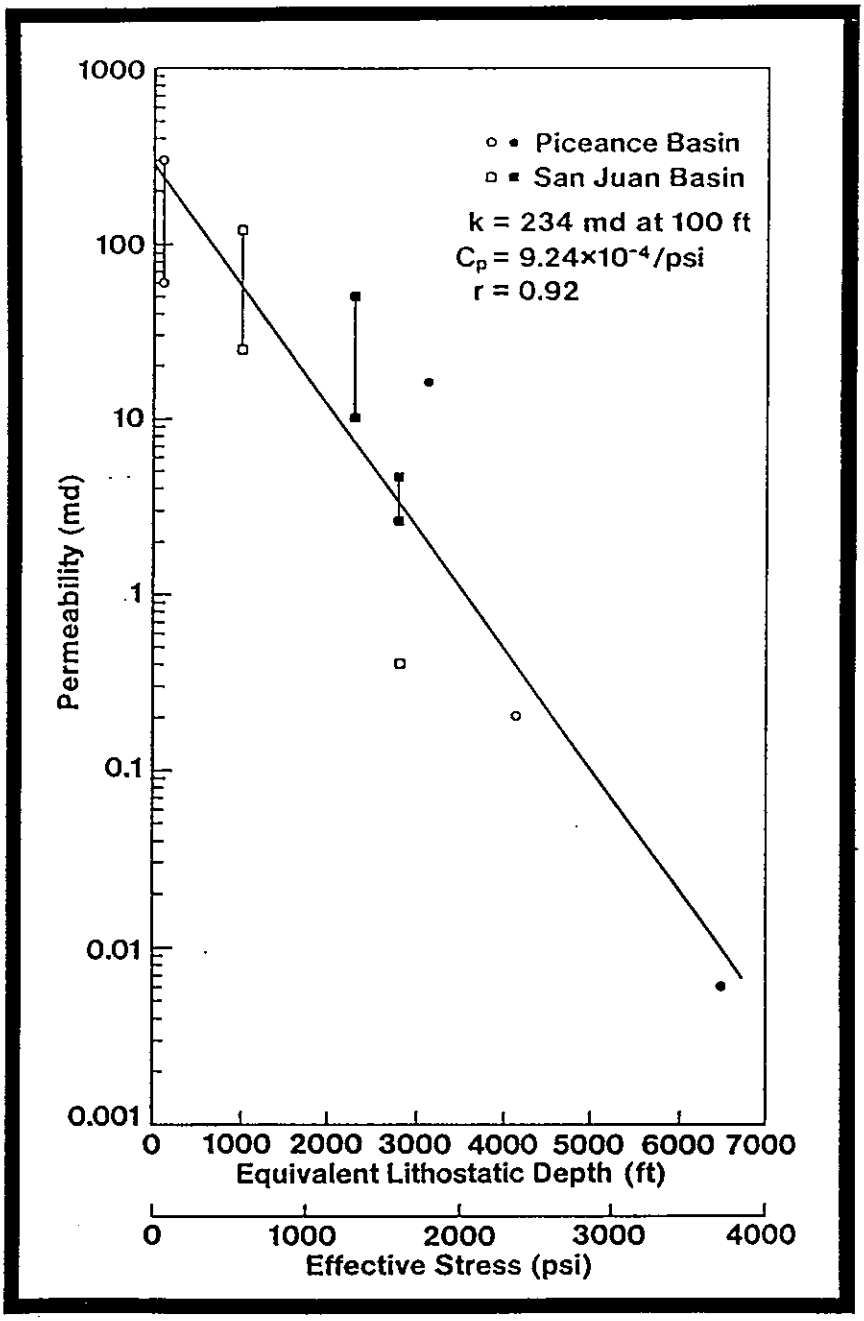

Figure 21 - Semilog plot of field measured and estimated coal interval permeabilities in the San Juan and Piceance Basins (from McKee et al., 1988).

that stresses involved with well testing may affect permeability calculations. That is, in situ coal interval permeability may be significantly different from permeabilities calculated using well test data. Existing well test data over Fruitland coal intervals will be summarized and discussed later in this study.

REGIONAL HEAD DISTRIBUTION DATA

Data to define the regional head distribution for the Fruitland Formation has been gathered, analyzed and mapped as part of this study. This data base includes drill-stem test data from oil and gas wells over the Fruitland and Pictured Cliffs interval and direct water-level data, primarily from around the periphery of the basin.

Drill-Stem Test Data

A drill-stem test is a temporary completion of a well, normally while it is being drilled, in order to determine the production potential of the tested interval. To run a drill-stem test (DST) a special DST tool is used to isolate the test interval from the column of drilling fluid and allow the formation fluid to flow into the drill-pipe while continuously recording pressure. In general, a DST includes a short initial flow period, a short shut-in period, a longer flow period and a relatively long final shut-in period. Figure 22 (Earlougher, 1977) is a schematic diagram showing a typical pressure response for a two-cycle test. Good quality DST data can be used to estimate reservoir pressure, formation permeability, and formation skin-factor by using pressure build-up analysis techniques. For this study DST data was only used to estimate reservoir pressure.

Drill-stem test data over the Fruitland and Pictured Cliffs interval was collected for 117 wells. For many of these wells,

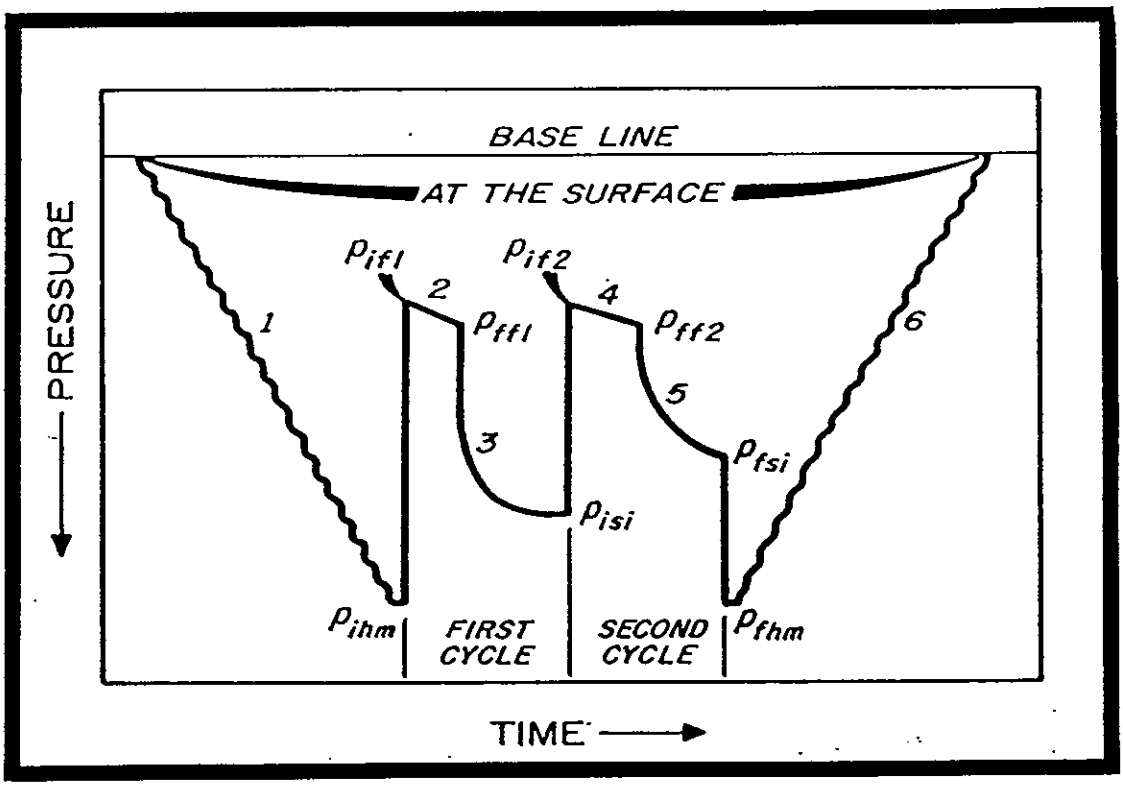

Figure 22 - Schematic of a DST chart: (1) going into hole; (2) initial flow period; (3) initial shut-in period; (4) final flow period; (5) final shut-in period; and (6) coming out of hole. p (ihm) = initial hydrostatic mud pressure; p (if1) = initial flowing pressure in first flow period; p (ff1) = final flowing pressure in first flow period; p (isi) = initial shut-in pressure; p (if2) = initial flowing pressure in second flow period; p (ff2) = final flowing pressure in second flow period; p (fsi) = final shut-in pressure; and p (fhm) = final hydrostatic mud pressure (from Earlougher, 1977).

multiple tests were available. Data collected on all these wells include:

- well name, location and elevation
- Fruitland/Pictured Cliffs stratigraphy as interpreted from available geophysical logs
- all available DST data including flow and shut-in times, associated pressures and fluid recovery.

In general, DST pressure data was available for only the end points of the flow and shut-in periods. Final flow periods range from 15 to 285 minutes with 60 minutes being the mode. Final shut-in pressures range from 15 to 210 minutes with 30 minutes being the mode. Analyses of DST's with continuous pressure data indicate that for final flow periods of 60 minutes or less, final shut-in pressures of 30 minutes come within 95% of final projected reservoir pressure. Therefore, final shut-in pressures are assumed to be representative of in situ reservoir pressure. Formation hydraulic head was estimated from final shut-in pressure. This pressure was converted to equivalent fresh-water hydraulic head using .433 psi/ft. This pressure head was then added to elevation of the measuring point to determine total hydraulic head.

After analysis and review of all DST data, data from 51 wells were used to calculate Fruitland Formation hydraulic head at different locations in the basin. Table 1 identified these wells. In 22 of these wells, there were complimentary DST's in the Pictured Cliffs Sandstone. Table 2 identifies these wells. Comparison of these tables indicates that in general, north of township 28 North, Fruitland Formation hydraulic head is greater than Pictured Cliffs hydraulic head. Therefore, in the area of this study, a contour plot of

Table 1. Summary of Fruitland Formation hydraulic head calculated from DST data - San Juan Basin, southwestern Colorado and northwestern New Mexico

WELL NAME	LOCATION TWP	RNG	SEC	GROUND SURFACE ELEVATION (ft. MSL)	DST DATA DST #	DEPTH INTERVAL (ft)	MP* (ft. MSL)	FSIP (psi)	HYDRAULIC HEAD (ft. MSL)
CONSOL O&G #1-17 Spring Creek	34N	06W	17	7192	1	2900-3397	4043	1350	7161
OCCIDENTAL #1-22 Davie	34N	08W	22	6645	1	2427-2476	4213	1250	7100
GREAT WESTERN #1 Thompson	34N	09W	20	6719	2	2628-2740	4035	1320	7083
BYRD OIL #1 Simon A	34N	09W	22	6816	2	2623-2725	4142	1250	7029
PNWP #3-36 Bondad 34-10	34N	10W	36	6214	1	2405-2450	3786	1315	6823
SUN #1 Ilamae Dunagan	33N	05W	28	6157	1	2641-2725	3474	1258	6379
CONSOL O&G #1-6 Superior Ute	33N	06W	06	6709	1	2756-2916	3873	1240	6737
STANOLIND #4 Ute Indian B	33N	07W	17	6570	1	2426-2488	4113	1400	7346
STANOLIND #1 Ute Gas Unit A	33N	07W	19	6551	1	2580-2827	3847	1370	7011
STANOLIND #1 Unit B Tiffany	33N	07W	35	6378	1	2295-2604	3928	1450	7277
STANOLIND #1 Ford	33N	08W	10	6692	1	2615-2895	3937	1395	7159
STANOLIND #1 Gallegos	33N	08W	12	6586	1	2432-2730	4005	1525	7527
NWPL Bondad 33-9 #5-3	33N	09W	03	6281	2	2392-2490	3840	1380	7027
NWPL Bondad 33-9 #13-6	33N	09W	06	6489	1	2460-2560	3979	1280	6935
MESA #8-A Southern Ute	33N	09W	11	6546	1	2505-2965	3811	1386	7012
NCRA #1-X Brown	33N	09W	15	6712	4	2877-2980	3783	1420	7062
STANOLIND #1 McCarville	33N	09W	14	6763	1	2790-3107	3814	1420	7093
GREAT WESTERN #1 Spatter	33N	09W	31	6044	4	2423-2523	3751	1390	6781
STANOLIND S.J. Unit 32-5 #3	32N	05W	10	7550	1	3830-4050	3610	1425	6901
STANOLIND S.J. Unit 32-5 #2	32N	05W	35	6320	1	2944-3029	3333	1550	6913
NWPL Arboles Unit 32-6 #2-13	32N	06W	13	6208	1	2600-2729	3543	1450	6892
STANOLIND Bixler Gas Unit #1	32N	06W	14	6153	3	2450-2627	3614	1500	7078
NWPL Arboles Unit 32-6 #3-15	32N	06W	15	6177	1	2438-2570	3673	1410	6929
GREENBRIAR #1 Schofield	32N	07W	05	6330	1	2585-2670	3702	1480	7120
SOHIO #9 Southern Ute	32N	07W	14	6379	1	2761-2859	3569	1533	7109
PHILLIPS Mesa Unit 32-7 #3-18	32N	07W	18	6253	2	2860-2930	3358	1650	7169
KOCH #3 Gardner	32N	08W	31	6520	1	3306-3384	3175	1675	7043
PHILLIPS #1-17 Aztec A	32N	10W	17	6745	2	3286-3420	3392	1520	6902
AMOCO Keys Gas Com-A #2	32N	10W	27	5947	1	2726-2761	3190	1603	6892
MESA Hamilton Fed #1-A	32N	10W	30	6091	1	2608-2650	3462	1479	6878
NWPL NW Cedar Hill 32-10 #2-20	32n	10W	20	6466	3	3000-3147	3390	1375	6566
Greenbriar #1 Maddox	32N	11W	14	6302	1	2749-2950	3478	1450	6826
Colorado O&G Rosa Unit #6	31N	05W	27	6775	1	3555-3606	3194	1550	6774
Blackwood & Nichols NEBU #212	31N	07W	01	6515	1	3067-3209	3469	1665	7314
Blackwood & Nichols NEBU #213	31N	07W	12	6535	1	3129-3234	3353	1671	7212
Blackwood & Nichols NEBU 52-15	31N	07W	15	6531	1	3134-3294	3312	1700	7238
Southern Union #9 Seymour	31N	09W	23	6156	**	2640-2962	3355	1374	6528
EPNG S.J. Unit 30-4 #4	30N	04W	27	7478	2	4130-4165	3330	1300	6332
Phillips Mesa 30-5 #2-29	30N	05W	29	6749	1	3480-3628	3195	1700	7121
EPNG Governador Strat Test #1-2	30N	06W	25	6553	2	3383-3400	3161	1780	7272
Phillips Mesa 30-6 #4-35	30N	06W	35	6676	1	3330-3491	3265	1695	7180
H. Birdseye #1-24 Carpenter	30N	14W	24	5694	1	1290-1310	4394	425	5376
Magnolia Cleveland-Fed #1	27N	09W	29	6333	1	1940-2056	4335	507	5506
Caulkins Breech D-D140	26N	06W	11	6588	1	2915-2931	3665	1035	6055
Magnolia Ingwersen Fed B-2	24N	02W	21	7163	1	2936-2995	4197	945	6379

Table 1 (con't)

WELL NAME	LOCATION TWP	RNG	SEC	GROUND SURFACE ELEVATION (ft. MSL)	DST DATA DST #	DEPTH INTERVAL (ft)	MP* (ft. MSL)	FSIP (psi)	HYDRAULIC HEAD (ft. MSL)
Standard Tx #1 Fed 1-27	24N	07W	27	7011	1	2150-2215	4828	635	6285
Humble Jicarilla C #1	23N	05W	04	6634	1	2076-2138	4527	720	6190
Humble Jicarilla #1	23N	05W	15	6854	1	2239-2340	4564	780	6365
Union Jicarilla #1-0-32	22N	05W	32	7271	1	1627-1697	5609	408	6551
WEXPRO Armijo Res. #1	21N	04W	16	7183	1	1678-1786	5451	426	6435
SKELLY R.C. White #1	21N	04W	07	7200	1	1687-1837	5438	465	6512

* assumed to be at mid-point of tested interval

** hydraulic head estimated from surface shut-in pressure

MP - measuring point

FSIP - final shut-in pressure

Table 2. Summary of Pictured Cliffs Sandstone hydraulic head calculated from DST data - San Juan Basin, southwestern Colorado and northwestern New Mexico (wells in this table also have had Fruitland Formation DST's)

WELL NAME	LOCATION TWP	RNG	SEC	GROUND SURFACE ELEVATION (ft. MSL)	DST DATA DST #	DEPTH INTERVAL (ft)	MP* (ft. MSL)	FSIP (psi)	HYDRAULIC HEAD (ft. MSL)
CONSOL O&G #1-6 Superior Ute	33N	06W	06	6709	2	2926-3150	3671	160	4041
Empire State #1 Daniels	34N	06W	32	6819	2	3095-3226	3658	240	4212
Sunray #1 South Ute	34N	07W	23	6696	2	2845-2890	3828	150	4174
BYRD #1 Simon A	34N	09W	22	6816	3	2894-3035	3951	1310	6976
Mesa #8-A Southern Ute	33N	09W	08	6193	2	3135-3152	3619	305	4323
STANOLIND S.J. 32-5 Unit 3	32N	05W	10	7550	2	4043-4131	3463	910	5565
STANOLIND S.J. 32-5 #2	32N	05W	35	6320	3	3155-3270	3107	250	3684
Greenbriar #1 Schoefield	32N	07W	05	6330	6	2949-3040	3335	1600	7030
Phillips Mesa Unit 32-7 #3-18	32N	07W	18	6253	4	3107-3200	3099	260	3699
AMOCO Rosa Unit #33	31N	04W	22	7212	2	4090-4180	3077	190	3516
Blackwood & Nichols #33-12	31N	07W	12	6541	3	3358-3600	3062	450	4101
Blackwood & Nichols NEBU #213	31N	07W	12	6535	4	3452-3590	3014	1484	6441
Blackwood & Nichols NEBU #52-15	31N	07W	15	6531	2	3310-3485	3128	540	4375
EPNG Govenardor #1-2	30N	06W	25	6553	3	3544-3548	3007	540	4254
EPNG Govenardor Gomez #1	30N	06W	33	6330	5	3289-3397	2987	120	3264
Phillips Mesa Unit 30-6 #4-35	30N	06W	35	6676	2	3606-3702	3022	1435	6336
Henry Birdseye #1-24 Carpenter	30N	14W	24	5694	2	1398-1422	4284	460	5346
Southland Royalty #1 Trujillo	29N	04W	01	6957	2	3843-3920	3075	91	3285
Phillips 29-6 Unit #2-14	29N	06W	14	6703	2	3614-3698	3047	225	3567
SKELLY J.F. Hickman #1	28N	06W	17	6784	2	3659-3689	3120	0	5920
EPNG S.J. Unit 27-4 #4	27N	04W	31	6871	2	3705-3755	3141	975	5373
STANOLIND Joe Quinn #1	27N	05W	14	6670	3	3510-3624	3103	445	4131

* assumed to be at mid-point of tested interval

MP - measuring point
FSIP - final shut-in pressure

Fruitland Formation hydraulic heads will best define the potentiometric surface for a Fruitland/Pictured Cliffs interval.

Water Level Data

Water-level data from the Fruitland Formation were obtained for 59 locations around the periphery of the basin. Most of these data were obtained from coal-mine permits. Table 3 identifies these data.

Potentiometric Surface

Fruitland Formation hydraulic head data from DST's identified in Table 1 and water-level measurements identified in Table 3 are plotted up to define the regional hydraulic-head distribution.

Plate I is the Fruitland Formation potentiometric surface map for the entire San Juan Basin as defined by hydraulic head data gathered for this study. Figure 23 shows this same map for the northern half of the basin which encompasses the area of this study. Review of this figure indicates that within the study area, flow is generally from north toward the south or southwest with an approximate hydraulic gradient of .01 m/m. Comparison of this figure with the potentiometric surfaces of the overlying and underlying aquifer units (Figures 8 and 9) indicates that within the study area, the Fruitland Formation has higher hydraulic potential than either the Ojo Alamo or the Mesa Verde Group Sandstones.

AQUIFER TESTS

Aquifer test data within the Fruitland Formation compiled as part of this study include 38 shallow tests and 3 deep tests. Shallow test data were obtained in coal mine areas on the basin periphery and reported as part of the mine permit environmental assessments. Deep test data include one test associated with coalbed gas reservoir

Table 3. Summary of water level data from wells completed in the Fruitland Formation - San Juan Basin, southwestern Colorado and northwestern New Mexico

WELL NAME	LOCATION				GROUND LEVEL ELEVATION (ft. MSL)	APPROXIMATE WATER LEVEL (depth-ft.)	HYDRAULIC HEAD ELEVATION (ft. MSL)	DATA SOURCE
	TWP	RNG	SEC	QTR				
Black Water	19N	05W	03	NWSE	6630	~5	6625	1
Coal Spring	19N	05W	09	NWSE	6635	@ surface	6635	1
Kimbeto Coal	22N	10W	04	SWNW	6280	69	6211	1,3
Kimbeto Ob.1	22N	10W	10	SESW	6300	93	6207	1,3
DH-4K Coal	22N	10W	17	NESE	6330	115	6215	1,3
DK-2K	22N	10W	18	NWNE	6290	87	6203	1,3
TL7-2 Coal	23N	12W	07	SWNE	5920	84	5836	1,3
TL8-1	23N	12W	08	NWNW	5925	63	5862	1,3
PSC Well C	30N	15W	15	SESE	5260	21	5239	1
PSC Well D	30N	15W	16	SWSW	5255	22	5233	1
Westwater A	30N	15W	21	NWSW	5212	19	5193	1
CDOB	30N	15W	24	NESE	5330	121	5209	1
PSC Well G	30N	15W	28	NWSE	5185	32	5153	1
PSC Well E	30N	15W	29	SESE	5170	22	5148	1
20NSW36	20N	05W	36	NWSW	6619	85	6534	2
---	19-20N	06-07W	--	--	6621	34	6587	3
---	19-20N	06-07W	--	--	6675	68	6607	3
---	30N	15W	--	--	5370	159	5211	3
CCR-23	19N	06W	01	--	~6700	96	6604	4
CCR-24	20N	07W	24	--	~6685	170	6515	4
B 1/2 - 11 1/2	21N	09W	04	--	6366	49	6317	5
C-19	21N	09W	02	--	6438	86	6352	5
E-13	21N	09W	09	--	6484	164	6320	5
E-16	21N	09W	10	--	6510	184	6326	5
I-21	21N	09W	11	--	6517	178	6339	5
M 5/6 - 25	21N	08W	19	--	6506	120	6386	5
M 5/6 - 25 OBS	21N	08W	19	--	6508	122	6386	5
M 35	21N	08W	21	--	6469	94	6375	5
M 35 OBS	21N	08W	21	--	6469	96	6373	5
Q-31	21N	08W	20	--	6494	123	6371	5
KF-2	29N	15W	28	SW	5374	Dry @ 172	5202*	6
KF-3	28N	15W	07	NE	5395	Dry @ 149	5246*	6
KF-4	28N	15W	17	SW	5335	110	5225	6
KF-5	28N	16W	24	--	5397	159	5238	6
KF-6	28N	16W	26	SE	5405	Dry @ 181	5224*	6
KF-7	28N	16W	34	C	5445	Dry @ 199	5246*	6
KF-8	27N	16W	10	--	5399	112	5287	6
KF-9	27N	16W	23	NW	5402	138-195**	5264-5207	6
KF-10	27N	16W	23	SW	5409	146-160**	5263-5249	6
KF-11	29N	15W	15	NW	5265	95	5170	6
KF-83-2	30N	15W	10	SWNE	5446	125	5321	7
KF-83-3	30N	15W	10	NESW	5344	22	5322	7
KF-83-6	30N	15W	22	NESE	5255	129	5126	7
KF-83-7	30N	15W	27	NESW	5211	157	5054	7
KF-83-8	30N	15W	27	SESE	5233	117	5116	7

Table 3 (con't)

WELL NAME	LOCATION TWP	RNG	SEC	QTR	GROUND LEVEL ELEVATION (ft. MSL)	APPROXIMATE WATER LEVEL (depth-ft.)	HYDRAULIC HEAD ELEVATION (ft. MSL)	DATA SOURCE
KF-83-9	30N	15W	34	NENW	5233	140	5093	7
KF-83-10	30N	15W	34	SENW	5291	151	5140	7
KF-83-17C	30N	15W	22	SENW	5230	93	5137	7
KF-83-18C	30N	15W	21	NESE	5224	119	5105	7
BD-OB-2	32N	13W	28	--	6038	107	5931	8
BD-OB-3	32N	13W	28	--	6066	117	5949	9
BD-OB-5	32N	13W	28	--	6038	102	5936	9
81-17-4-KF	32N	13W	17	--	5943	1-13	5930-42	9
81-13-13-KF1	32N	13W	13	--	6044	104-114	5930-40	9
81-18-24-#1	32N	13W	18	--	5909	0-11	5909-20***	9
81-18-24-#2	32N	13W	18	--	5909	0-12	5900-21***	9
81-18-24-#3	32N	13W	18	--	5907	4-7	5900-03	9
81-22-2-#1	32N	13W	22	--	5898	0-74	5898-5924***	9
81-22-2-#2	32N	13W	22	--	5897	7	5890	9

Data Source:

1. Hydrologic Report No. 6, New Mexico Bureau of Mines and Mineral Resources
2. New Mexico Bureau of Mines Hydrologic Data Base
3. USGS WRI 85-4251
4. Star Lake mine permit
5. Gallo Wash mine permit
6. Navajo mine permit
7. San Juan mine permit
8. Black Diamond mine permit
9. La Plata mine permit

* Minimum hydraulic head elevation

** Multizone completion

*** Water flowing @ surface

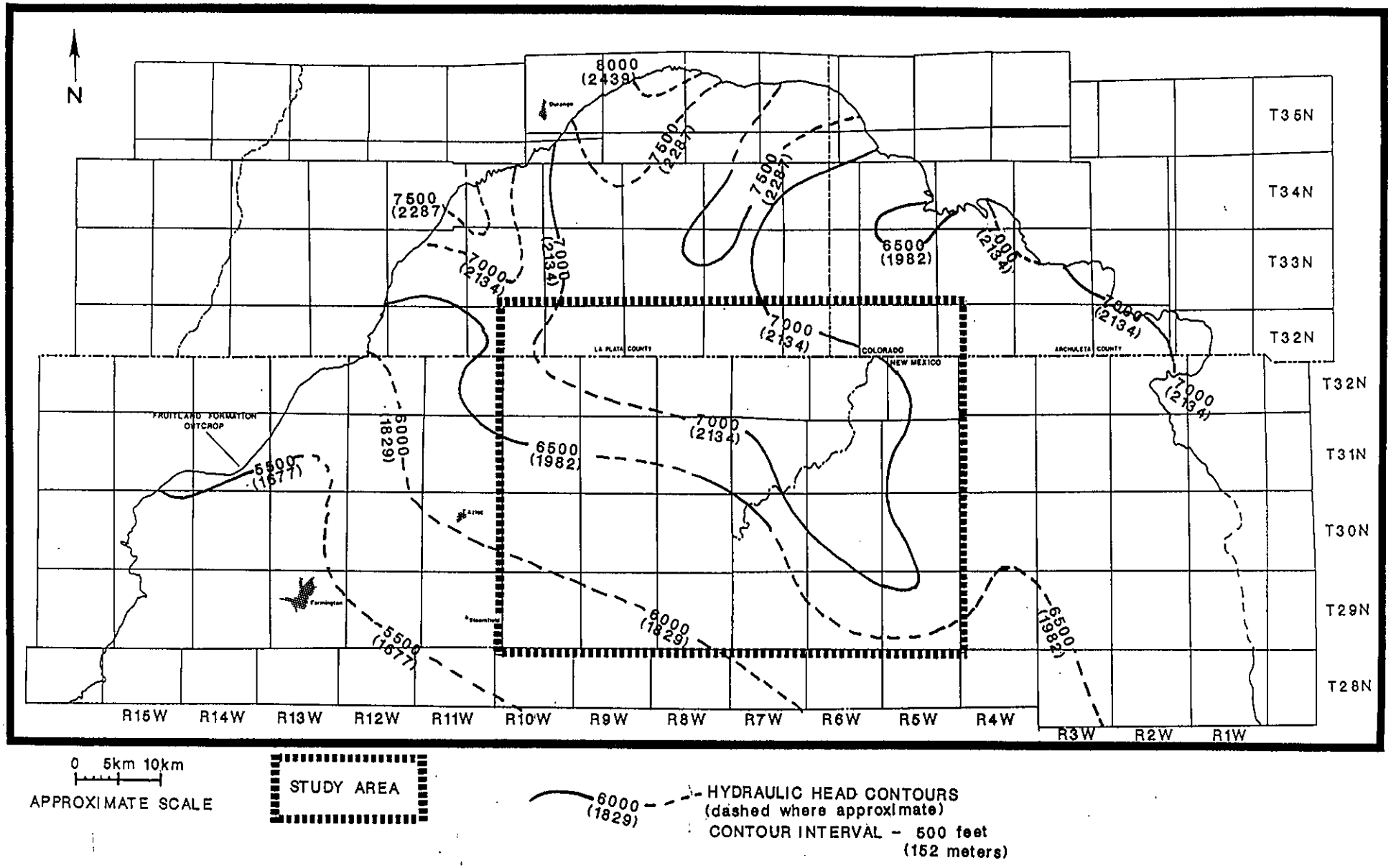

Figure 23 - Potentiometric surface of the Fruitland Formation

analysis, one drill-stem test over the Fruitland coal interval, and a multi-well analysis of the Cedar Hills Coalbed Gas Unit. Table 4 summarizes the analyzed aquifer parameters from shallow Fruitland Formation testing. This table shows hydraulic conductivity ranging over four orders of magnitude (7.9×10^{-4} cm/sec to 3.50×10^{-8} cm/sec). Table 5 summarizes the analyzed reservoir parameters from deep Fruitland Formation tests. Review of this table shows intrinsic permeabilities ranging from 3.3 to 15.3 millidarcies. Assuming density and viscosity for pure water, equivalent hydraulic conductivities range from 3.26×10^{-6} to 1.51×10^{-5} cm/sec. However, as indicated in the discussion on coal permeability, these test-acquired hydraulic conductivity values may underestimate the in situ hydraulic conductivity because of the stress-sensitive nature of coal permeability.

An indirect method for estimating hydraulic conductivity which does not involve aquifer testing utilizes hydraulic head gradients and groundwater specific discharge calculated from temperature data. Rearranging Darcy's Law and solving for hydraulic conductivity results in:

$$K_H = V_x \, (\Delta h/\Delta \ell)^{-1} \tag{36}$$

K_H = hydraulic conductivity

$\Delta h/\Delta \ell$ = hydraulic head gradient

V_x = lateral groundwater specific discharge

The rest of this study consists of a detailed discussion of Fruitland Formation thermal characteristics within the study area and the

Table 4. Summary of aquifer parameters obtained from analyses of shallow test data

WELL NAME	LOCATION TWP	RNG	SEC	AQUIFER PARAMETERS* b	K	S	TYPE OF AQUIFER TEST ANALYSIS	DATA SOURCE
B - 1/2 - 11 1/2	22N	10W	18	30.5	3.5×10^{-6}	1.0×10^{-2}	Jacob drawdown	1
E-13	21N	09W	09	2.4	3.5×10^{-4}	---	Jacob recovery	1
I-21	21N	09W	11	20.7	1.1×10^{-5}	---	Jacob step-drawdown	1
M 5/6 - 25 OBS	21N	08W	19	24.4	1.8×10^{-4}	1.0×10^{-4}	Theis	1
M-35 OBS	21N	08W	21	61.0	3.5×10^{-5}	---	Jacob drawdown	1
Q-31	21N	08W	20	45.7	1.4×10^{-4}	---	Jacob recovery	1
KF-1	29N	15W	22	6.7	6.9×10^{-4}	---	-----	2
KF-4	28N	15W	17	5.2	1.9×10^{-4}	---	-----	2
KF-8	27N	16W	10	25.9	3.8×10^{-4}	---	-----	2
KF-83-3	30N	15W	10	4.7	9.2×10^{-5}	---	Jacob recovery	3
KF-83-3	30N	15W	10	4.7	3.2×10^{-6}	---	McWhorter modified recovery	3
KF-83-9	30N	15W	34	5.3	2.8×10^{-6}	---	Jacob recovery	3
KF-83-9	30N	15W	34	5.3	2.8×10^{-7}	---	McWhorter modified recovery	3
KF-83-8	30N	15W	27	4.6	3.5×10^{-8}	---	Jacob recovery	3
KF-83-8	30N	15W	27	4.6	3.5×10^{-4}	---	McWhorter modified recovery	3
81-23-3 (Lower Seam)	32N	13W	28	11.0	7.9×10^{-4}	6.2×10^{-4}	Jacob recovery	4
81-23-3 (Lower Seam)	32N	13W	28	11.0	3.5×10^{-5}	---	Theis	4
81-23-3 (Middle Seam)	32N	13W	28	4.6	2.5×10^{-5}	4.2×10^{-5}	Jacob recovery	4
81-23-3 (Middle Seam)	32N	13W	28	4.6	2.5×10^{-5}	---	Theis	4
81-23-3 (Upper Seam)	32N	13W	28	4.0	4.3×10^{-4}	2.5×10^{-6}	Slug test analysis	4
81-17-4 KF	32N	13W	17	12.2	2.1×10^{-4}	---	Jacob recovery	4
81-17-4 KF	32N	13W	17	12.2	1.7×10^{-4}	---	Theis	4
81-22-2 (Lower Seam)	32N	13W	22	11.0	2.0×10^{-4}	---	Jacob recovery	4
81-22-2 (Lower Seam)	32N	13W	22	11.0	1.7×10^{-4}	---	Theis	4
81-13-13 KF (Lower Seam)	32N	13W	13	4.9	6.7×10^{-4}	---	Jacob recovery	4
81-13-13 KF (Lower Seam)	32N	13W	13	4.9	6.0×10^{-4}	---	Theis	4
81-22-2 (Middle Seam)	32N	13W	22	4.6	1.4×10^{-5}	---	Jacob recovery	4
81-13-13 KF (Middle Seam)	32N	13W	13	4.6	9.5×10^{-5}	---	Jacob recovery	4
81-13-13 KF (Middle Seam)	32N	13W	13	4.6	9.5×10^{-5}	---	Theis	4
81-18-24 (Upper Seam)	32N	13W	18	3.7	8.8×10^{-4}	2.5×10^{-6}	Slug test analysis	4
81-18-24 (Upper Seam)	32N	13W	18	3.7	4.6×10^{-4}	2.5×10^{-5}	Slug test analysis	4
81-13-13 KF (Upper Seam)	32N	13W	13	4.0	1.2×10^{-4}	---	Jacob recovery	4
81-13-13 KF (Upper Seam)	32N	13W	13	4.0	1.1×10^{-4}	---	Theis	4

* b = aquifer thickness, m
K = hydraulic conductivity, cm/sec
S = storage coefficient, dimensionless

Data Source:

1. Gallo Wash mine permit
2. Navajo mine permit
3. San Juan mine permit
4. La Plata mine permit

Table 5. Summary of aquifer parameters obtained from analyses of deep test data

WELL NAME	LOCATION TWP	RNG	SEC	APPROXIMATE DEPTH INTERVAL (m)	AQUIFER PARAMETERS n	b	RSP	k	TYPE OF AQUIFER TEST	DATA SOURCE
Tiffany Glover #1	32N	06W	2	900-950	3.0-5.7	23.8	--	3.3	McKinley type curve-drawdown	1
Tiffany Glover #1	32N	06W	2	900-950	---	23.8	--	3.4	McKinley type curve-drawdown	1
Tiffany Glover #1	32N	06W	2	900-950	---	23.8	1483	3.5	Horner fall-off - injection	1
Tiffany Glover #1	32N	06W	2	900-950	---	23.8	1483	3.5	Horner fall-off - injection	1
Amoco Cedar Hills Field	32N	10W	33	800-915	---	--	--	10.0	Field performance	2
Blackwood & Nichols NEBU #212	31N	07W	1	935-977	---	43.4	1670	15.2	Horner analysis - DST data	3
Blackwood & Nichols NEBU #212	31N	07W	1	935-977	---	43.4	1679	15.3	Horner analysis - DST data	3

* n = porosity, %
  b = aquifer thickness, m
  RSP = reservoir, static pressure, psi
  k = permeability, millidarcies

Data Source:

1. GRI Final Report 85/0033
2. Presentation at field site, 1988 coalbed methane symposium field trip
3. Drill-stem test report from files of New Mexico Oil and Gas Commission, Aztec, New Mexico

application of temperature data to the calculation of lateral specific discharge.

THERMAL CHARACTERISTICS

The important thermal characteristics of the Fruitland Formation include:

- thermal conductivities for the formation lithologies
- vertical and lateral (horizontal) temperature gradients
- interval heat flow

Wells with temperature data utilized in this study are identified in Table 6.

Thermal Conductivity

Detailed thermal conductivity measurements and profiles through the Fruitland Formation are not available. Therefore, thermal conductivity data are generally limited to measurements on lithologic types. For purposes of this study, only two lithologies are assumed to comprise the Fruitland Formation aquifer interval. These lithologies are coal and sandy shale. Table 7 summarizes measured thermal conductivity values for these rock types and for water (used for porosity-correction).

The thermal conductivity of coal is low. The values shown in the table were obtained from chip samples using previously described techniques and include a correction of water-filled porosity. However, in situ coalbeds also include a cleat system which is assumed to be water-filled. Therefore, since there will be some amount of increased water-content in the coalbeds, it is expected that these measured values will be lower than the in situ thermal conductivity. For

Table 6. Wells with temperature data through the Fruitland Formation utilized in this study

WELL	LOCATION SEC	TWP	RNG	FRUITLAND DEPTH INTERVAL (m below GL)	CUMULATIVE COAL THICKNESS (m)	TEMPERATURE DATA DENSITY
Southern Ute 2-2	2	32N	9W	1085 - 1193	17.7	3 m
Kelly A #3A	15	31N	10W	835 - 911	15.2	30 m
Atlantic State #6	16	30N	10W	886 - 938	9.8	30 m
Allison #59	20	32N	6W	844 - 892	12.5	3 m
Com-G #8	32	31N	8W	945 - 1020	23.8	30 m
Roelofs A #1A	10	29N	8W	857 - 899	19.8	30 m

Table 7. Measured thermal conductivities for water, coal and sandy shale

LITHOLOGY	THERMAL CONDUCTIVITY ($x10^{-3}$ cal $cm^{-1}sec^{-1}{}^{\circ}C^{-1}$)	REFERENCE
Water	1.522 (at 47°C)	CRC Handbook of Physics and Chemistry
Coal	.88	Minier, 1987
	1.02	Reiter, unpublished data
Sandy Shale	4.80 - 5.09	Reiter and Mansure, 1983
	5.30 - 5.95	Minier, 1987
	5.15	Vacquier et al., 1988

calculations requiring coal thermal conductivity, a conservative (low) value of 1.02×10^{-3} cal $cm^{-1}sec^{-1}{}^{\circ}C^{-1}$ will be used.

Thermal conductivity values for sandy shale obtained by Reiter and Mansure (1983) range from 4.8 to 5.09×10^{-3} cal $cm^{-1}sec^{-1}{}^{\circ}C^{-1}$. Other values for this lithologic type found in the literature include 5.30 to 5.95×10^{-5} cal $cm^{-1}sec^{-1}{}^{\circ}C^{-1}$ (Minier, 1987) and 5.15×10^{-3} cal $cm^{-1}sec^{-1}{}^{\circ}C^{-1}$ (Vacquier and others, 1988). In this study a value of 5.15×10^{-3} cal $cm^{-1}sec^{-1}{}^{\circ}C^{-1}$ will be assumed for all calculations requiring the thermal conductivity of sandy shale.

Lateral Temperature Gradient

As previously discussed, geothermal studies in the San Juan Basin indicate a systematic decrease in heat flow from the San Juan Mountains, north of the basin, southward into the basin (Figure 10). This change in heat flow suggests that a lateral (horizontal) temperature gradient should exist. To determine a lateral temperature gradient, temperatures from the same stratigraphic interval at approximately the same depth from two or more locations on a line trending perpendicular to the isoheat-flow contours need to be determined. From the six wells selected for use in this study, five well sets with these characteristics are available. Table 8 identifies these well sets and summarizes the calculations for the lateral temperature gradients. Review of this table indicates that north-south lateral temperature gradients in the study area range from 1.0×10^{-4} to 4.8×10^{-4} °C/meter.

Vertical Temperature Gradients

As previously discussed vertical temperature profiles were obtained from numerous wells in the San Juan Basin by Reiter et al. as

Table 8. Wells and temperature data used to estimate lateral temperature gradients

WELL COMBINATION	FRUITLAND FORMATION ELEVATION INTERVAL (m-msl)	DISTANCE BETWEEN WELLS (m)	TEMPERATURE AT MIDDLE OF FRUITLAND FORMATION (°C)	ESTIMATED LATERAL TEMPERATURE GRADIENTS ($x10^{-4}$ °C/m)
Southern Ute 2-2/Kelly A #3A	1077-1022/1061- 985	17,931	54.3/45.8	4.8
Kelly A #1A/Atlantic State #6	1061- 985/1085-1034	10,163	45.8/43.2	2.5
Southern Ute 2-2/Atlantic State #6	1077-1022/1085-1034	28,094	54.3/43.2	4.0
Allison #59/Com G #8	844- 900/ 945-1023	23,185	48.4/46.1	1.0
Allison #59/Roelofs A #1A	844- 900/ 849- 932	34,937*	48.4/41.0	2.1

* Distance along assumed flow line

part of a regional study to define the geothermal and heat flow characteristics of this area. In general, temperature data from shale units below the Fruitland Formation (i.e., Lewis and Mancos Shales) were utilized for the heat flow calculations. However, temperature data were obtained through the Fruitland interval at fifteen locations. Figure 24 shows a temperature versus depth plot from the surface through the Fruitland Formation into the Lewis shale at one of these locations. Review of this figure indicates a gradient increase through the Fruitland Formation. This increase is typical of all the temperature data obtained in the basin.

Variations in temperature gradients through a stratigraphic interval primarily reflect changes in thermal conductivity. Generally, the lower the thermal conductivity, the higher the temperature gradient. Therefore, since the Fruitland Formation contains a significant proportion of coal (low thermal conductivity), it is not surprising that the temperature gradient increases through this unit. However, other factors including groundwater flow can impact temperature gradients. For example, upward vertical flow and lateral flow from a region of higher temperature to a region of lower temperature can increase temperature gradients. Since the latter case is generally operative in the San Juan Basin (see Figure 10 and 23), some amount of the increase in Fruitland Formation temperature gradient may also be due to lateral advection.

Figure 25 is a composite study area map showing the wells used in this study in relationship to the conductive heat flow contours (Figure 10) and the Fruitland Formation potentiometric surface (Figure 23). Selection of these wells for this study was done for two reasons. The first reason was good data density (3 m) in the Fruitland interval.

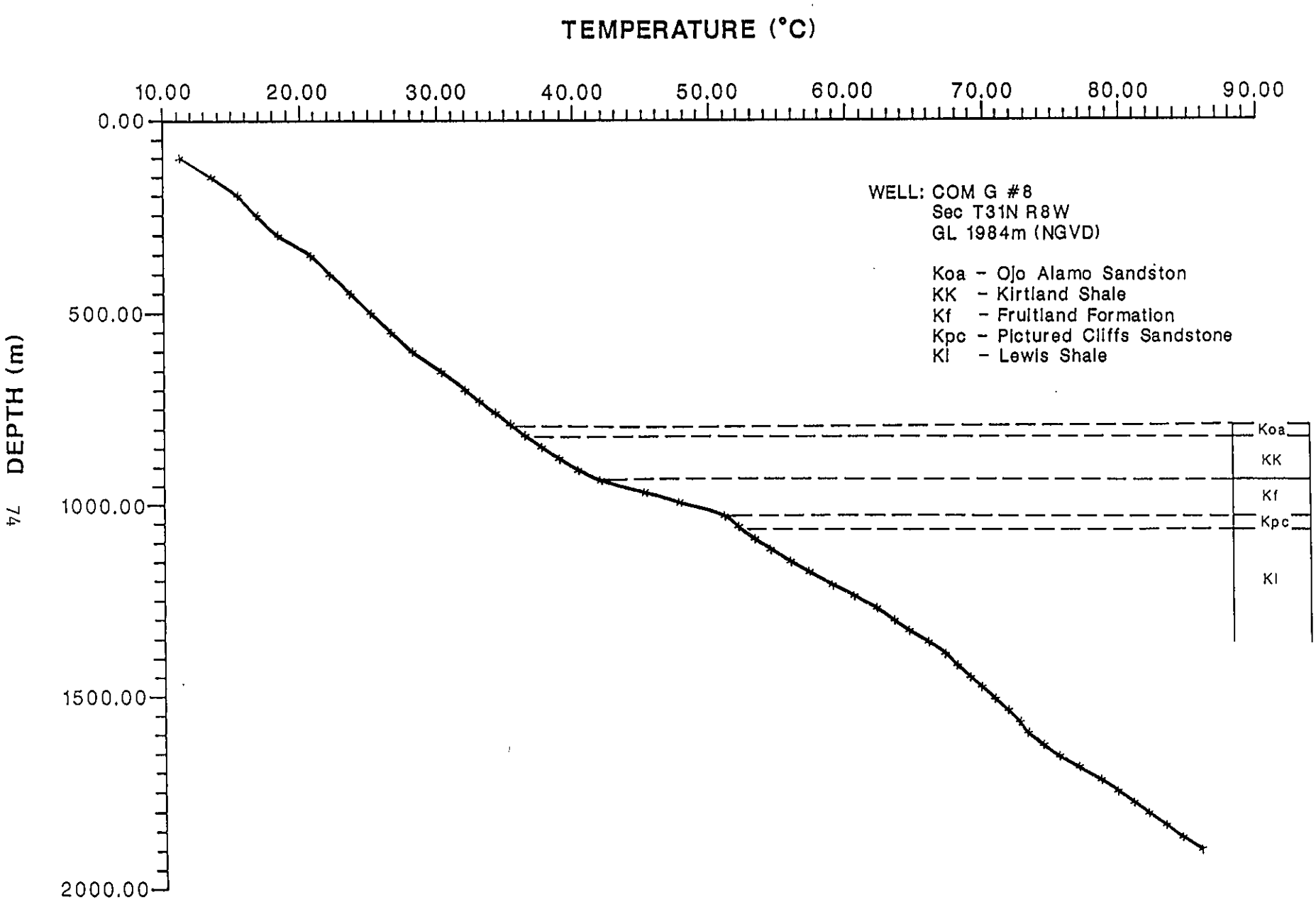

Figure 24 - Typical temperature versus depth plot of San Juan Basin temperature data

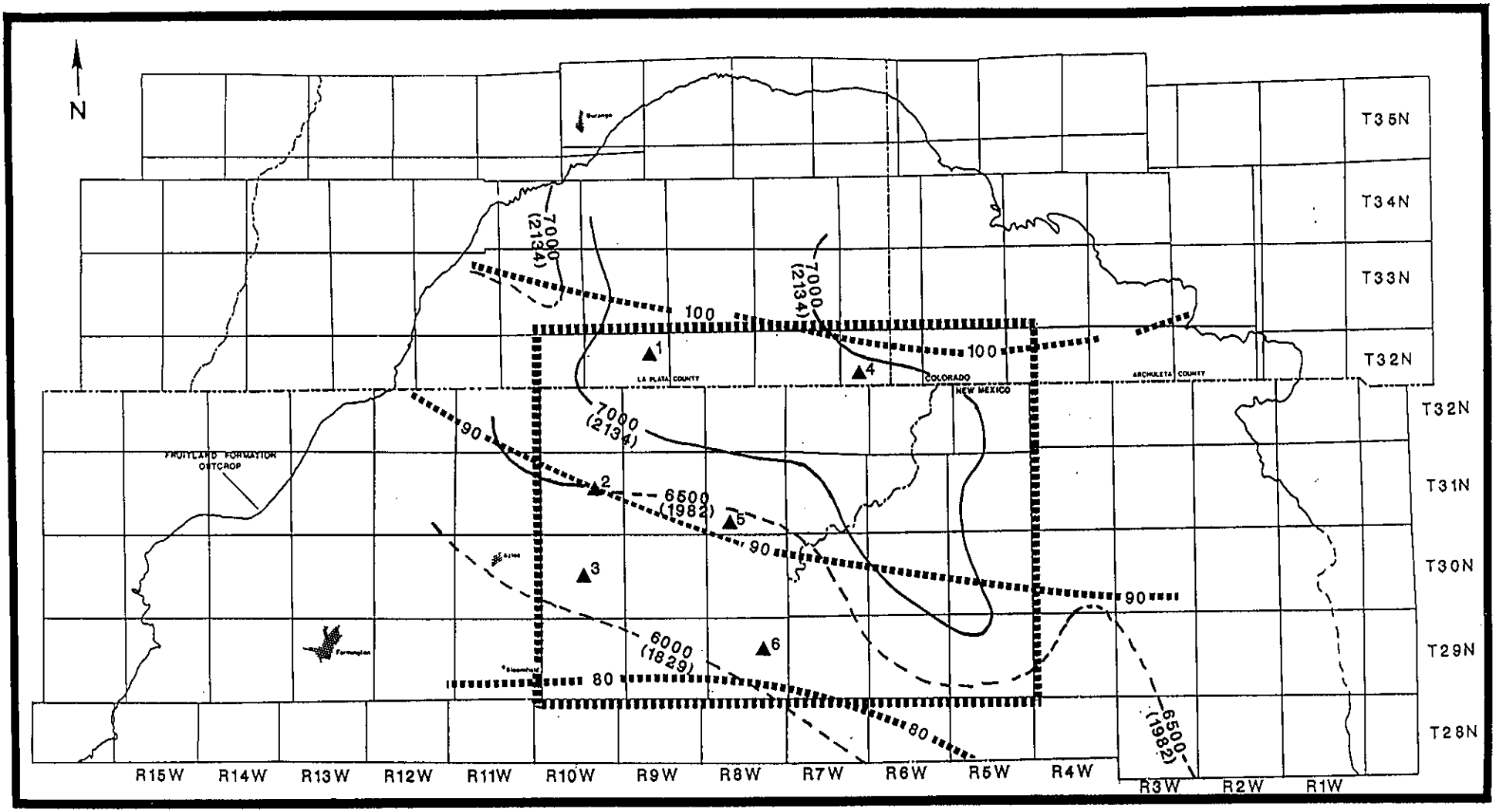

0 5km 10km
APPROXIMATE SCALE

STUDY AREA

▲1 Location of wells used in this study
1. Southern Ute #2-2
2. Kelly A#3A
3. Atlantic State #6
4. Allison #59
5. Com G#8
6. Roelofs A#1A

90 HEAT FLOW CONTOURS
CONTOUR INTERVAL - 10 mW/m^2

6000 (1829) FRUITLAND FM
HYDRAULIC HEAD CONTOURS
(dashed where approximate)
CONTOUR INTERVAL - 500 feet
(152 meters)

Figure 25 - Composite study area map

The second reason was that the lateral comparison of Fruitland Formation temperature data between the selected wells was approximately from the same elevation datum perpendicular to heat flow contours (Figure 10) and parallel to groundwater flow direction (Figure 23). Figures 26, 27 and 28 are Fruitland Formation stratigraphic cross-sections in the study area. Review of these figures indicates that the Fruitland Formation is generally between the elevations of 950 to 1100 meters.

Figures 29 and 30 show detailed (3 m) temperature data through the Fruitland Formation and their relationship to the stratigraphic position of coalbeds in Southern Ute 2-2 and Allison #59. Interpretations of Fruitland Formation coal intervals for the wells utilized in this study were done using geophysical logs, primarily compensated formation density logs, from either the actual well or from the nearest off-set well with available logs. In the cases where off-set well logs were used, interval elevation corrections were employed. Figure 29 (Southern Ute 2-2) shows a significant increase in the temperature gradient between the depths of 1110 and 1140 meters. This 30 meter interval includes approximately 17 meters of coal in individual seams ranging from 1 meter to 9 meters in thickness. The temperature gradient increases from a range of .036 to .069 °C/m in the immediately underlying units (tongue of Pictured Cliffs sandstone and thin Fruitland interval) up to .174 °C/m near the top of the basal Fruitland coal interval. Figure 30 (Allison #59) shows a somewhat more complicated profile. In this well the Fruitland Formation contains two well-developed coal intervals between the depths of 845 and 893 meters. The temperature gradient through this interval shows two distinct peaks of approximately .185 - .190 °C/m generally correlatable to the main

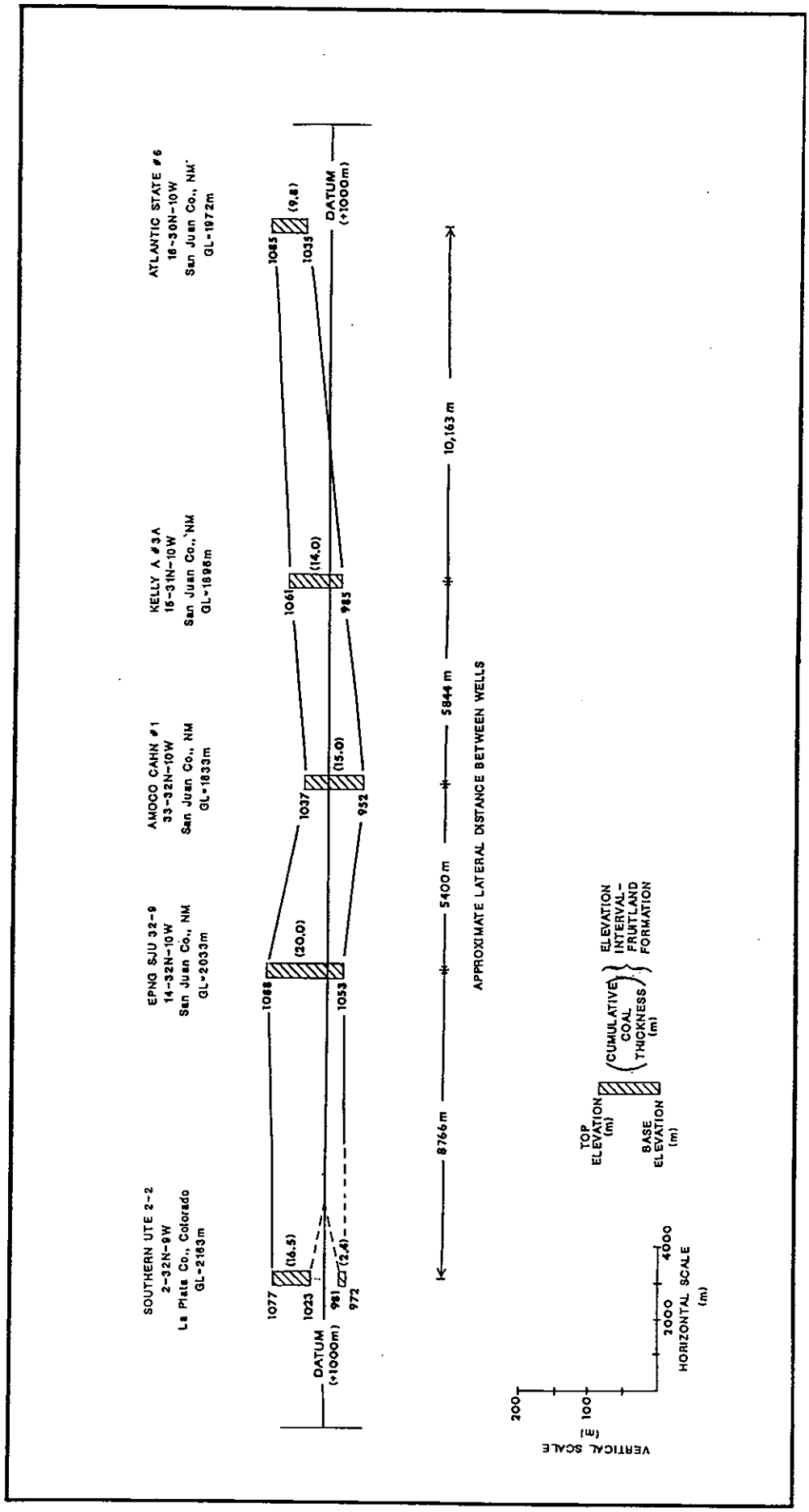

Figure 26 - Schematic cross-section of the Fruitland Formation between Southern Ute #2-2 and Atlantic State #6

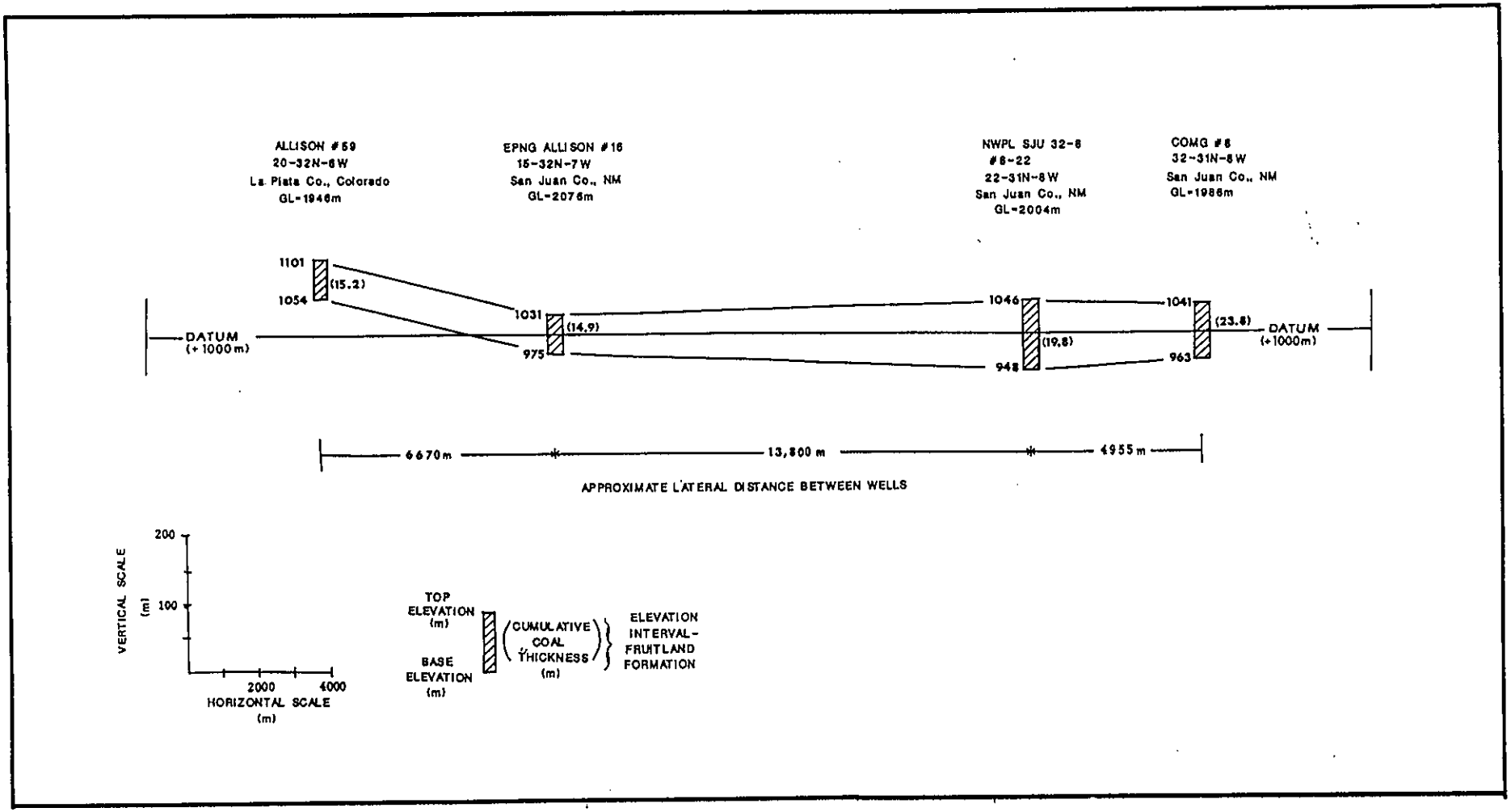

Figure 27 – Schematic cross-section of the Fruitland Formation between Allison #59 and COMG #8

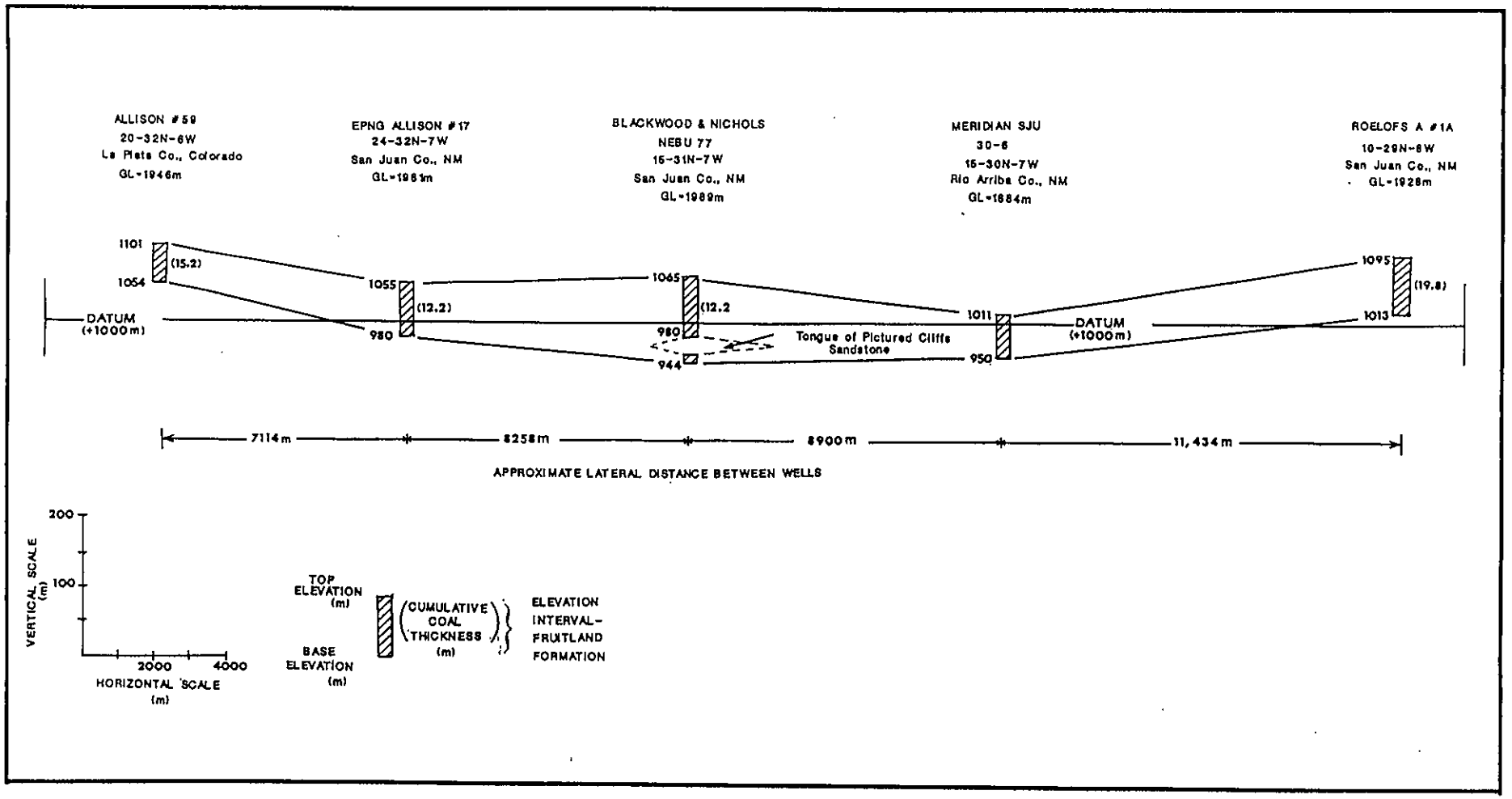

Figure 28 - Schematic cross-section of the Fruitland Formation between Allison #59 and Roelofs A #1A

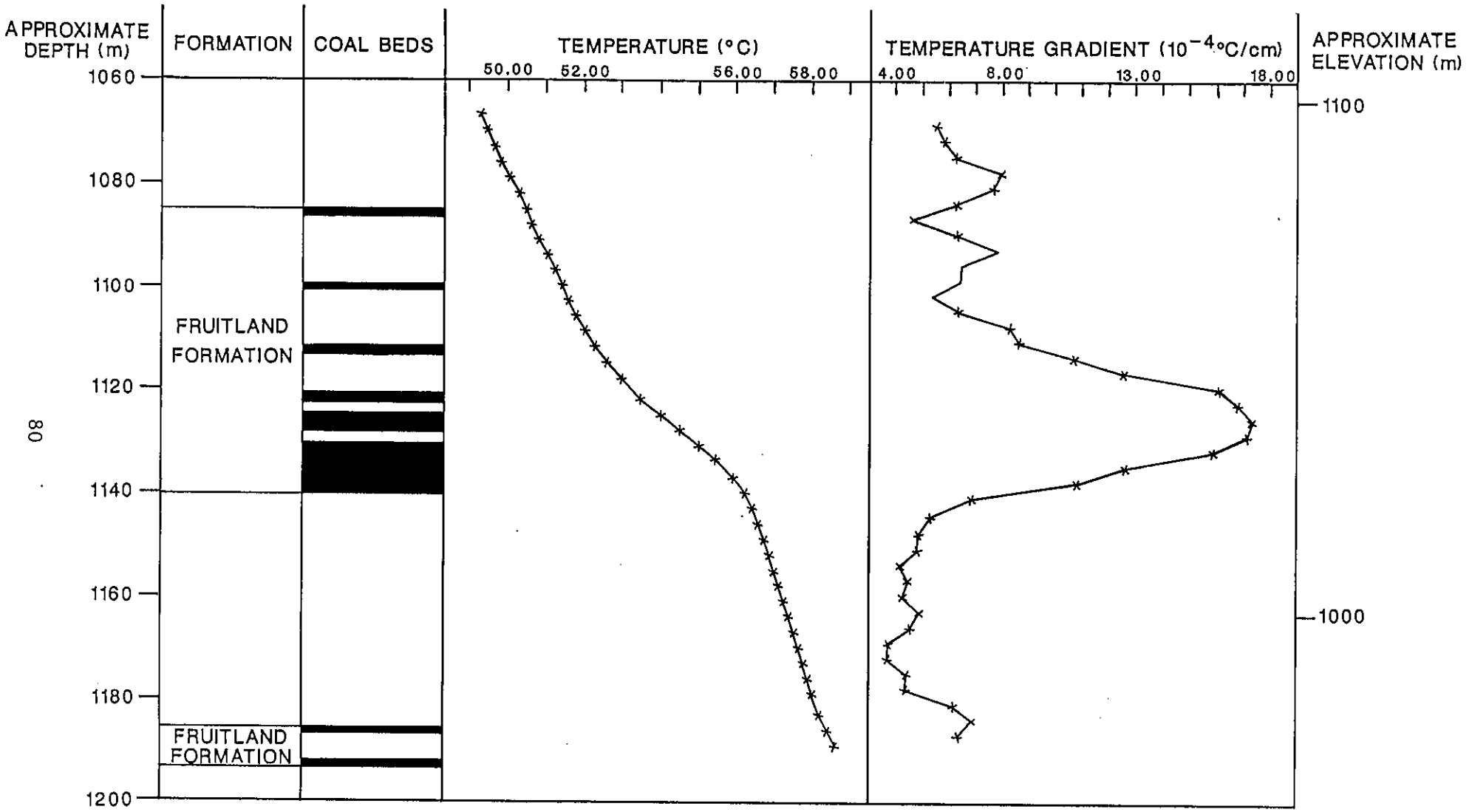

Figure 29 – Plots of Fruitland Formation temperature and temperature gradient versus depth at the Southern Ute 2-2 well.

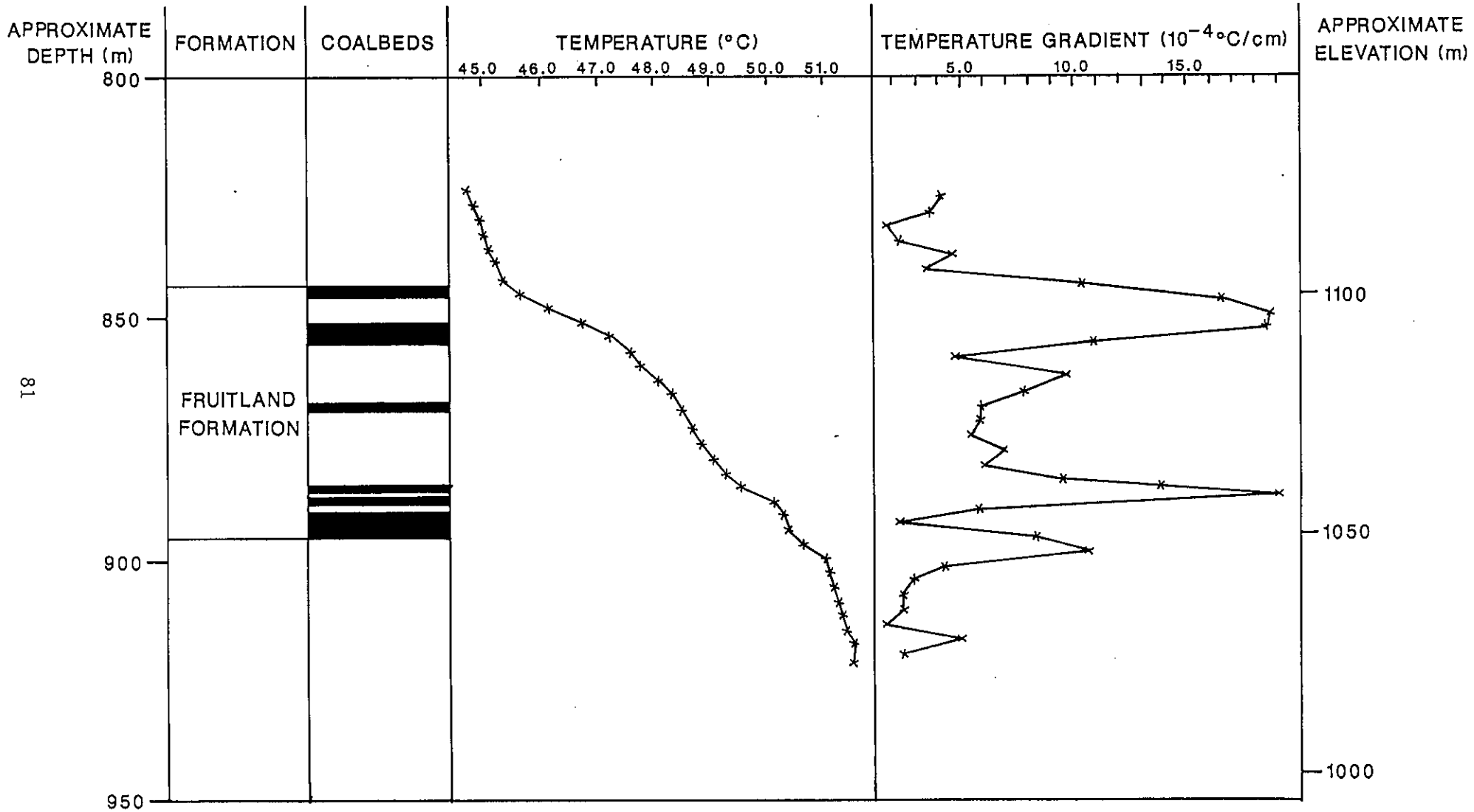

Figure 30 – Plots of Fruitland Formation temperature and temperature gradient versus depth at the Allison #59 well.

coal intervals. These peaks and the intervening temperature gradient of .05 to .07 °C/m are higher than the temperature gradients of the immediately underlying and overlying units (.02 to .04 °C/m).

Figure 31, 32, 33, and 34 show less detailed (30 meters) temperature data through the Fruitland Formation. Review of these figures, indicates that while detailed correlations between high gradients and well developed coal intervals are not possible, a general trend of significantly increased temperature gradients within the Fruitland Formation is apparent.

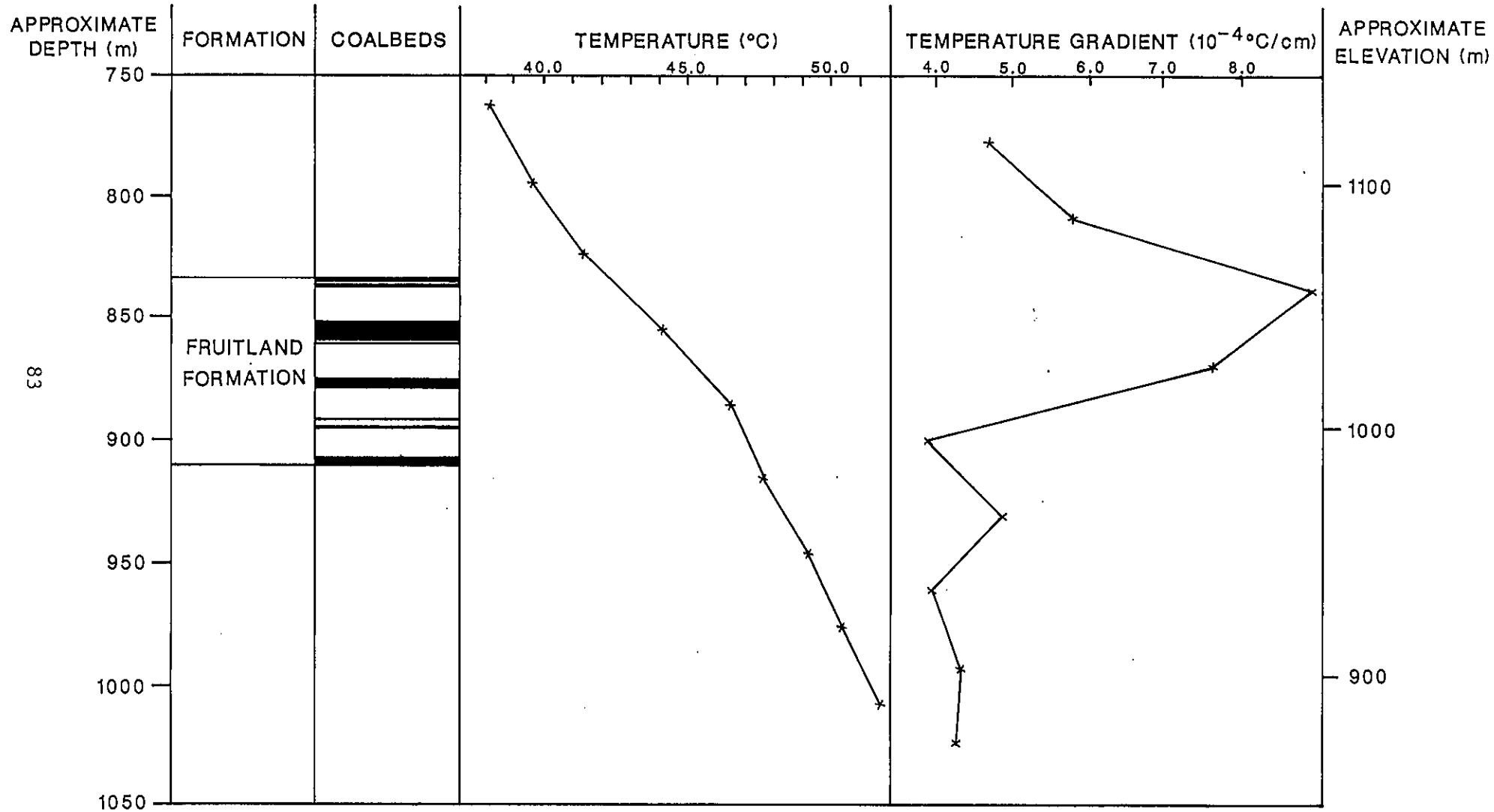

Figure 31 - Plots of Fruitland Formation temperature and temperature gradient versus depth at the Kelly A #3A well.

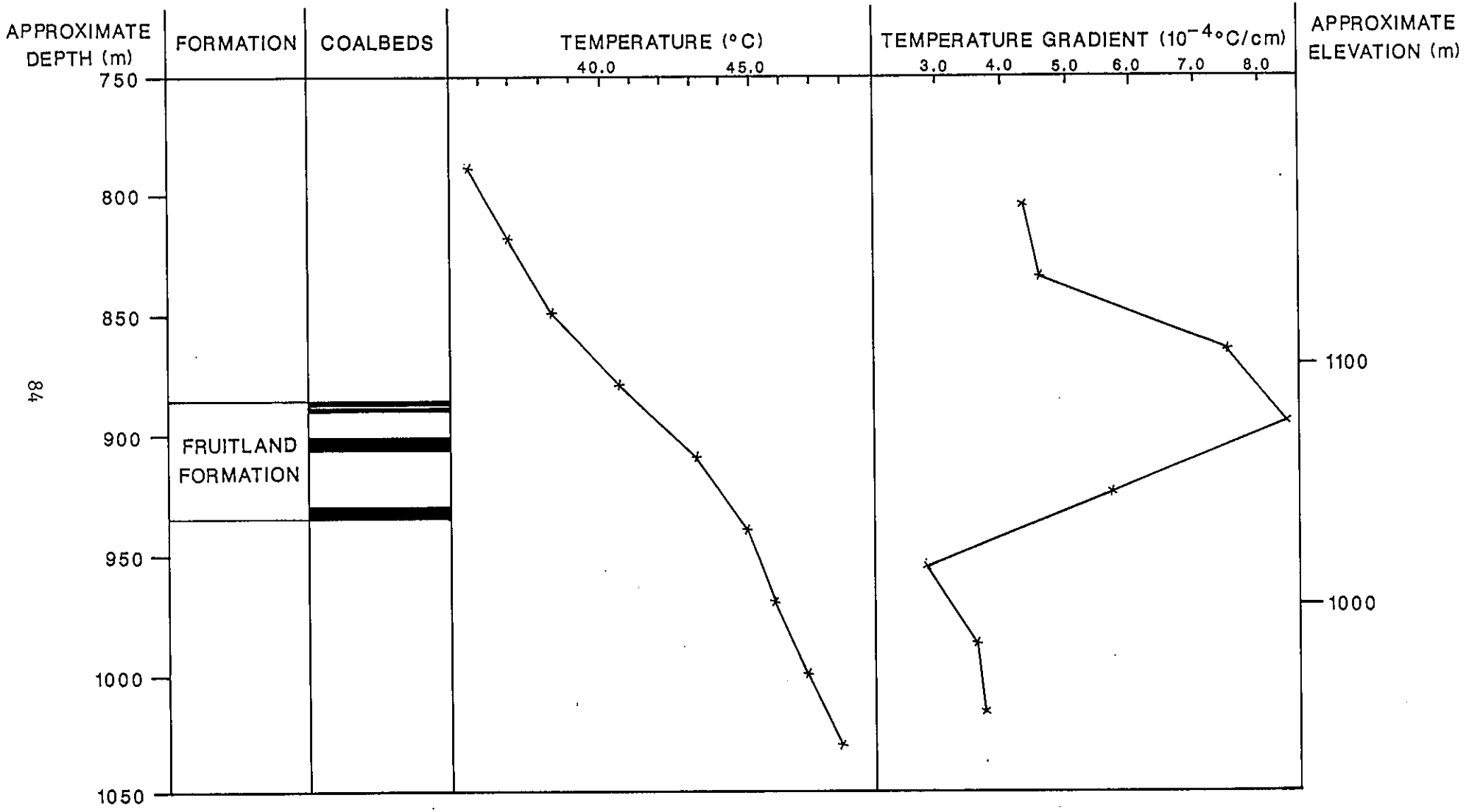

Figure 32 – Plots of Fruitland Formation temperature and temperature gradient versus depth at the Atlantic State #6 well.

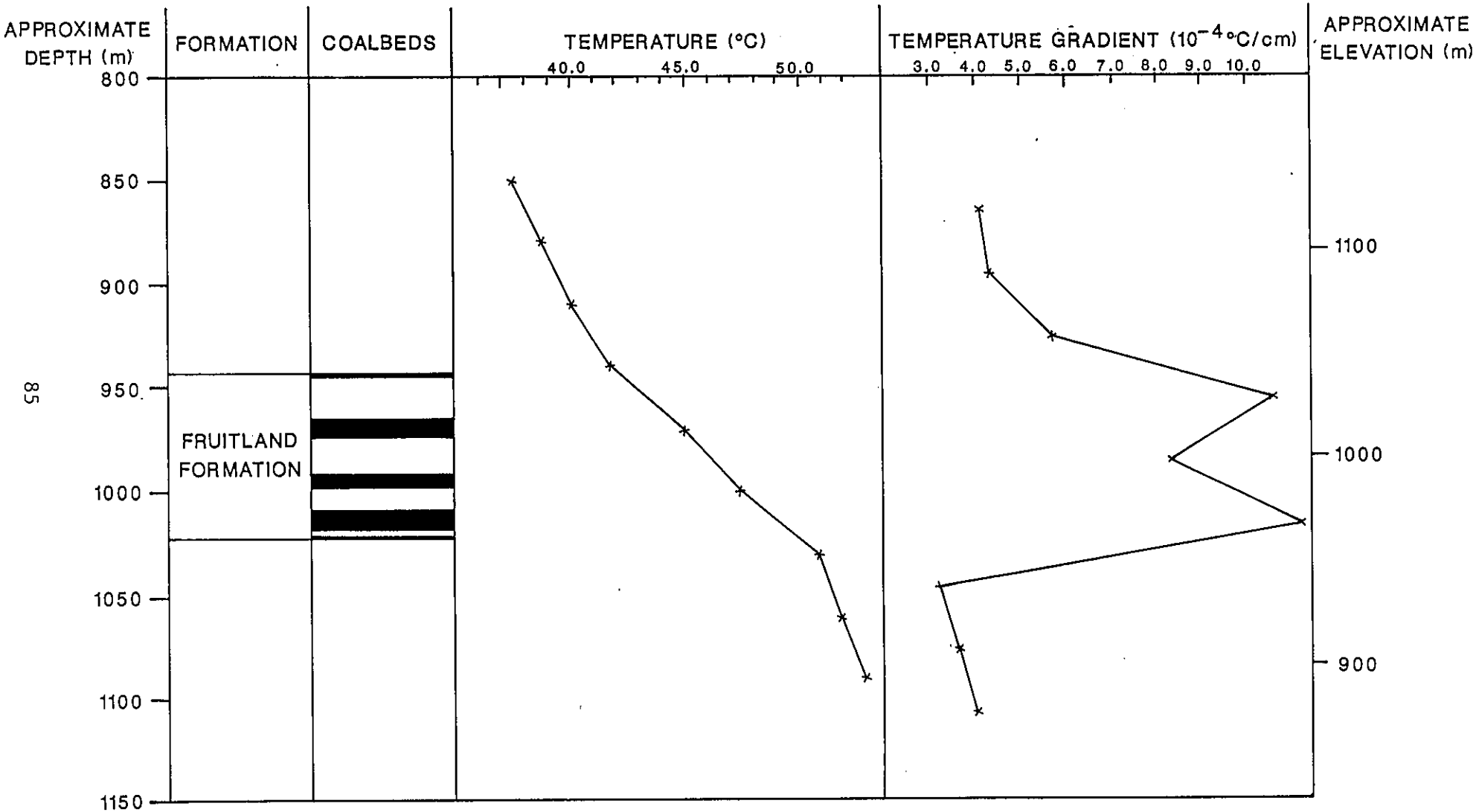

Figure 33 – Plots of Fruitland Formation temperature and temperature gradient versus depth at the Com G #8 well.

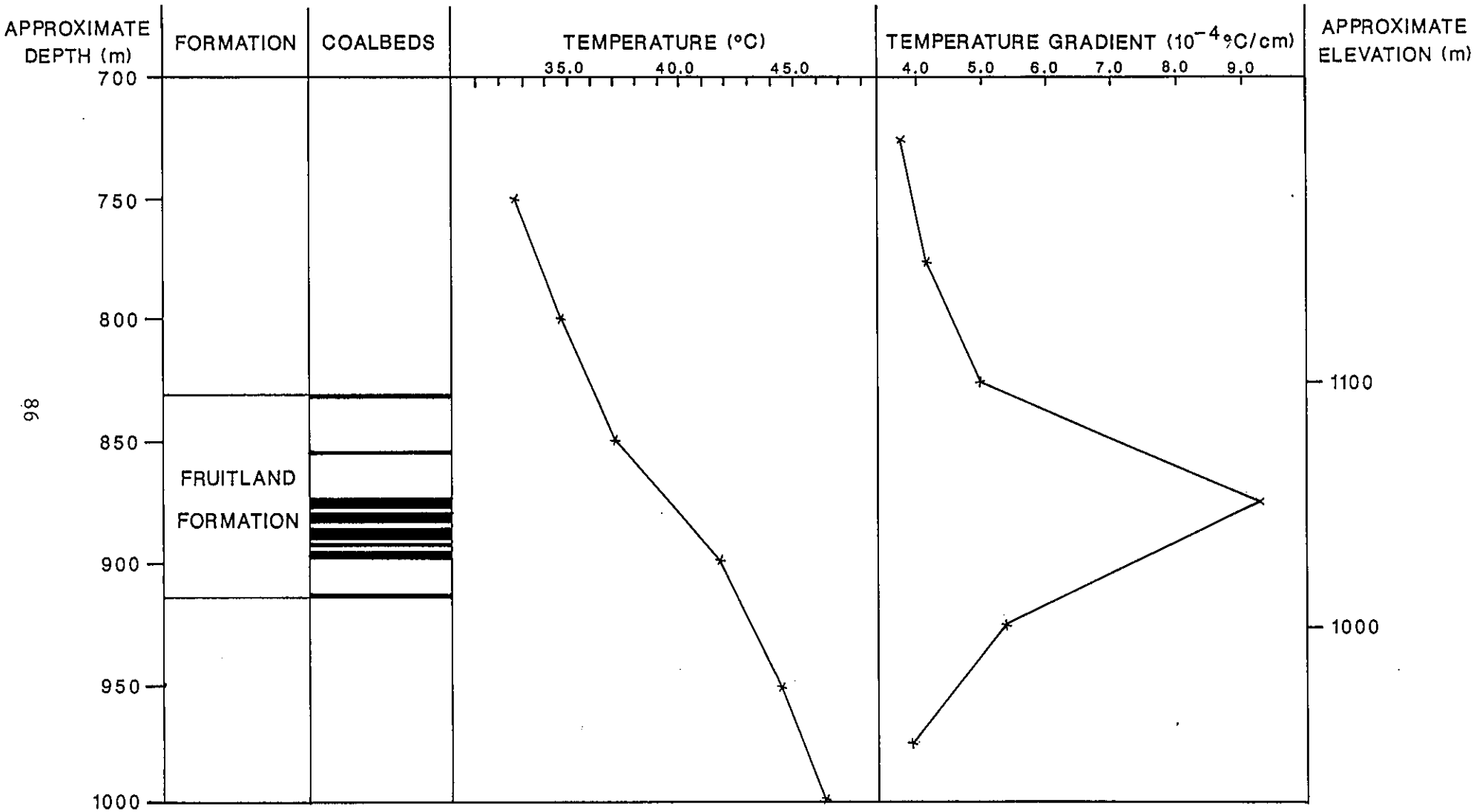

Figure 34 – Plots of Fruitland Formation temperature and temperature gradient versus depth at the Roelofs A #1A well.

Interval Heat Flow

Interval heat flow is the product of the vertical temperature gradient and the harmonic mean thermal conductivity across the interval. In a steady-state, non-perturbed thermal system, interval heat flow equals conductive heat flow at that site. Perturbations to the thermal system include local topography, climatic changes, erosion/sedimentation and groundwater advection. In general the effects of these perturbations tend to dampen out with increasing depth. However, groundwater advection can influence interval heat flows to the depths considered in this study.

One method of presenting and analyzing interval heat flow data is to plot heat flow ($K_T \Delta T/\Delta z$) versus temperature (T). In general, if there is no perturbations caused by lateral groundwater flow, this type of plot should show linear trends. Mansure and Reiter (1979), uses this type of plot to analyze vertical groundwater advection. A discussion of this technique was presented previously in this study. However if these plots are not linear and exhibit some significant heat flow variation, then some additional factors besides vertical advection must be operative in the perturbed interval. In intervals that show an elevated heat flow these factors could include laterally advected heat transport from a region of higher heat flow, lower than assumed interval thermal conductivity, or in-place heat generation. For purposes of this study, the first factor, lateral advection, is considered to be the primary reason for observed elevated heat flow. While differences in interval thermal conductivity are certainly a possibility, the necessary thermal conductivity data are generally lacking. The assumed thermal conductivity values for the Fruitland Formation lithologies are intended to be conservative (low) but

realistic. However, it is recognized that a lower interval thermal conductivity is possible. In the Fruitland Formation, thermal conductivity is most sensitive to cumulative coal thickness. Using the assumed coal and sandy shale values of 1.02×10^{-3} cal $cm^{-1}sec^{-1}{}^{\circ}C^{-1}$ and 5.15×10^{-3} cal $cm^{-1}sec^{-1}{}^{\circ}C^{-1}$, respectively, an increase in coal thickness of 10 percent will result in an approximate 5 percent decrease in interval thermal conductivity. The last factor, the potential for in-place heat generation, is not considered in this study.

Figures 35 and 36 compare temperature gradient versus temperature ($\Delta T/\Delta z$ vs. T) plots and calculated heat flow versus temperature (K_T $\Delta T/\Delta z$ vs. T) plots across the Fruitland Formation for the wells with 3 meter data density. Review of the K_T $\Delta T/\Delta z$ vs. T plot in Figure 35 (Southern Ute 2-2) does not show any significant linear trends. However, heat flow peaks in this figure generally correspond to coal intervals, with the largest peak (8.9×10^{-6} cal $cm^{-2}sec^{-1}$) occurring in the thickest coal interval. In general, these same characteristics are shown in Figure 36 (Allison #59).

Figures 37, 38, 39 and 40 are the same types of plots for the wells with 30 meter data density. Heat flow peaks in these figures are not as well correlated with the coals. Over-all, these figures indicate that heat flow in the Fruitland Formation is generally elevated and shows very few linear trends. These characteristics, coupled with the regional conductive heat flow trend (Figure 10) and the groundwater flow patterns (Figure 23), suggest that the elevated heat flow is associated with lateral advection in the Fruitland Formation coal intervals.

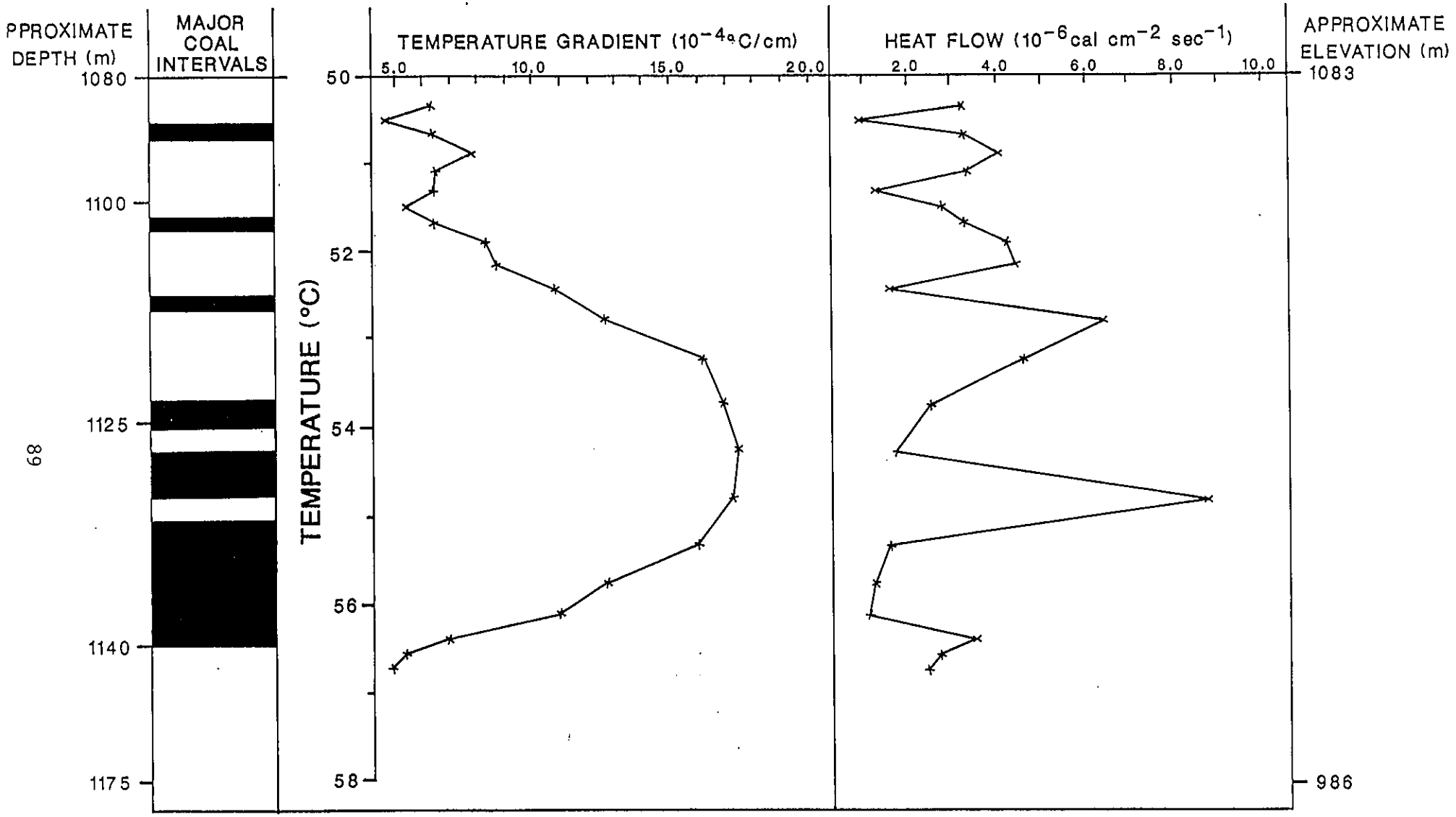

Figure 35 - Plots of Fruitland Formation temperature gradient and calculated heat-flow versus temperature at the Southern Ute 2-2 well.

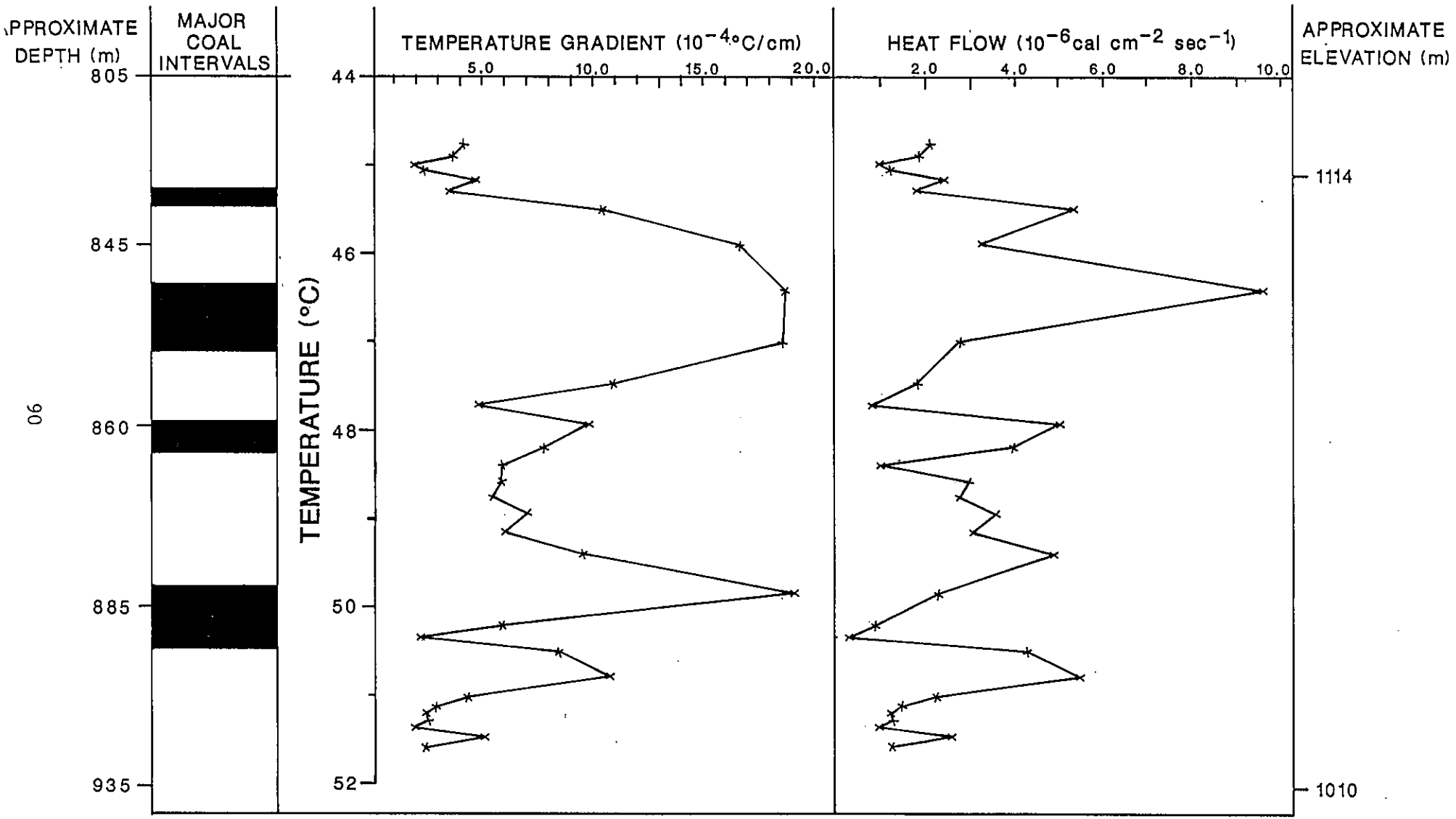

Figure 36 – Plots of Fruitland Formation temperature gradient and calculated heat-flow versus temperature at the Allison #59 well.

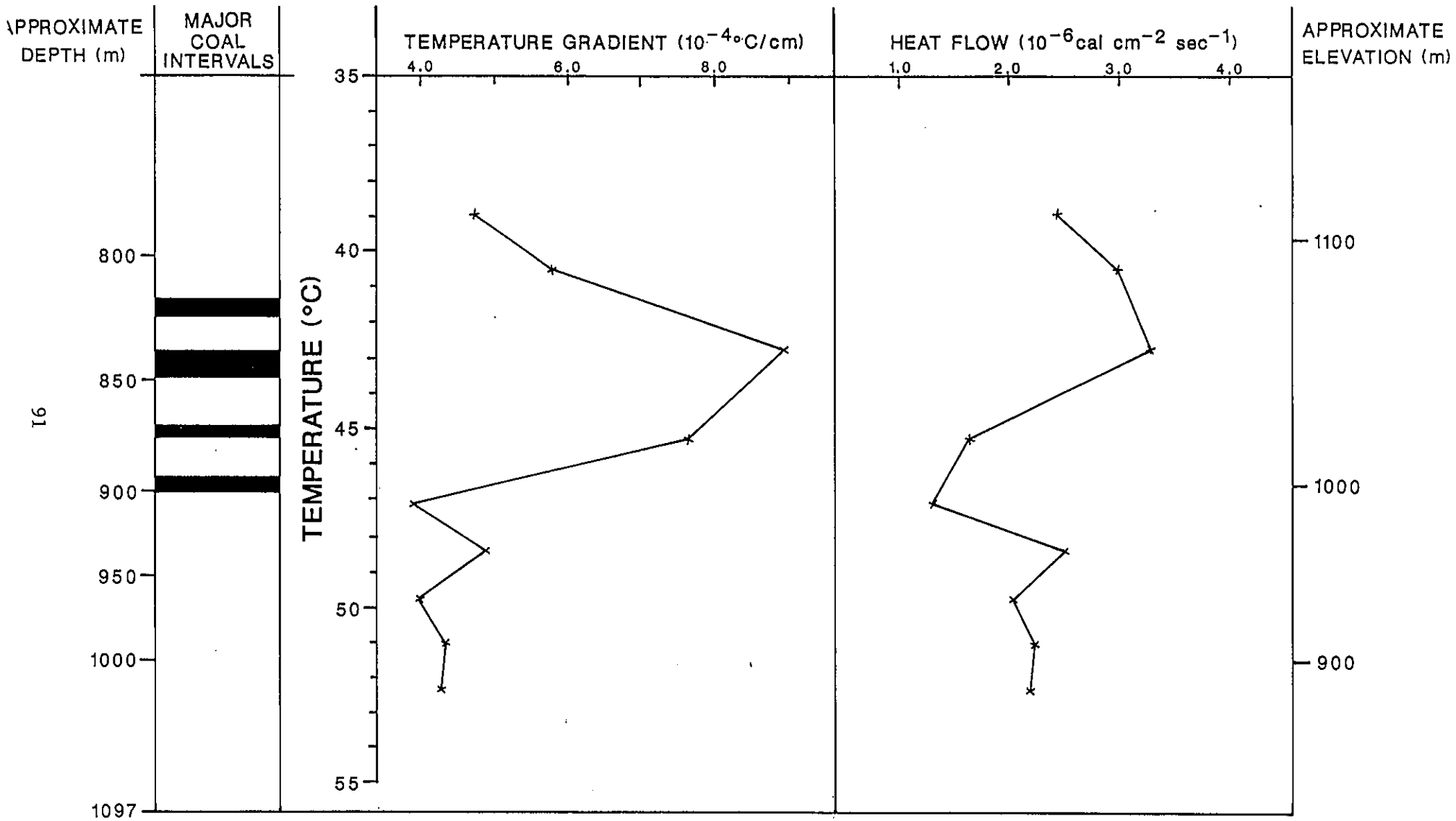

Figure 37 - Plots of Fruitland Formation temperature gradient and calculated heat-flow versus temperature at the Kelly A #3A well.

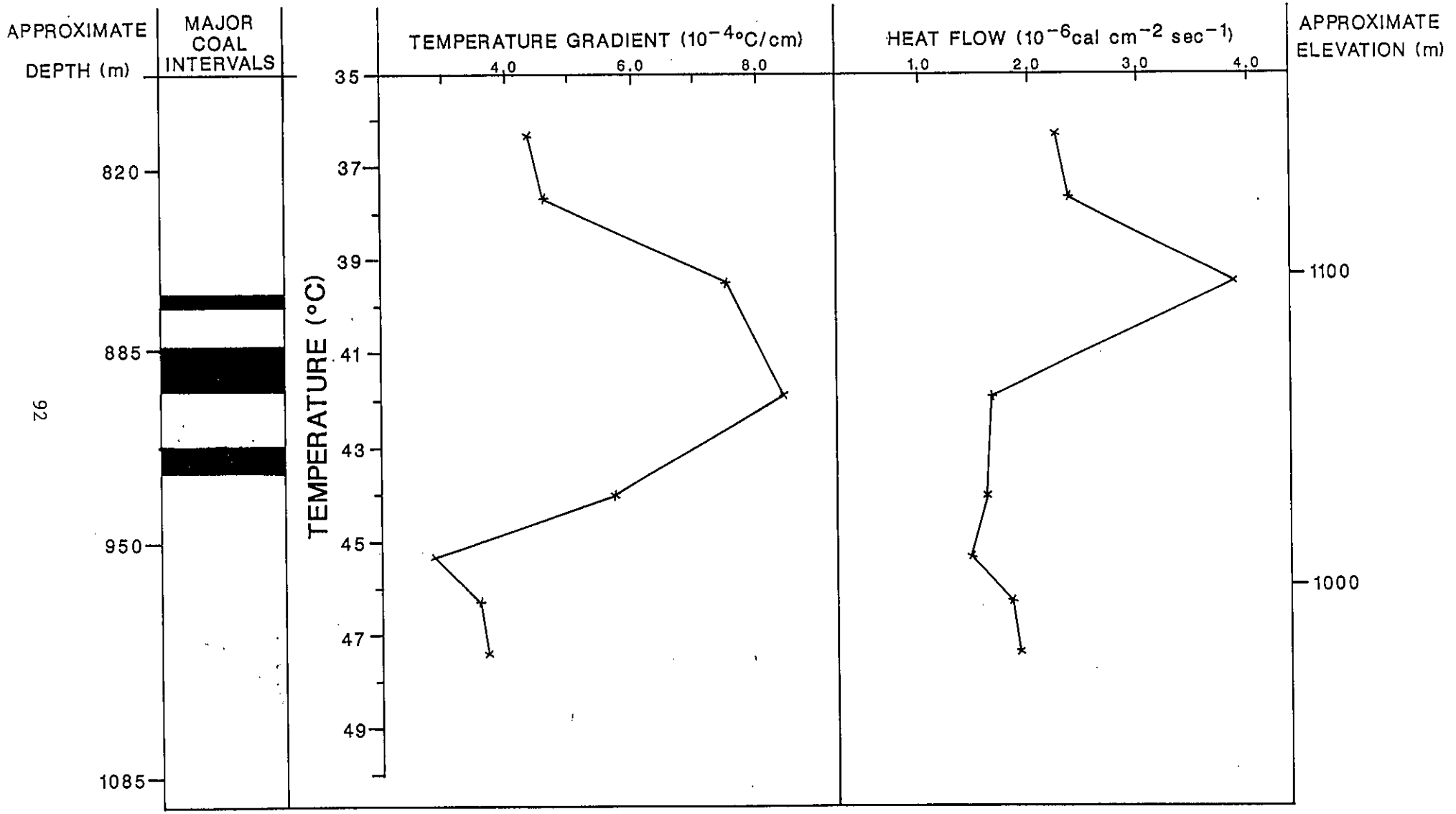

Figure 38 – Plots of Fruitland Formation temperature gradient and calculated heat-flow versus temperature at the Atlantic State #6 well.

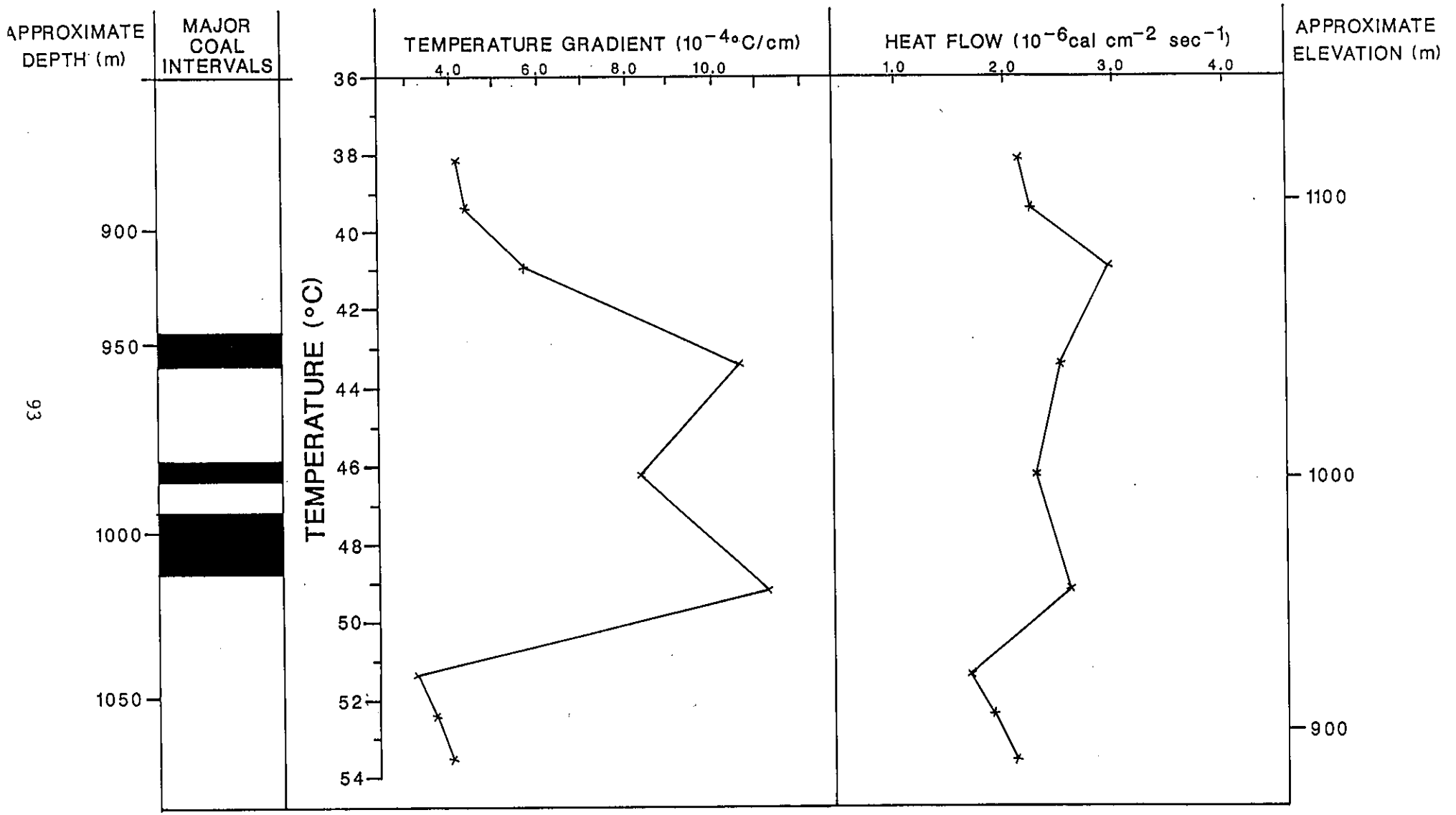

Figure 39 – Plots of the Fruitland Formation temperature gradient and calculated heat-flow versus temperature at the Com G #8 well.

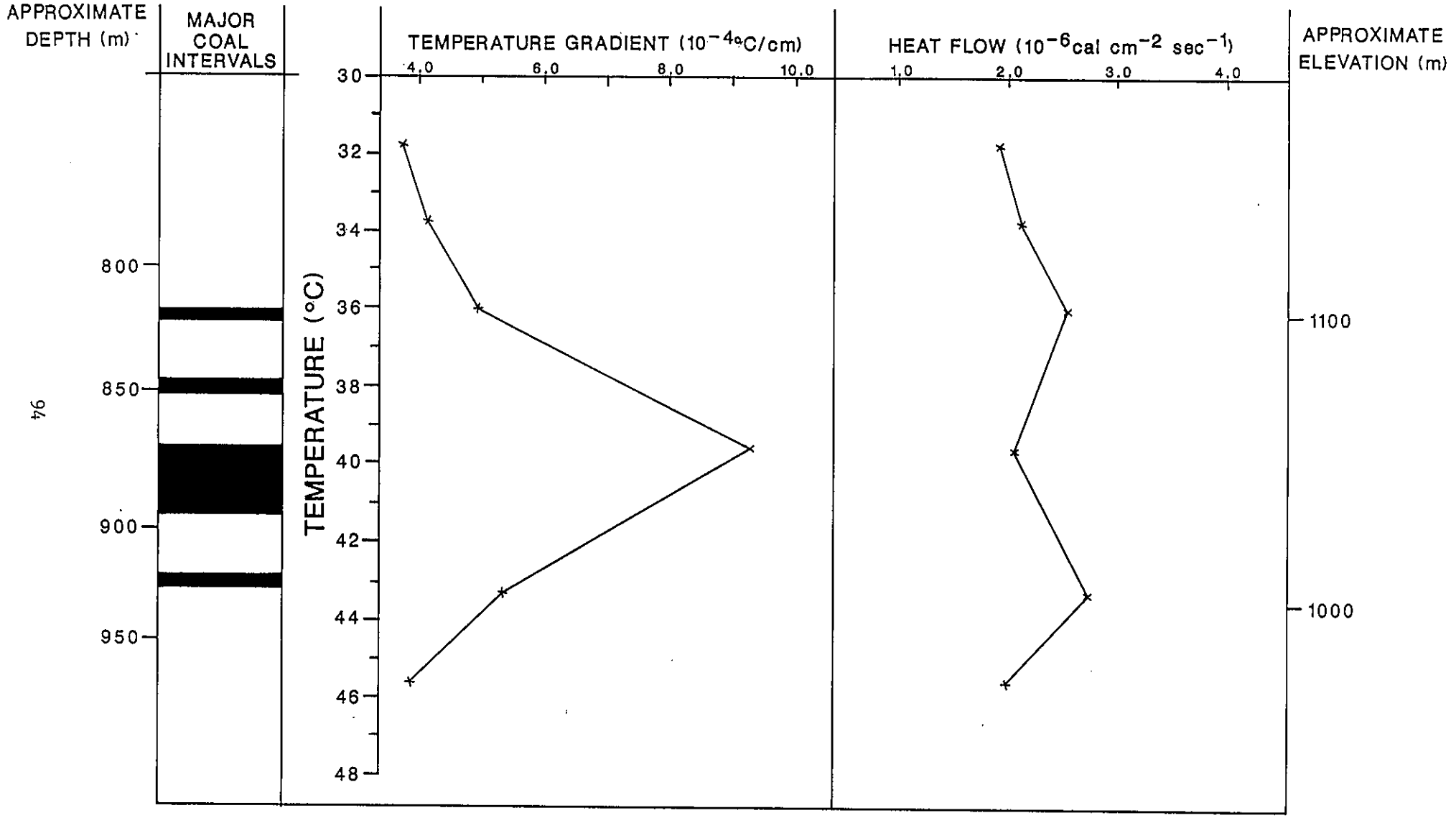

Figure 40 – Plots of Fruitland Formation temperature gradient and calculated heat-flow versus temperature at the Roelofs A #1A well.

SUMMARY

In this section characteristics important to defining a Fruitland Formation coal interval aquifer have been discussed. These characteristics can be summarized as follows.

1. Coalbeds are the most laterally continuous lithologies in the Fruitland Formation. Lateral continuity of thick coalbeds has been shown to range from approximately 24 to 40 km. Within the study area two or more thick coalbeds overlap in an echelon fashion. Assuming some degree of hydraulic connection between these overlapping coalbeds, a laterally continuous thick coalbed can be hypothesized.

2. Measurements of coal porosity and permeability are difficult and may not provide the complete picture of the aquifer/reservoir characteristics of coals. Fracture porosity and permeability are critical parameters that are difficult to estimate due to laboratory limitations and the stress-dependent nature of fracture aperture.

3. Aquifer/reservoir tests in coal intervals indicate the hydraulic conductivity is within the 10^{-5} to 10^{-6} cm/sec orders of magnitude. However, these values may be affected by the stress-sensitive nature of coal permeability.

4. Comparison of Fruitland Formation hydraulic head within the study area with the estimated potentiometric surfaces of the overlying and underlying aquifers (Ojo Alamo and Mesa Verde Group sandstones, respectively) suggests that the Fruitland Formation has the highest hydraulic potential in this group. This would indicate that the Fruitland Formation is a significant regional aquifer.

5. Elevated heat flow through the Fruitland Formation is interpreted to be due to laterally advected heat from areas of higher conductive heat flow toward areas of lower conductive heat flow.

In addition to these characteristics, temperature distribution data within the study area can be analyzed to give an estimate of lateral groundwater velocity. Approaches to this analysis and results from several well combinations are discussed in the following section.

ESTIMATION OF LATERAL GROUNDWATER VELOCITY

APPROACHES TO ANALYSES

Two approaches to the analysis of temperature distribution data for estimation of lateral groundwater velocity in the Fruitland Formation are used in this study. The first of these approaches is based on solutions to the differential equation defining conductive and advective heat transfer. The second approach is based on the analyses of vertical variation in heat flow and is herein referred to as the Excess Heat Flow approach.

Solutions to Governing Equation

Equation 27 is the most general form of the differential equation defining three-dimensional conductive and advective heat transfer within a control volume. To adapt this equation to analyze the effects of lateral fluid flow on heat transfer, the following simplifying assumptions are made (Stallman, 1963):

1. Both the thermal and flow field are at steady-state.
2. Groundwater flow is important only in the x-direction.
3. Heat flow is important only in the z-direction.

Using these assumptions, Equation 27 simplifies to:

$$\frac{\partial^2 T}{\partial z^2} = \frac{c_{pw}\rho_w}{K_T} (V_x) \frac{\partial T}{\partial x} \qquad (37)$$

where,

T = temperature

c_{pw} = specific heat of pure water

ρ_w = density of water

K_T = thermal conductivity of the fluid saturated porous media

V_x = groundwater velocity (specific discharge) in the x-direction

Solutions to this equation provide the basis for the first of two approaches to the analysis of temperature distribution data to determine lateral groundwater velocity.

Implicit Analytical Solution

Using all the previously stated assumptions, the governing partial differential equation (PDE) describing conductive and advective heat transfer is equation 37. This equation can be reformulated as a second-order ordinary differential equation (ODE) by assuming that:

$$\frac{\partial T}{\partial x} - \frac{T(z)-T_o}{\Delta x}$$

where

T_o = T at x = 0 (up-gradient temperature)

$\Delta x = x - x_o$ (distance between location of T_o and location of T(z))

The resulting ODE is:

$$\frac{d^2T}{dz^2} = \frac{c_{pw}\rho_w V_x}{K_T} \frac{(T(z)-T_o)}{\Delta x} \qquad (38)$$

In this equation the thermal advective leakage factor is defined as:

$$B = \left[\frac{K_T \Delta x}{c_{pw}\rho_w V_x}\right]^{1/2} \qquad (39)$$

Subtracting the right-hand side of equation 38 and substituting equation 39 results in:

$$\frac{d^2T}{dz^2} - \frac{(T(z)-T_o)}{B^2} = 0 \qquad (40)$$

This equation is analogous to the 1-D equation describing head distribution in a steady-state, isotropic, homogeneous, confined leaky aquifer, and describes 1-D (vertical) conductive heat flux through an isotropic, homogeneous layer, with some amount of heat either added to or subtracted from this layer due to lateral advection (leakage). Figure 41 is a schematic diagram showing conductive heat transfer and laterally advected heat flux (leakage) in an aquifer unit. Figure 41 shows that the boundary conditions for equation 40 are:

@ z = 0 T(z) = T1

@ z = L T(z) = T2

Assuming a finite domain and solving for these boundary conditions results in the following analytical solution:

$$T(z) = T_o + \frac{T2-T_o}{\sinh(L/B)} \sinh(z/B) + \frac{T1-T_o}{\sinh(L/B)} \sinh\left[\frac{L-z}{B}\right] \qquad (41)$$

In this study the unknown parameter is lateral groundwater velocity (V_x). This parameter is embedded in the leakage factor (B) and cannot be solved for directly using this approach. However, given a measured temperature profile it can be solved for implicitly by matching the measured temperature with a calculated temperature by varying V_x. This approach is used in a Fortran program developed for this study. In this program the secant method is used to minimize the following function:

$$\text{Tempfn} = \text{Tzm} - \text{Tzc} \qquad (42)$$

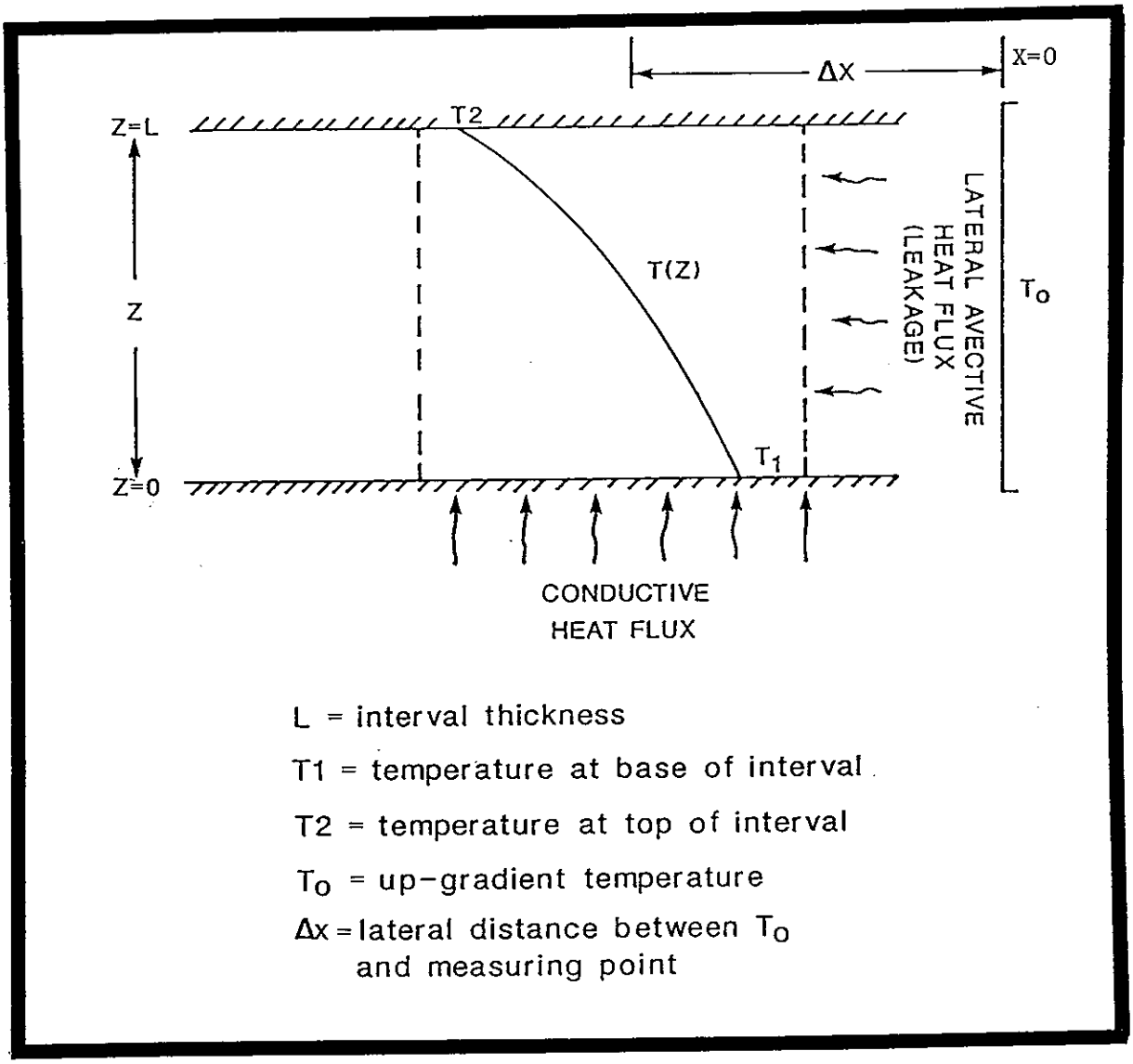

Figure 41 - Schematic diagram showing 1-D (vertical) conductive heat flux with leakage of laterally advected heat flux in an aquifer unit.

Tzm = measured temperature at middle of interval

Tzc = calculated temperature at middle of interval

The Fortran program code is included in Appendix 1.

Approximate Solution

Making all previously stated assumptions, the governing equation can be expressed as:

$$\frac{d^2T}{dz^2} = \frac{c_{pw}\rho_w V_x}{K_T} \frac{\Delta T}{\Delta x} \tag{43}$$

where,

$\Delta T/\Delta x$ = constant lateral temperature gradient

The finite-difference approximate solution to this equation is:

$$4 \frac{(T_1 - 2T_c + T_2)}{L^2} \approx \frac{c_{pw}\rho_w V_x}{K_T} \frac{\Delta T}{\Delta x} \tag{44}$$

where

T_2 = temperature at the top of the interval of interest

T_c = temperature at the center of the interval of interest

T_1 = temperature at the base of the interval of interest

Solving for V_x,

$$V_x = \frac{4(T_t - 2T_c + T_b)}{L^2} \left(\frac{K_T}{c_{pw}\rho_w \frac{\Delta T}{\Delta x}} \right) \tag{45}$$

The sign on V_x will either be positive when heat is being removed from the interval ($2T_c < T_t + T_b$), or negative when heat is being added to

the interval ($2T_c > T_t + T_b$). When the temperature gradient through the interval is linear ($2T_c = T_t + T_b$), $V_x = 0$.

Vertical Variation in Heat Flow

Assuming that, at a given location, the conductive (vertical) heat flow and the thermal conductivity profile are known, then vertical variations from this conductive heat flow will be due to groundwater advection. In the San Juan Basin, Reiter and Mansure (1983) have calculated heat flow at numerous sites. Generally, these site heat flow (SHF) calculations were made using data from deep, thick shale intervals (Lewis and Mancos Shales). Deep, thick shales usually will present a more homogeneous thermal conductivity, and due to their depth and low permeability, perturbations due to advection should be small. Therefore, heat flow values measured in these types of units are assumed to represent the local conductive heat flow. Table 9 summarizes the site heat flows at the wells in the study area. Note, that the site heat flow (SHF) calculated for the Southern Ute 2-2 Well is from data in the Fruitland Formation and probably is not representative of conductive heat flow at this location.

In an area which has a lateral temperature gradient, like the San Juan Basin, heat flow over an aquifer interval (Interval Heat Flow or IHF) might be expected to show some difference relative to the SHF. This differences is herein referred to as Excess Heat Flow (EHF), and is assumed to be the amount of heat transferred within the aquifer interval due to lateral advection. EHF will be positive when the direction of lateral flow is from a region of higher heat flow toward a region of lower heat flow. EHF will be negative when the opposite is true.

Table 9. Summary of Calculated Site Heat Flows (Reiter and Mansure, 1983) At Wells in the Study Area

WELL	LOCATION	SITE HEAT FLOW ($x10^{-3}$ cal cm^{-2} sec^{-1})	STRATIGRAPHIC UNIT
Southern Ute 2-2	2-32N-9W(Co.)	2.37	Fruitland
Allison #59	20-32N-6W(Co.)	2.29	Lewis/Mancos
Kelly A #3A	15-31N-10W	2.15	Lewis
Atlantic State #6	16-30N-10W	2.08	Lewis
Com G #8	32-31N-8W	2.17	Lewis/Menefee
Roelofs A #1A	10-29N-8W	1.96	Lewis

The velocity of lateral advection can be estimated using the following relationship.

$$EHF = c_{pw}\rho_w \left(\frac{\Delta T}{\Delta x}\right) V_x L \tag{46}$$

or

$$V_x = EHF \left(\frac{\Delta x}{\Delta T}\right) \left(\frac{1}{c_{pw}\rho_w L}\right) \tag{47}$$

where

L = thickness of the aquifer

VELOCITY CALCULATIONS

Lateral groundwater velocity calculations in the study area are performed using temperature data from the following well combinations:

- Southern Ute 2-2 - Kelly A #3A
- Kelley A #3A - Atlantic State #6
- Southern Ute 2-2 - Atlantic State #6
- Allison #59 - Com G #8
- Allison #59 - Roelofs A #1A

The results of all calculations will be the an estimate of lateral groundwater velocity between each well in a given combination. Table 10 summarizes all data required for the different calculation approaches for each of these well combinations. Table 11 summarizes the results from all calculations. For calculations using some form of the simplified governing equation, lateral groundwater velocity in the study area ranges between 5.24×10^{-5} and 11.2×10^{-5} cm/sec. Calculations using the Excess Heat Flow approach result in velocities approximately one order of magnitude smaller (2.57×10^{-6} to 7.9×10^{-6}

Table 10. Summary of Data used for Calculations of Lateral Groundwater Velocity

WELL COMBINATION	DATA FOR CACULATIONS											
	C	D	K_T	ΔX	L	Z	T_o	T_1	T_2	T_C	ΔT/Δx	EHF
Southern Ute 2-2 Kelly A #3A			2.905	1.7931	7.986	3.993	54.301	47.660	42.457	45.753	4.767	2.589 (Kelly)
Kelly A #3A/ Atlantic State #6			3.107	1.0163	6.005	3.003	45.753	44.895	40.654	43.184	2.527	1.136 (Atlantic)
Southern Ute 2-2/ Atlantic State #6	1.0 (assumed)	1.0 (assumed)	3.107	2.8094	6.005	3.003	54.301	44.895	40.654	43.184	3.957	1.136 (Atlantic)
Allison #59/ Com G #8			2.301	2.3185	7.772	3.886	48.426	50.012	41.798	46.100	1.002	2.570 (Atlantic)
Allison #59/ Roelofs A #1A			2.620	3.4937	8.260	4.130	48.426	43.614	37.289	41.027	2.117	0.450 (Roelofs)

C - specific heat of pure water, (cal gm^{-1} $°C^{-1}$)
D - density of pure water, (gm cm^{-3})
K_T - thermal conductivity of saturated porous rock, (10^{-3} cal cm^{-1} sec^{-1} $°C^{-1}$)
X - horizontal, up-gradient distance between wells, (cm)
L - interpreted thickness of Fruitland Formation flow interval, (cm)
T_o - up-gradient temperature near middle of Fruitland Formation interval, (cm)
T_1 - temperature at base of Fruitland Formation flow interval, (°C)
T_2 - temperature at top of Fruitland Formation flow interval, (°C)
T_C - temperature in center of Fruitland Formation flow interval, (°C)
ΔT/Δx - lateral temperature gradient between wells (10^{-6} °C/cm)
EHF - Excess Heat Flow at downstream well, (10^{-7} cal cm^{-2} sec^{-1})
Z - vertical distance up from base of flow interval, (cm)

Table 11. Summary of calculated lateral groundwater velocity between wells in the study area

WELL COMBINATION	CALCULATED LATERAL GROUNDWATER VELOCITY, cm/sec		
	IMPLICIT ANALYTICAL SOLUTION	FINITE DIFFERENCE APPROXIMATION	EXCESS HEAT FLOW
Southern Ute 2-2/Kelly A #3A	5.24×10^{-5}	5.30×10^{-5}	6.80×10^{-6}
Southern Ute 2-2/Atlantic State #6	7.10×10^{-5}	7.14×10^{-5}	4.78×10^{-6}
Kelly A #3A/Atlantic State #6	1.09×10^{-4}	1.12×10^{-4}	7.48×10^{-6}
Allison #59/Com G #8	5.84×10^{-5}	5.99×10^{-5}	7.9×10^{-6}
Allison #59/Roelofs A #1A	8.24×10^{-5}	8.35×10^{-5}	2.57×10^{-6}

cm/sec). Possible reasons for this order of magnitude difference include:

- The Site Heat Flow determined in the deep shale units and assumed to represent conductive heat flux, may be impacted by vertically advected heat flux from the overlying Fruitland aquifer. This would result in estimated conductive heat flux that is lower than the actual value and minimize the difference between Site Heat Flow and Interval Heat Flow. Therefore, the estimated Excess Heat Flow and the resulting calculated groundwater velocity would be too low. To determine if this is potential for downward leakage from the Fruitland Formation at a given site requires that the hydraulic head of all aquifers in the regional system be known at that site. In the study area this data is not available. However, computer modelling by Frensel and Lyford (1982) indicates that there is the potential for downward leakage in at least the northeast half of the study area.

- The lack of a detailed temperature profile across the assumed flow interval results in an over-estimation of T(z) relative to T_1 and T_2 (or T_c relative to T_1 and T_2 for the finite-difference approximation). This would result in groundwater velocities calculated using the implicit analytical/finite-difference approach that are too high. Since the same thermal conductivity for the assumed flow interval was used in both approaches, this parameter does not contribute to the difference in calculated velocities.

DISCUSSION

The most critical parameter involved in the calculation of lateral groundwater velocity from temperature data is the temperature data itself. Temperature data utilized in this study were obtained using high-precision equipment as part of a regional heat flow investigation. Measured temperatures are therefore assumed to be accurate and correlatable. However, in all the down-gradient wells for the well combinations analyzed in this study, temperature data were obtained at 30-50 meter intervals. This low density of data required linear interpolation to estimate some of the temperatures used in the calculations. This assumption of a linear trend between data points 30 to 50 meters apart is probably not correct, but is the only reasonable alternative. A decrease in the interval between data points to 3 meters would significantly improve confidence in the velocity calculations.

The sensitivity of velocity estimate to variation in the other parameters in the analytical solutions was investigated over reasonable ranges of these parameters, for the Southern Ute 2-2 to Kelly A #3A well combination. In these analyses V_x was calculated by varying a single parameter (i.e., K_T) while holding the other parameters constant. The assumed range for thermal conductivity is between 1.02×10^{-3} to 5.15×10^{-3} cal $cm^{-1}sec^{-1}{}^{\circ}C^{-1}$. The measured range of the up-gradient temperature for the Fruitland interval at Southern Ute 2-2 is between 52.05 to 56.11 °C. The assumed range for fluid heat capacity ranges between 1.02 and .998 cal $cm^{-1}sec^{-1}{}^{\circ}C^{-1}$. This range was estimated by calculating the effects of increased temperature on both the specific heat and density of pure water, and the effect of an increase in dissolved solid concentration to 20,000 mg/ℓ on density.

Figure 42 summarizes the results of these analyses. This figure indicates that V_x is most sensitive to variations in thermal conductivity and least sensitive to variations in heat capacity of water over their assumed ranges.

SUMMARY AND CONCLUSIONS

The objective of this study has been to develop an understanding of a Fruitland Formation coal interval aquifer. The approach to this investigation was to compile and analyze all data appropriate to defining the head distribution of this interval and its general aquifer characteristics. Among the data used to assess aquifer characteristics is lateral and vertical temperature distribution data.

Data to establish the regional distribution of Fruitland Formation hydraulic head included direct water-level measurements around the periphery of the basin and reservoir pressure data obtained from drill-stem tests (DST). Plate I is the resulting basin-wide potentiometric surface map for the Fruitland Formation. Figure 23 reproduces this map, but only in the vicinity of the study area. Review of Plate I indicates that the recharge areas for this aquifer are primarily on the north and south flanks of the basin with flow directed south and west, and north and west respectively. The main discharge areas are along the western boundary of the basin into the San Juan River and tributaries to the Chaco River. In the vicinity of the study area, the hydraulic gradient is approximately 0.01 m/m to the south and southwest. In addition to establishing the potentiometric surface for this aquifer, the hydraulic potential between the Fruitland Formation, and the overlying Ojo Alamo Sandstone and underlying Pictured Cliffs and Cliff House Sandstones was investigated. DST data defining the

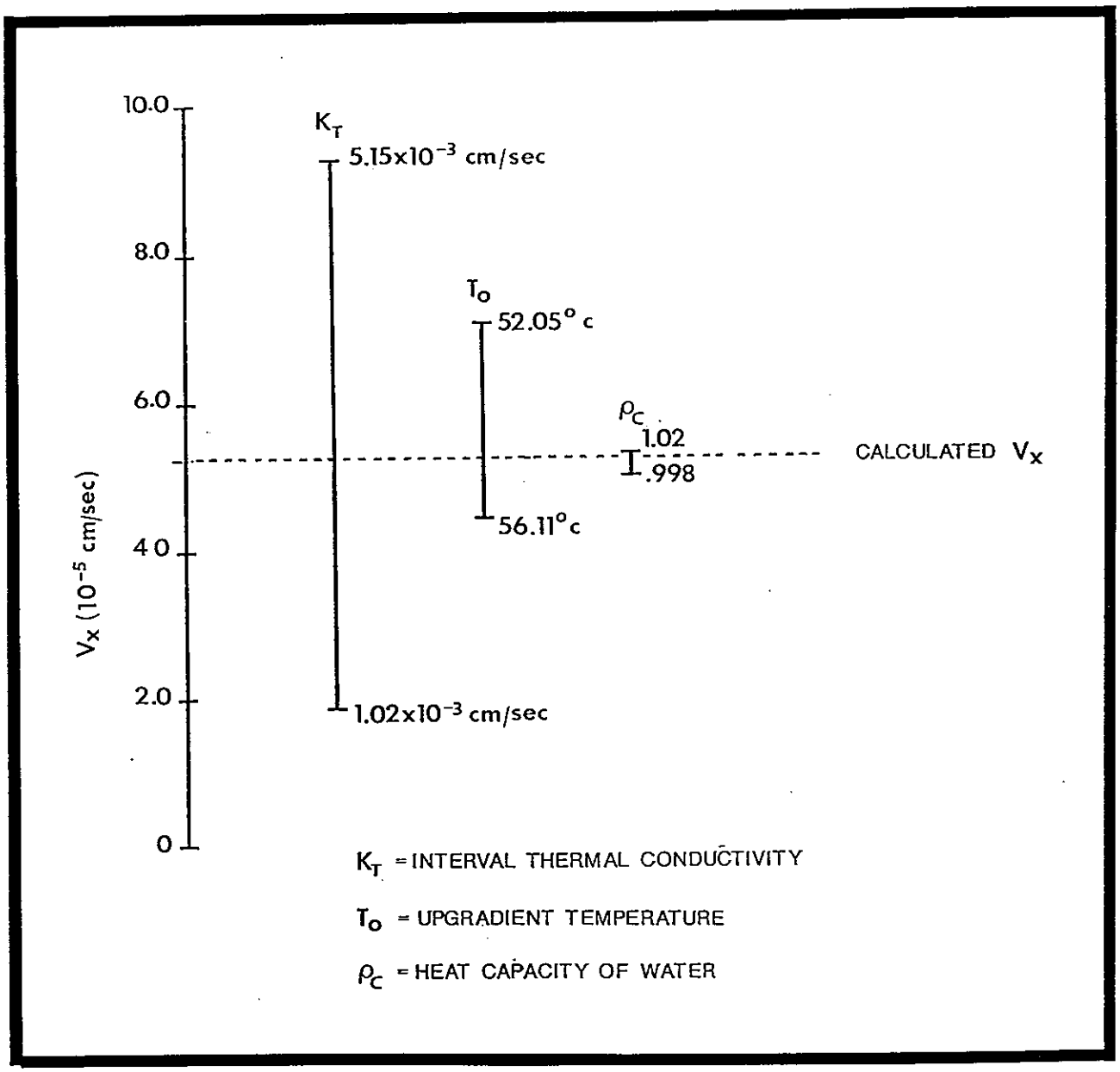

Figure 42 - Variability of calculated lateral groundwater velocity over the expected ranges of interval thermal conductivity, up-gradient temperature and fluid heat capacity for the Southern Ute 2-2 to Kelly A #3A well combination.

Pictured Cliffs hydraulic head relative to Fruitland Formation head was obtained in 22 wells. In those wells in the study area with DST's in both intervals, Fruitland Formation head potential is generally higher than Pictured Cliff head potential (Tables 1 and 2). However, the data indicate that this relationship reverses south of township 28N. Data defining the hydraulic head distribution for the Ojo Alamo and Cliff House Sandstones are sparse in the vicinity of the study area. However, the available data, shown on Figure 8 and 9, indicate that in this area, the Fruitland Formation has the highest hydraulic potential in the Ojo Alamo to Cliff House Sandstone interval.

The Fruitland Formation consists of interbedded shales, siltstones, fine-grained channel sandstones, and coal. Thick coals ranging from approximately 3 meters to 9 meters in thickness are the most laterally continuous lithology. In the study area, four individual thick coalbeds have been shown to extend from between 24 to 40 km on a southwest-northeast trend. In addition, these coalbeds form an echelon pattern and tend to overlap each other with vertical separations of less than 80 meters. Therefore, if these coalbeds are assumed to be hydraulically connected over these vertical separations, a thick laterally extensive coal can be expected to underlie the entire study area. This coal would comprise the primary flow interval in the Fruitland Formation aquifer.

Since a thick coalbed is hypothesized to be the primary flow interval within the Fruitland Formation aquifer, porosity and permeability of coal are important in defining aquifer characteristics. Coal has a low primary porosity composed primarily of micropores (<20 Å). Measured porosity ranges from less than 5% to approximately 9%. In addition, mercury injection capillary pressure data indicates

that Fruitland Formation coal exhibits very high irreducible water saturations. These characteristics indicate that the primary porosity is not an important factor relative to the hydraulic conductivity of coal.

Coal permeability is primarily due to the genetic fracture system called cleat. Locally, this fracture system can be enhanced by geologic structure. One important characteristic of this fracture permeability is that it is stress-sensitive. Laboratory analyses show that coal permeability decreases with increasing stress. In addition, review of permeability values obtained from field tests indicates that coal permeability decreases with increasing depth. In recent well tests the stress-dependent nature of coal permeability has been recognized and tests adjusted to minimize its impact. However, the ability to drill and test coal intervals without damaging permeability is still questionable. Intrinsic permeability values obtained from deep aquifer/reservoir tests and well performance analyses over the Fruitland coal interval range from 3.4 to 15.3 millidarcies. Assuming that water density and dynamic viscosity are 1000 kg m^{-3} and 1.124×10^{-3} kg $m^{-1}sec^{-1}$ respectively, calculated hydraulic conductivities range between 1.51×10^{-5} cm/sec to 3.26×10^{-6} cm/sec. Hydraulic conductivity values obtained from shallow aquifer tests over Fruitland Formation coal intervals range between 7.9×10^{-4} cm/sec and 3.5×10^{-8} cm/sec.

In this study, temperature distribution data was used to estimate lateral groundwater velocity. Lateral and vertical temperature distribution data was obtained in the San Juan Basin as part of a regional heat flow study. Two characteristics of this temperature data base suggested that it might aid in the analyses of a Fruitland

Formation aquifer. The first of these characteristics was the presence of a north-south trending change in conductive heat flow. Conductive heat flow is shown to change from approximately 3.4×10^{-6} cal $cm^{-2}sec^{-1}$ in the San Juan Mountains just to the north of the basin to 1.6×10^{-6} cal $cm^{-2}sec^{-1}$ on the Chaco Slope. This change in conductive heat flow implies that there is a lateral temperature gradient. In the study area this lateral temperature gradient at the approximate elevation interval of the Fruitland Formation ranges between 1.0×10^{-4} °C/m and -4.8×10^{-4} °C/m. The second of these characteristics is that there is typically a significant change in the vertical temperature gradient over the Fruitland interval. Part of this gradient change is certainly due to the lower thermal conductivity of this coal-bearing interval. However, the curvature of the gradient in wells with temperature data obtained at 3 meter intervals suggests that some additional heat is being advected into the Fruitland interval at these locations. Considering that, in the study area, the hydraulic potential of the Fruitland Formation is higher than either the Pictured Cliffs and Cliff House Sandstones (the two aquifer units below the Fruitland), vertical advection bringing heat from below can be discounted. Review of Figures 10 and 23 indicate that, in the study area, lateral groundwater flow is generally from areas of higher heat flow towards areas of lower heat flow. Therefore it is reasonable to assume that any additional heat in the Fruitland aquifer has been added by lateral advection.

In this study two approaches were used to estimate lateral groundwater velocity using temperature distribution data. The first approach is based on the general analytical solution to coupled conductive and advective heat transfer developed by R. W. Stallman

(1963). The second approach is based on vertical variation in heat flow.

To simplify Stallman's general analytical solution to consider only lateral advection, the following assumptions were made:

1. Both the thermal and flow fields are at steady-state.
2. Groundwater flow is only important in the x-direction.
3. Conductive heat flow is only important in the z-direction.

This resulted in equation (36):

$$\frac{\partial^2 T}{\partial z^2} = \frac{c_{pw}\rho_w}{K_T} (V_x) \frac{\partial T}{\partial x}$$

This partial differential equation was then further simplified by assuming a constant lateral temperature gradient. Both the resulting ordinary differential equation (equation 41) and its finite difference approximation (equation 43) were used to calculate lateral groundwater velocity (V_x) between various well combinations in the study area. Results of these calculations indicate that lateral groundwater velocity in the study area ranges between 5.24×10^{-5} cm/sec and 1.12×10^{-4} cm/sec.

Temperature data from the wells in the study area indicate that heat flow in the Fruitland Formation is higher than the conductive heat flow obtained in deeper shale units. The difference between the conductive heat flow at a site is the amount of heat added to the interval due to lateral advection and can be analyzed using equation (46). Using this approach, calculated lateral groundwater velocity ranges between 2.57×10^{-6} cm/sec and 7.90×10^{-6} cm/sec.

Lateral groundwater velocities calculated from temperature distribution data can be combined with the Fruitland Formation

hydraulic head gradient to estimate hydraulic conductivity for this aquifer. Table 12 summarizes the estimated Fruitland Formation aquifer hydraulic conductivity between the given well combinations. This table indicates that Fruitland Formation aquifer hydraulic conductivities estimated from the calculated lateral velocities and the estimated head distribution tend to be significantly higher than those obtained from aquifer/reservoir testing.

1. Lateral groundwater velocities calculated from temperature data are too high.
2. Hydraulic conductivity values calculated from aquifer/reservoir test data are low.
3. The direction and magnitude of hydraulic head gradients are different.
4. A combination of two or more of the above factors.

Examination of elements of the first factor indicates that while the approach and general assumptions seem reasonable, assumptions related to critical temperature and thermal conductivity parameters may be incorrect. The need for these assumptions can be eliminated by decreasing the vertical distance between temperature measurements in a single well and by determining a detailed thermal conductivity profile at wells where the temperature data is obtained. Examination of the second factor indicates analyses of data obtained from coal interval aquifer/reservoir tests may indeed underestimate permeability. This is because the coal fracture permeability is stress-dependent and probably easily damaged by drilling operations. Finally, examination of the third factor indicates that, within the limitations of the data, the interpretation of the regional head distribution and indicated gradients seems reasonable.

In conclusion, the hydrogeologic data presented in this study suggest that a laterally extensive, Fruitland Formation coal interval

Table 12. Summary of Fruitland Formation aquifer hydraulic conductivities estimated from calculated groundwater velocities and regional hydraulic head distribution

WELL COMBINATION	ESTIMATED HYDRAULIC HEAD GRADIENT (m/m)	CALCULATED LATERAL GROUNDWATER VELOCITY (cm/sec)		ESTIMATED HYDRAULIC CONDUCTIVITY (cm/sec)	
		IAS*	EHF**	IAS*	EHF**
Southern Ute 2-2/ Kelly A #3A	.012	5.24×10^{-5}	6.8×10^{-6}	4.37×10^{-3}	5.67×10^{-4}
Southern Ute 2-2/ Atlantic State #6	.010	7.10×10^{-5}	4.78×10^{-6}	7.10×10^{-3}	4.78×10^{-4}
Kelly A #3A/ Atlantic State #6	.006	1.09×10^{-4}	7.48×10^{-6}	1.82×10^{-2}	1.25×10^{-3}
Allison #59/ Com G #8	.009	5.84×10^{-5}	7.9×10^{-6}	6.48×10^{-3}	8.78×10^{-4}
Allison #59/ Roelofs A #1A	.008	8.24×10^{-5}	2.57×10^{-6}	1.03×10^{-2}	3.21×10^{-4}

* IAS - lateral velocity calculated using Implicit Analytical Solution

** EHF - lateral velocity calcualted using Excess Heat Flow approach

aquifer does exist and that, at least in the center of the basin, should be considered a major aquifer. The potential of this interval to be a major aquifer may be important in understanding the regional hydrodynamics in the basin, and water/gas production characteristics associated with development of Fruitland Formation coalbed methane reservoirs. In addition, the temperature distribution data available in the San Juan Basin can be analyzed to calculate lateral groundwater velocity. Innovative techniques to perform these calculations are developed in this study. Application of the analyticl solution technique has resulted in groundwater velocities and hydraulic conductivities that seem unreasonably high. Velocities and conductivities calculated using the Excess Heat Flow Approach are at the upper end of expected ranges for these parameters and overlay with the highest aquifer test values. However, these techniques are conceptually correct and given more detailed vertical temperature and thermal conductivity profiles, should result in reliable estimations of lateral groundwater velocity.

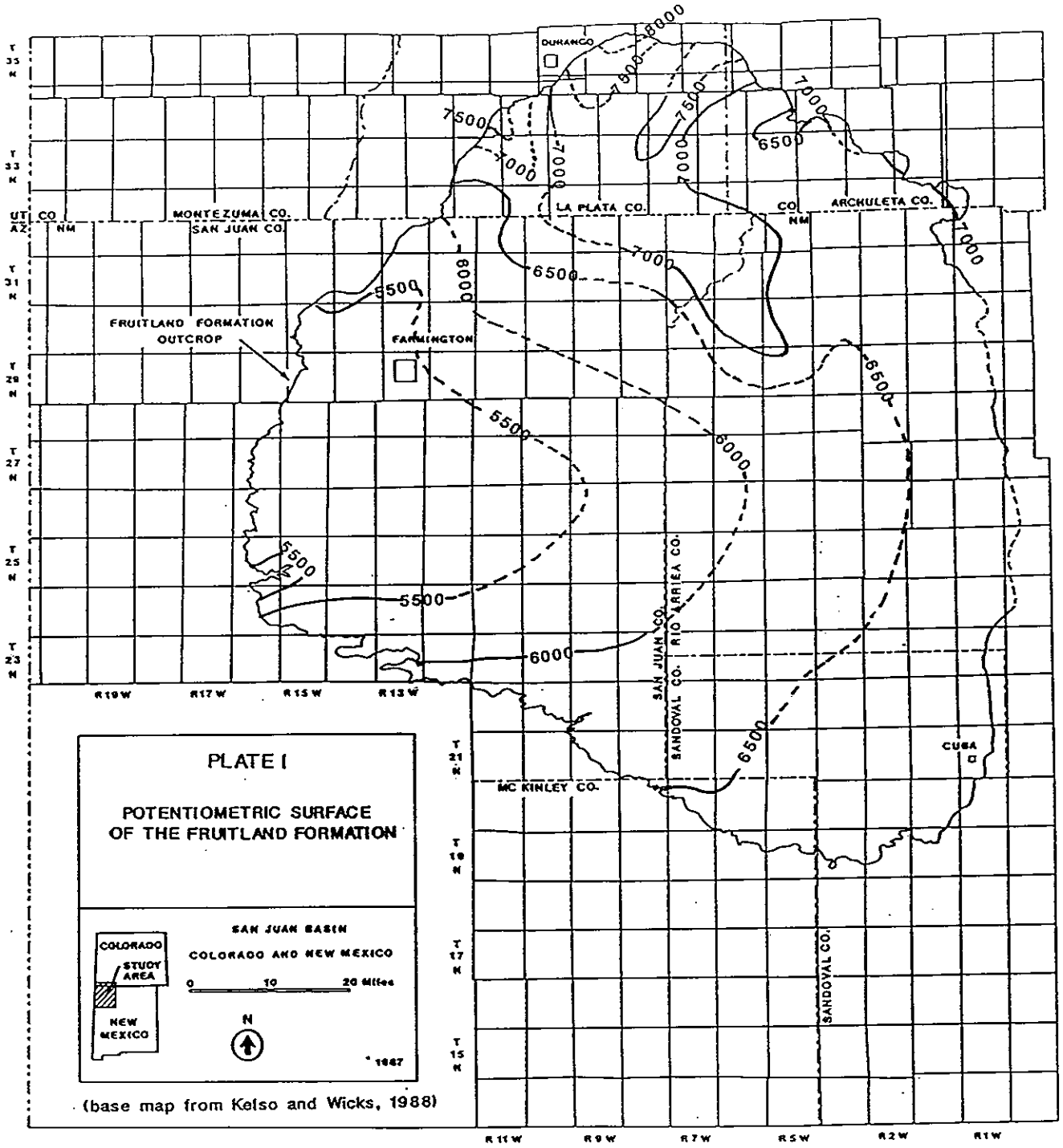
DURANGO
LA PLATA CO.
MONTEZUMA CO.
SAN JUAN CO.
ARCHULETA CO.
FRUITLAND FORMATION OUTCROP
FARMINGTON
SAN JUAN CO.
RIO ARRIBA CO.
SANDOVAL CO.
MC KINLEY CO.
CUBA
SANDOVAL CO.
8000
7500
7000
6500
6000
5500
R19W
R17W
R15W
R13W
R11W
R9W
R7W
R5W
R2W
R1W
PLATE I
POTENTIOMETRIC SURFACE OF THE FRUITLAND FORMATION
SAN JUAN BASIN
COLORADO AND NEW MEXICO
COLORADO
STUDY AREA
NEW MEXICO
0 10 20 Miles
N
1987
(base map from Kelso and Wicks, 1988)
6000
HYDRAULIC HEAD CONTOUR
(dashed where approximate)
CONTOUR INTERVAL - 500 feet

REFERENCES

Averitt, P., 1975. Coal resources of the United States, USGS Bulletin 1412, 131 p.

Berry, F.A.F., 1959. Hydrodynamics and geochemistry of the Jurassic and Cretaceous Systems in the San Juan Basin, Northwestern New Mexico and Southwestern Colorado: Ph.D. Thesis, Stanford University, 192 p.

Bredehoeft, J.D., and Papadopulos, I.S., 1965. Rates of vertical groundwater movement estimated from the earth's thermal profile, Water Resources Research, Vol. 1, No. 2, pp 325-328.

Brimhall, R.M., 1973. Groundwater hydrology of Tertiary rocks of the San Juan Basin, New Mexico, Four Corners Geological Society Memoir, pp 197-207.

Choate, R., 1984. Upper Cretaceous geology, coal, and the potential for methane recovery from coalbeds in San Juan Basin - Colorado and New Mexico, AAPG Studies in Geology Series 17, pp 185-222.

Clarkson, G., and Reiter, M., 1987. The thermal regime of the San Juan Basin since Late Cretaceous times and its relationship to San Juan Mountains thermal sources, Journal of Volcanology and Geothermal Research, v. 31, pp 217-237.

Domenico, P.A., and V.V. Palciauskas, 1973. Theoretical analysis of forced convective heat transfer in regional groundwater flow, GSA Bulletin, Vol. 84, pp 3803-3814.

Earlougher, R.C., 1977. Advances in Well Test Analysis, SPE Monograph, Vol. 5, p 258.

Fassett, J.E., 1988. Geometry and depositional environment of Fruitland Formation coal beds, San Juan Basin, New Mexico and Colorado: Anatomy of a giant coal-bed methane deposit, RMAG Geology and Coal-bed Methane Resources of the Northern San Juan Basin, Colorado and New Mexico, pp 23-38.

Fassett, J.E., and Hinds, J.S., 1971. Geology and field resources of the Fruitland Formation and Kirtland Shale of the San Juan Basin, New Mexico and Colorado, USGS Professional Paper 676, p. 76.

Four Corners Geological Society, 1978-1983. Oil and Gas Field of the Four Corners Area, Four Corners Geological Society, Vol. I, II and III, p. 1143.

Frenzel, P.F., and Lyford, F.P., 1982. Estimates of vertical hydraulic conductivity and regional ground-water flow rates in rocks of Jurassic and Cretaceous age, San Juan Basin, New Mexico and Colorado, USGS Water Resources Investigations, No. 82-4015, p. 59.

Geoguel, J., 1976. Geothermics, ed. by S.P. Clark, translated by A. Rite, McGraw-Hill Book Company.

Harpalani, S., and Mcpherson, J.J., 1985. Effect of stress on permeability of coal, GRI Quarterly Review of Methane from Coal Seams Technology, Vol. 3, No. 2, pp 23-28.

Jones, A.H. et al., 1984. Methane production characteristics for a deeply buried coalbed reservoir in the San Juan Basin, GRI Quarterly Review of Methane from Coal Seams Technology, Vol. 2, No. 1, pp 19-33.

Jones, A.H., et al., 1985. Methane production characteristics of deeply buried coalbed reservoirs, GRI Final Report, TR 85-40R, p. 176.

Jones, A.H., Bell, G.J., and Schraufnagel, R.A., 1988. A review of the physical and mechanical properties of coal with implications for coal-bed methane well completion and production, RMAG Geology and Coal-bed Methane Resources of the Northern San Juan Basin, Colorado and New Mexico, pp 169-181.

Kappelmeyer, O., and Haenel, R., 1974. Geothermics - with special reference to application, Gebruder Borntraeger, p 234

Kelley, V.C., 1950. Regional structure of the San Juan Basin, New Mexico Geological Society, Guidebook, first field conference, pp 101-108.

Kelley, V.C., 1951. Tectonics of the San Juan Basin, New Mexico Geological Society, Guidebook, second field conference, pp 124-131.

Kelso, B.S., and Wicks, D.E., 1988. A geologic analysis of the Fruitland Formation coal and coal-bed methane resources of the San Juan Basin, Southwestern Colorado and Northwestern New Mexico, RMAG Geology and Coal-bed Methane Resources of the Northern San Juan Basin Colorado and New Mexico, pp 69-79.

Kissell, F., Mculloch, C., and Elder, C., 1973. The direct method of determining methane content of coalbeds for ventilation design, U.S. Bureau of Mines Report of Investigations, R.I. 7767.

Law, B.E., et al., 1983. Geologic implications of coal dewatering, AAPG Bulletin, Vol. 67, pp 2255-2260.

Mansure, A.J., and Reiter, M., 1979. A vertical groundwater movement correction for heat flow, Journal of Geophysical Research, Vol. 84, pp 3490-3496.

McKee, C.R., et al., 1986. Using permeability-vs-depth correlations to assess the potential for producing gas from coal seams, GRI Quarterly Review of Methane from Coal Seams Technology, Vol. 4, No. 1, pp. 15-26.

McKee, C.R., et al., 1988. Stress-dependent permeability and porosity of coal, RMAG Geology and Coal-bed Methane Resources of the Northern San Juan Basin, Colorado and New Mexico, pp 143-153.

Meissner, F.F., 1984. Cretaceous and lower Tertiary coals as sources for gas accumulations in the Rocky Mountain area, RMAG Hydrocarbon Source Rocks of the Greater Rocky Mountain Region, pp 401-431.

Minier, J.D., 1984. A geothermal study in west-central New Mexico, Ph.D. thesis, New Mexico Institute of Mining and Technology, p. 229.

Myers, R.G., and Villanueva, E.D., 1986. Geohydrology of the aquifers that may be affected by the surface Mining of coal in the Fruitland Formation in the San Juan Basin, Northwestern New Mexico, USGS Water Resources Investigation Report No. 85-4251, p. 41.

Reiter, M., and Clarkson, G., 1983, Geothermal studies in the San Juan Basin and the Four Corners Area of the Colorado Plateau, II. Steady-state models of the thermal source of the San Juan Volcanic Field, Tectonophysics, Vol. 91, pp 253-269.

Reiter, M., and Hartman, H., 1971. A new steady-state method for determining thermal conductivity, Journal of Geophysical Research, Vol. 76, pp 7047-7051.

Reiter, M., and Mansure, A.J., 1983. Geothermal studies in the San Juan Basin and the Four Corners Area of the Colorado Plateau, I. Terrestrial heat-flow measurements, Tectonophysics, Vol. 91, pp 233-251.

Rose, R.E., and Foh, S.E., 1984. Liquid permeability of coal as a function of net stress, SPE/DOE/GRI Paper 12856, pp 253-259.

Sato, T., 1981. Methane recovery from coalbeds: Surface and physical properties of Western United Stated coal, M.S. thesis, University of New Mexico, p. 78.

Sears, J.D., Hunt, C.F., and Henricks, T.A., 1941. Transgressive and regressive Cretaceous deposits in southern San Juan Basin, New Mexico, USGS Professional Paper 193-F, pp 101-121.

Silver, C., 1951. Cretaceous stratigraphy of the San Juan Basin, New Mexico Geological Society, Guidebook, second field conference, pp 104-118.

Sorey, M.L., 1971. Measurement of vertical groundwater velocity from temperature profiles in wells, Water Resources Research, Vol. 7, No. 4, pp 963-970.

Stone, W.J., et al., 1983. Hydrogeology and water resources of the San Juan Basin, New Mexico, New Mexico Bureau of Mines and Mineral Resources Hydrologic Report No. 6, p. 70.

Stallman, R.W., 1963. Computation of groundwater velocity from temperature data, USGS Water-supply Paper 1544-H, pp 36-46.

Tansey, M.K., 1984. An integrated isotopic/physical approach to a numerical model of groundwater flow in the San Juan Basin, M.S.

Independent Study, New Mexico Institute of Mining and Technology, p. 153.

Vacquier, V., et al., 1988. Experiment on estimating thermal conductivity of sedimentary rocks from oil well logging, AAPG Bulletin Vol. 72, No. 6, pp 758-764.

Van Krevelen, D.W., 1981. Coal, Typology-Chemistry-Physics-Constitution, Elsevier Scientific Publishing Company, p. 514.

Weast, R.C., editor, 1981. CRC Handbook of Physics and Chemistry, CRC Press, 61st. edition.

APPENDIX 1

FORTRAN PROGRAM TO IMPLICITLY SOLVE

THE ANALYTICAL SOLUTION

```
C
C
C
C          THIS FORTRAN CODE IS DESIGNED TO SOLVE THE PARTICULAR
C          SOLUTION FOR THE ODE DESCRIBING VERTICAL TEMPERATURE
C          DISTRIBUTION COUPLING CONDUCTIVE HEAT FLUX WITH LEAKAGE
C          FROM LATERALLY ADVECTED HEAT FLUX. THIS 1-D,
C          QUASI-ANALYTICAL SOLUTION IS SIMILIAR TO 1-D,
C          STEADY-STATE HEAD DISTRIBUTION IN A CONFINED, HOMOGENEOUS,
C          ISOTROPIC AQUIFER WITH VERTICAL LEAKAGE. IN THIS APPLICATION
C          THE TEMPERATURE DISTRIBUTION IS KNOWN. THE UNKNOWN IS LATERAL
C          GROUNDWATER VELOCITY ( VX ) WHICH IS EMBEDDED IN THE
C          LEAKAGE TERM. VX CANNOT BE SOLVED FOR DIRECTLY. RATHER AN
C          ITERATIVE SOLVER USING THE SECANT METHOD IS USED TO MATCH
C          THE MID-POINT MEASURED TEMPERATURE.
C*************************************************************************
C*************************************************************************
C
C     VARIABLE       TYPE           DESCRIPTION
C
C     INPUT          SUBROUTINE     GETS ALL TERMINAL INPUT
C     OUTPUT         SUBROUTINE     DUMPS ALL CALCULATED RESULTS TO THE SCREEN
C                                   AND PRINTS ALL INPUT DATA/CALCULATED RESULTS
C     SECANT         SUBROUTINE     CALCULATES THE ROOT OF THE EVALUTED FUNCTION
C     TEMPFN         FUNCTION       FUNCTION TO BE EVALUATED BY SECANT, COMPUTES
C                                   THE VALUE OF[T(COMPUTED)-T(MEASURED)]
C     TZM            REAL           THE TEMPERATURE MEASURED AT SOME VERTICAL
C                                   POSITION Z
C     TZC            REAL           THE TEMPERATURE CALCULATED AT Z
C     Z              REAL           THE VERTICAL POSITION AT WHICH TEMPERATURE
C                                   IS CALCULATED
C     D              REAL           DENSITY
C     C              REAL           SPECIFIC HEAT
C     TK             REAL           THERMAL CONDUCTIVITY
C     T1             REAL           MEASURED TEMPERATURE AT BASE OF THE INTERVAL
C     T2             REAL           MEASURED TEMPERATURE AT TOP OF THE INTERVAL
C     T0             REAL           MEASURED TEMPERATURE UP-GRADIENT
C     X              REAL           DISTANCE UP-GRADIENT BETWEEN T0 AND
C                                   EVALUATION POINT
C     RL             REAL           INTERVAL THICKNESS
C     VX1            REAL           FIRST GUESS FOR LATERAL VELOCITY
C     VX2            REAL           SECOND GUESS FOR LATERAL VELOCITY
C     TOL            REAL           TOLERANCE USED FOR ITERATIVE SOLUTION
C     ITMAX          INTEGER        MAXIMUM NUMBER OF ITERATIONS ALLOWED
C     VX             REAL           CALCULATED LATERAL VELOCITY
C
C*************************************************************************
C
      EXTERNAL TEMPFN
C
      COMMON /TEMP/C,D,TK,T1,T2,T0,X,RL,TZM,Z
C
      OPEN(UNIT=25,FILE='outwc1',STATUS='unknown')
C
C*******************************************************
C
C     ENTER ALL PARAMETERS
C
C*******************************************************
C
```

```
 12   FORMAT( ' THERMAL CONDUCTIVITY (CAL/(CM-SEC-oC)=    ',F7.5,//)
C
      WRITE(25,13)T1
 13   FORMAT( ' TEMPERATURE @ BASE OF INTERVAL (oC)=    ',F6.3,//)
C
      WRITE(25,14)T2
 14   FORMAT( ' TEMPERATURE @ TOP OF INTERVAL (oC)=    ',F6.3,//)
C
      WRITE(25,15)T0
 15   FORMAT( ' UPGRADIENT TEMPERATURE (oC)=    ',F6.3,//)
C
      WRITE(25,16)X
 16   FORMAT( ' DISTANCE TO UPGRADIENT TEMPERATURE (CM)=    ',E12.5,//)

C
      WRITE(25,17)RL
 17   FORMAT( ' THICKNESS OF VERTICAL INTERVAL (CM)=    ',F6.1,//)
C
      WRITE(25,18)Z
 18   FORMAT( ' Z POSITION FOR TEMPERATURE CALCULATION (CM)=    ',
     *F6.1,//)
C
      WRITE(25,19)TZM
 19   FORMAT( ' TEMPERATURE MEASURED @ Z (oC)=    ',F6.3,//)
C
      WRITE(25,20)VX1
 20   FORMAT( ' FIRST INITIAL GUESS OF VELOCITY (CM/SEC)=    ',E10.3,/)
C
      WRITE(25,24)VX2
 24   FORMAT( ' SECOND INTIAL GUESS OF VELOCITY (CM/SEC)=    ',E10.3,//)
C
      WRITE(25,21)TOL
 21   FORMAT( ' TOLERANCE FOR CALCULATED VELOCITY (CM/SEC)=  ',F10.8,//)
C
      WRITE(25,22)ITMAX
 22   FORMAT(' MAXIMUM NUMBER OF ITERATIONS=     ',I3,////)
C
      RETURN
      END
C
C
C
      SUBROUTINE SECANT(FN,P0,P1,TOL,ITMAX,P)
C*************************************************************************
C     ROUTINE TO RETURN THE ROOT OF A FUNCTION NAMED "FN"
C     P0,P1 :    TWO INITIAL GUESS OF THE ROOT
C     P     :    THE FINAL ROOT VALUE
C     TOL   :    THE CONVERGENCE CRITERIA
C     ITMAX :    MAXIMUM NUMBER OF ITERATIONS TO BE DONE
C     FN    :    FUNCTION TO BE EVALUATED, MUST BE DECLARED EXTERNAL IN THE
C                CALLING PROGRAM
C*************************************************************************
C
      Q0 = FN(P0)
      Q1 = FN(P1)
      DO 100 I=1,ITMAX
C
         P = P1 -Q1*(P1-P0)/(Q1-Q0)
         FNP = FN(P)
         TEST1 = ABS(P-P1)
```

```
      SUBROUTINE INPUT(VX1,VX2,TOL,ITMAX)
C*************************************************************************
C
C   ROUTINE TO INPUT DATA AND SEND TO OUTPUT FILE
C
C*************************************************************************
C
      COMMON/ TEMP/C,D,TK,T1,T2,T0,X,RL,TZM,Z
C
      WRITE(6,*)' ENTER FLUID SPECIFIC HEAT (CAL/CC) '
      READ(5,*)C
C
      WRITE(6,*)' ENTER FLUID DENSITY (GM/CC) '
      READ(5,*)D
C
      WRITE(6,*)' ENTER THERMAL CONDUCTIVITY (CAL/(CM-SEC-oC) '
      READ(5,*)TK
C
      WRITE(6,*)' ENTER TEMPERATURE @ BASE OF INTERVAL (oC) '
      READ(5,*)T1
C
      WRITE(6,*)' ENTER TEMPERATURE @ TOP OF INTERVAL (oC) '
      READ(5,*)T2
C
      WRITE(6,*)' ENTER UPGRADIENT TEMPERATURE (oC)'
      READ(5,*)T0
C
      WRITE(6,*)' ENTER DISTANCE TO UPGRADIENT TEMPERATURE (CM) '
      READ(5,*)X
C
      WRITE(6,*)' ENTER THICKNESS OF VERTICAL INTERVAL (CM) '
      READ(5,*)RL
C
      WRITE(6,*)' ENTER Z POSITION FOR TEMPERATURE CALCULATION (CM) '
      READ(5,*)Z
C
      WRITE(6,*)' ENTER TEMPERATURE MEASURED @ Z (oC) '
      READ(5,*)TZM
C
      WRITE(6,*)' ENTER FIRST GUESS OF VELOCITY (CM/SEC) '
      READ(5,*)VX1
C
      WRITE(6,*)' ENTER SECOND GUESS OF VELOCITY (CM/SEC) '
      READ(5,*)VX2
C
      WRITE(6,*)' ENTER THE TOLERANCE FOR THE VELOCITY (CM/SEC) '
      READ(5,*)TOL
C
      WRITE(6,*)' ENTER THE MAXIMUM NUMBER OF ITERATIONS'
      READ(5,*)ITMAX
C
C
      WRITE(25,10)C
 10   FORMAT('1','*****INPUT DATA*****',///,
     *'FLUID SPECIFIC HEAT (CAL/CC)=  ',F5.3,//)
C
      WRITE(25,11)D
 11   FORMAT( ' FLUID DENSITY (GM/CC)=   ',F5.3,//)
C
      WRITE(25,12)TK
```

```
      CALL INPUT(VX1,VX2,TOL,ITMAX)
C
C*********************************************************
C
C     CALL SECANT TO EVALUATE VX
C
C*********************************************************
C
      CALL SECANT(TEMPFN,VX1,VX2,TOL,ITMAX,VX)
C
C*********************************************************
C
C     OUTPUT ALL COMPUTED VALUES
C
C*********************************************************
      CALL OUTPUT(VX1,VX2,TOL,ITMAX,VX)
      END
C
C
C
      REAL FUNCTION TEMPFN(VX)
C*******************************************************
C
C     FUNCTION TO COMPUTE THE TEMPERATURE AT VELOCITY VX
C
C*******************************************************
C
      COMMON /TEMP/C,D,TK,T1,T2,T0,X,RL,TZM,Z
C
C
C*******************************************************
C
C     CALCULATE LEAKAGE FACTOR
C
C*******************************************************
C
      B=SQRT((TK*X)/(C*D*VX))
C
C*******************************************************
C
C     CALCULATE TEMPERATURE @ Z
C
C*******************************************************
C
         TZC=T0+((T2-T0)/SINH(RL/B))*SINH(Z/B)+
     *((T1-T0)/SINH(RL/B))*SINH((RL-Z)/B)
C
C*******************************************************
C
C     THE FUNCTION SHOULD BE ZERO AT ( TZM - TZC)
C
C*******************************************************
C
         TEMPFN = TZM - TZC
         write(6,*)'vx, tempfn =',vx,tempfn
         RETURN
         END
C
C
C
```

```
          TEST2 = ABS(Q0-Q1)
          TEST = TEST1 + TEST2
          IF((TEST .LT. 2.*TOL).or. ( abs(fnp).lt.tol))THEN
             WRITE(6,*)'ROOT FOUND'
             WRITE(6,*)'FUNCTION VALUE = ',FNP
             WRITE(6,*)'ROOT VALUE = ',P
             RETURN
           ENDIF
           P0 = P1
           P1 = P
           Q0 = Q1
           Q1 = FNP
100     CONTINUE
         RETURN
         END
C
C
      SUBROUTINE OUTPUT(VX)
C*************************************************************************
C
C       ROUTINE TO OUTPUT CALCULATED OUTPUT
C
C*************************************************************************
      COMMON/ TEMP/C,D,TK,T1,T2,T0,X,RL,TZM,Z
C

C
      WRITE(25,23)VX
 23   FORMAT( '***** CALCULATED OUTPUT*****',//,
     *'VX (CM/SEC)=  ',E11.5,//)
C
C
         RETURN
         END
```

NEW MEXICO INSTITUTE OF MINING AND TECHNOLOGY
OFFICE OF GRADUATE STUDIES

REPORT OF M.S. ADVISORY COMMITTEE GEOSCIENCE

This form is to be used by the advisor to transmit information to the Graduate Office. Use the same form for each meeting of the advisory committee.

Student's Name JOHN PHILIP MCCORD Date _____

Members Present _____

Degree Program being Followed: Master of Science ( ) with thesis
(X) without thesis

Course Program

Hyd 411 - Groundwater Hydrology Fall 86	Hyd 534 - Advanced Groundwater Sp
Hyd 412 - Surface Water Hydrology Spring 87	Hyd 542 - Numerical Methods Spri
Hyd 525 - Hydrogeochemistry Fall 86	Hyd 590 - Independent Study Spri
Hyd 535 - Applied Groundwater Spring 87	Math 335 - Applied Analysis Spri
Hyd 491 - Quantitative Hydrology Fall 87	Math 410 - Numerical Analysis Fal
Hyd 538 - Vadose Zone Hydrology Fall 87	Math 332 - Vector Analysis Spri

Advisers Acceptance Fred M. Phillips Date 8 Aug 88

Department Chairman _____ Date _____

Independent Study (X)

Title Hydrogeology of a Fruitland Formation Aquifer, San Juan Bas New Mexico and Colorado, With Emphasis on Using Temperature ~~Data~~ Distributio Data to Estimate Lateral Ground Water Velocity

Accepted: _____ Date _____

Thesis ( )

Title _____

_____

Defense Report: _____

Accepted: _____ Date _____

All Requirements Completed:

Department Chairman: _____ Date _____